TUNNELING IN QUANTUM FIELD THEORY AND SEMICLASSICAL GRAVITY

A Dissertation

Presented to the Faculty of the Graduate School

of Cornell University

in Partial Fulfillment of the Requirements for the Degree of

Doctor of Philosophy

by

Dan Funch Wohns

August 2011

TUNNELING IN QUANTUM FIELD THEORY AND SEMICLASSICAL GRAVITY

Dan Funch Wohns, Ph.D.

Cornell University 2011

In this dissertation we discuss aspects of the transitions between metastable vacua in scalar field theories. These transitions are caused by nucleation of bubbles of one vacuum in a background of another vacuum, and may have relevance in cosmology. Such processes are typically exponentially suppressed in the height and width of the barriers between the vacua. We demonstrate several scenarios where this intuition fails. We use a functional Schrödinger approach to show that tunneling of a scalar field through two barriers can be exponentially faster than tunneling through a single barrier. We determine the conditions that the effective potential must satisfy for a large enhancement in the tunneling rate to be possible. Both the tunneling rate to nearby vacua and to distant vacua in field space can be enhanced by this process. It may be possible to test this phenomenon using superfluid Helium-3. Nucleation of the B phase in samples of the supercooled A phase of superfluid Helium-3 is observed in seconds or minutes, while the characteristic decay time is calculated to be longer than the age of the universe. We propose a resolution to this discrepancy using resonant tunneling. This explanation makes the distinctive prediction that there exist multiple peaks in the nucleation probability as a function of temperature, pressure, and magnetic field. Next we investigate in detail Coleman-de Luccia tunneling. We show that there are four types of tunneling, depending on the importance of thermal and horizon effects. We estimate corrections to the

Hawking-Moss tunneling rate, which can be large. Finally, the tunneling rate for a scalar field described by the Dirac-Born-Infeld action is calculated in the Hawking-Moss limit using a stochastic approach.

BIOGRAPHICAL SKETCH

Daniel Funch Weinberg was born on March 15, 1984 in Rochester, NY. At the age of two, he changed his name to Daniel Funch Wohns, to restore the original family name or perhaps to conceal his identity. He moved to North Carolina in the same year. At the age of three he first learned about inelastic collisions, when he exploited a ten-second gap in his mother's attention to climb in the driver's seat and release the parking brake of a car parked on a slope.

At the age of five he moved to Michigan where he began his education in the East Grand Rapids public school system. He showed an early interest in science and mathematics. In kindergarden he performed his first experiment, and measured the maximum height from which he could drop a block before it would destroy a pen resting on his parents' carpet.

Outside of academics, Dan's interests in middle and high school included skiing, running cross country and track, playing trumpet in the marching band, symphony band, and jazz band, and martial arts. In his seventh year of training in Tae Kwon Do, he was inspired by *The Lord of the Rings* to spend the final summer before his black belt test without wearing shoes. He received his black belt in 2000.

He enrolled at Leland Stanford Junior University in 2002 with the intention of studying mathematics. He quickly realized that he preferred physics to mathematics after several excellent classes during his freshman and sophomore years. Tired of playing organized music, he gave up the trumpet and began to play the mellophone in the Stanford Marching Band. Upon receipt of his Bachelor of Science in Physics with Honors and in Mathematics in 2006, he began his graduate studies at Cornell University. This dissertation is the result of his work there.

To Gang, with love.

ACKNOWLEDGEMENTS

First and foremost, I am indebted to my advisor Henry Tye for all of his guidance and advice throughout my graduate career. He has been an truly outstanding mentor. He has been generous with his time and knowledge, and his encouragement has been an indispensable aid in my development as a physicist. I would also like to thank Liam McAllister for sharing his insight and enthusiasm with me.

I have learned a great deal from many of the other faculty members at Cornell and would like to thank Csaba Csaki, Éanna Flannagan, Kurt Gottfried, Yuval Grossman, Chris Henley, André LeClair, Matthias Neubert, Jeevak Parpia, Maxim Perelstein, Kyle Shen, and Peter Wittich for sharing their wisdom inside and outside of the classroom.

I would like to thank the students and postdocs at Cornell for many interesting discussions, including Thomas Bachlechner, Josh Berger, Monika Blanke, David Curtin, Sergei Dyda, Sohang Gandhi, Girma Hailu, Ben Heidenreich, Johannes Heinonen, Naresh Kumar, David Marsh, Itay Nachshon, Andrew Noble, Enrico Pajer, Bibhushan Shakya, Stefan Sjörs, Flip Tanedo, Yu-Hsin Tsai, and Timm Wrase. I am especially grateful to my collaborators Yang Zhang and Jiajun Xu. I would also like to acknowledge Dan Balick, Adam Brown, Ed Copeland, Jason Ho, Doug Osheroff, Tony Padilla, Paul Saffin, Gary Shiu, Ben Shlaer, Grisha Volovik, and Erick Weinberg for valuable discussions about the work presented in this dissertation.

I am grateful for the financial support I received from the National Science Foundation under grant PHY- 0355005.

My friends including Bryan Daniels, Mohammad Hamidian, Yoav Kallus, Stefan Natu, Stephen Poprocki, Darren Puigh, Sumiran Pujari, and Tristan

Rocheleau made my time in Ithaca truly enjoyable.

The love and support of my parents, Wendy and David, and brothers, Dimitri and Sam, made this dissertation possible. Most of all I thank my lovely wife, Gang, for her love.

TABLE OF CONTENTS

Biographical Sketch . . . iii
Dedication . . . iv
Acknowledgements . . . v
Table of Contents . . . vii
List of Figures . . . ix

1 Introduction **1**
1.1 Cosmological Constant Problem . . . 1
1.2 String Landscape and Eternal Inflation . . . 2
1.3 Organization of this Dissertation . . . 7

2 Resonant Tunneling in Scalar Quantum Field Theory **10**
2.1 Introduction . . . 10
2.2 Resonant Tunneling in Quantum Mechanics . . . 14
2.3 Coleman's Euclidean Instanton Method . . . 17
2.4 Functional Schrödinger Method . . . 19
2.5 Resonant Tunneling in Scalar Quantum Field Theory . . . 29
2.5.1 Setup . . . 29
2.5.2 Ansatz . . . 30
2.5.3 Constraints . . . 34
2.5.4 Tunneling Probability . . . 40
2.5.5 Condition for Resonant Tunneling . . . 42
2.5.6 Generic Situation . . . 46
2.6 Remarks . . . 47

3 Resonant Tunneling in Superfluid Helium-3 **49**
3.1 Introduction . . . 49
3.2 Thermal and Quantum Tunneling . . . 54
3.3 Condition for Resonant Tunneling in Superfluid Helium-3 . . . 59
3.4 Some Predictions . . . 62
3.4.1 Comparison to Other Explanations . . . 62
3.4.2 A Plausible Prediction . . . 64
3.4.3 Growth of Bubbles . . . 67
3.5 Discussion and Remarks . . . 68
3.5.1 Some Subtleties . . . 69
3.5.2 Cosmic Landscape . . . 70
3.5.3 Eternal Inflation . . . 70

4 Coleman-de Luccia Tunneling and the Gibbons-Hawking Temperature **72**
4.1 Introduction . . . 72
4.2 Coleman-de Luccia Tunneling . . . 79

4.3 Tunneling Without Gravity 82
4.3.1 Case (II) 85
4.3.2 Case (I) 86
4.4 Turning on Gravity 88
4.5 The Four Scenarios of Tunneling in de Sitter Space 91
4.5.1 Case (IV) 92
4.5.2 Case (III) 98
4.5.3 Case (II) 100
4.5.4 Case (I) 102
4.6 Discussion 108
4.7 Thermal Tunneling 112
4.7.1 Case IV 114
4.7.2 Case II 115
4.7.3 Case I 116
4.8 Tunneling in the Cosmic Landscape 118
4.9 Summary and Remarks 123

5 Hawking-Moss Tunneling with a Dirac-Born-Infeld Action 127

Bibliography 136

LIST OF FIGURES

2.1 A one-dimensional potential in quantum mechanics with three local minima separated by two barriers. 11
2.2 A typical effective potential $V(\phi)$ with a false vacuum (A) and a true vacuum (B) 17
2.3 Reparameterization of a domain-wall solution 23
2.4 The most probable escape path is a path through field configuration space parameterized by λ 24
2.5 The position-dependent mass $m(\lambda)$ 25
2.6 Effective tunneling potential $U(\lambda)$ 26
2.7 Effective potential $V(\phi)$ for resonant tunneling 31
2.8 Field configuration for resonant tunneling 32
2.9 A typical effective tunneling potential $U(\lambda)$ for double tunneling 33
2.10 The position-dependent mass $m(\lambda)$ for resonant tunneling 34
2.11 The various regions that can be described by Euclidean time or by Lorentzian time in the double bubble nucleation process . . . 36
2.12 The allowed parameter region for resonant tunneling 38
2.13 Two examples where resonant tunneling is absent 40
2.14 Effective one-dimensional potentials for resonant tunneling . . . 42
2.15 Parameter regions where resonant tunneling is likely 43

3.1 Plot of the potential for superfluid Helium-3 as a function of the interpolating field ϕ 61
3.2 Predictions for He-3 experiments 63

4.1 Potential $V(\phi)$. 72
4.2 The log-log plot of the tunneling exponent B as a function of the Hubble parameter H for a fixed potential $V(\phi)$ except for its overall height as measured by H 77
4.3 Triangular potential $V(\phi)$ 83
4.4 The Euclidean bounce solution of $\phi(\xi)$ in the four cases 93
4.5 The function g(c) 97
4.6 The function $I(1/\gamma)$ 102
4.7 The contour plot of $(B_{tw} - B)/B$ as the function of $\tilde{\epsilon}$ and V_T 106
4.8 Comparison of the Euclidean action and the free energy divided by the GH temperature 119

CHAPTER 1

INTRODUCTION

1.1 Cosmological Constant Problem

The expansion of the universe is accelerating. All known forms of matter and radiation are gravitationally attractive and cause the expansion of the universe to decelerate. Some new gravitationally repulsive substance unlike anything previously discovered must be responsible.

The first observational evidence for the accelerated expansion came from measurements of the luminosity of type Ia supernovae [1]. When a white dwarf star accumulates enough mass from a companion star, it will explode resulting in a type Ia supernovae. The intrinsic luminosity of these events does not vary greatly and the variations are partially understood, allowing their use as standard candles. The most redshifted supernovae are dimmer than expected, implying that the universe was expanding at a slower rate in the past.

The simplest explanation[1] of this accelerated expansion of the universe is a cosmological constant. Einstein originally added a cosmological constant term to counteract the gravitational attraction of matter and radiation and allow for a stationary universe. Following Hubble's observation that the universe was expanding, Einstein remarked that the introduction of the cosmological constant was his biggest blunder. In the classical theory, explaining the observed value of the cosmological constant involves tuning a single parameter.

[1]Other possibilities include quintessence or a modification of Einstein's theory of gravitation. Even if these theories can successfully explain the expansion history of the universe, they generally do not escape from the problem discussed below.

The true problem is much worse than a single tuning, because the classical value of the cosmological constant receives many quantum corrections. The vacuum energy density has the form of a cosmological constant in Einstein's equation. This vacuum energy density arises because the vacuum in quantum field theory is a seething foam of virtual particle-antiparticle pairs, which gravitates. Each particle loop contributes to the vacuum energy density, and by dimensional analysis each of these contributions is of the order of the cutoff of the theory to the fourth power. Standard Model particles should each contribute at least $(1\,\mathrm{TeV})^4$ and as much as $(10^{18}\,\mathrm{GeV})^4$ to the vacuum energy density. Additional contributions come from the potentials of scalar fields. Although the energy density of the vacuum is seventy percent of the total energy density of the universe, the measured value is only $(10^{-3}\,\mathrm{eV})^4$, 60 to 120 orders of magnitude smaller than predicted. These contributions can have either sign, so there is no contradiction with cosmological observations, but the deep question of why these contributions cancel so precisely has been puzzling scientists for decades. This mystery is what is known as the cosmological constant problem.

Any fundamental theory of nature that unifies gravity and quantum field theory must at least be able to accommodate if not explain the observed value of the cosmological constant. String theory is a candidate theory of quantum gravity and arguably succeeds at least in this first aspect.

1.2 String Landscape and Eternal Inflation

String theory suggests that there exist a large number of classically metastable vacua known as the landscape. The total number of vacua is not known, but

typical estimates exceed 10^{500}. In each of these vacua, the cosmological constant, coupling constants, matter content, and even forces can differ. The existence of a large number of vacua with different cosmological constants admits the possibility that at least some of these vacua have a cosmological constant consistent with the measured value.

The reason that string theory predicts such a large number of vacua is related to the large number of additional four-dimensional fields that result from the ten-dimensional nature of string theory. If string theory describes our universe, six dimensions must be compactified. From a four-dimensional perspective, the sizes and shapes of these compactified dimensions are moduli, or massless scalar fields. Massless scalar fields can lead to modifications of gravity that contradict experiment [2], or they can overclose the universe [3]. This problem can be solved by introducing generalized magnetic fields known as fluxes in the compactified dimensions. The energy stored in these fluxes depends on the internal geometry, and contributes to the potential of the (pseudo-) moduli. The volume moduli are not lifted by flux and instead can acquire a potential through non-perturbative effects [4] or a combination of non-perturbative effects and α' corrections [5]. The low-energy physics will depend on the choice of fluxes and the resulting values of the stabilized moduli. These fluxes are quantized, and there are typically of order 100 distinct cycles that can support flux. Even a modest number of choices for the flux in each cycle leads to an extremely large number of vacua.

Quantum tunneling allows for transitions between these vacua. If the transitions are dominated by Coleman-de Luccia instantons [6] or the Hawking-Moss tunneling [7] process[2], then generically more volume is created by the expan-

[2]We will assume throughout that the vacua have a four-dimensional effective field theory

sion of a region of false vacuum than is lost due to transitions to other vacua, leading to eternal inflation. These tunneling processes describe the quantum mechanical nucleation of a bubble of the true vacuum from a region of spacetime in which a homogeneous scalar field is in a false vacuum state. The rate at which these bubbles nucleate is typically exponentially suppressed.

In the eternal inflation scenario [8], the multiverse is inhomogeneous on very large scales, with different regions of spacetime inflating in different vacua. Within this multiverse are bubbles created via quantum tunneling. Each of these bubbles is an open universe that is infinite in spatial extent. The majority of spacetime consists of these inflating bubbles, but regions exist where inflation has ended. Some regions of spacetime tunnel to a part of the landscape where inflation consistent with the observed cosmic microwave background (CMB) radiation can occur. Other regions may tunnel to vacua with negative cosmological constants, where a big crunch singularity will occur. Still other regions could tunnel to a supersymmetric vacuum with vanishing cosmological constant.

In an eternally inflating multiverse, every possible event or sequence of events occurs an infinite number of times because the volume of spacetime is infinite. To make predictions about the relative probability of two events if both of those events occur an infinite number of times requires some way of regulating the infinities. While it is possible to define probabilities in this way, the result depends strongly on the method of regularization. This issue is known as the measure problem [9].

A seemingly natural way to regulate these infinities is to consider the multiverse with a finite time cutoff and take the limit where the cutoff diverges.

description.

Such a scheme has several ambiguities, such as whether to weight each bubble universe equally or by its volume (or somewhere in between), and how to choose constant-time hypersurfaces when the multiverse is highly inhomogeneous. Different choices lead to vastly different predictions, and many such schemes are in violent conflict with observation.

If this picture of eternal inflation in the landscape is correct, then the cosmological constant is an environmental variable. Although it may be constant over vast distances in parts of the multiverse, over sufficiently large distances the cosmological constant varies. This idea was used by Weinberg [10] to predict the value of the cosmological constant. Weinberg argued that if the cosmological constant varied in spacetime, observers would only be found in those regions where structure, and more specifically galaxies could form. If the cosmological constant were much larger than $(10^{-3}\,\mathrm{eV})^4$, then it would dominate the energy density of the universe before galaxies could form. The universe would recollapse before the formation of galaxies if the cosmological constant were much smaller than $-(10^{-3}\,\mathrm{eV})^4$. If the cosmological constant can take many values and the prior probability distribution of cosmological constants is flat in this range, then a cosmological constant of the same order of magnitude as observed should be expected. A better understanding of the landscape, the correct measure, and the transitions between vacua is necessary to have confidence in the assumptions underlying this explanation.

It is possible that we may be able to observe the imprints of a tunneling event on the cosmic microwave background if our universe collided with another bubble just before the observable period of inflation [11]. If these collisions occurred too early all signatures would be stretched to unobservable super-

horizon scales, and if they occurred too late they would create unacceptably large anisotropies, but there is a window in which such collisions are potentially observable, and not already excluded. The surface of last scattering can only be affected within the future lightcone of such a collision. Because of the symmetry of the collision and this causality argument, the CMB will be modified within a circular region. The CMB could change discontinuously across the boundary of this region. No such signatures have been unambiguously detected, but observational data will improve considerably over the next few years.

The existence of only one observable universe disadvantages cosmologists who would like to perform repeatable, controlled experiments. Fortunately at least one system, namely superfluid Helium-3, shares many properties with the landscape and is more accessible. At a temperature of a few millikelvins, Helium-3 pairs condense and enter a superfluid phase in which the viscosity vanishes. These pairs carry net spin, so the order parameter has eighteen real components. The potential on this eighteen-dimensional "landscape" is complicated and has many local minima. As samples are essentially free from impurities, nucleation experiments using superfluid Helium-3 may be the best way to use experiment to shed light on cosmological quantum nucleation processes.

In this dissertation we will not directly attempt to solve the problems discussed above, although these issues motivate much of what follows. The existence of eternal inflation of the false vacuum type requires a vacuum with a sufficiently slow decay rate. To check this assumption, we need both a better understanding of the landscape and the decay processes. If tunneling processes can become exponentially faster than the Hawking-Moss or Coleman-de Luccia processes, then the question of whether eternal inflation of the false vacuum

type occurs could become more dependent on the details of the potential. In particular Hawking-Moss and Coleman-de Luccia transitions to distant vacua typically incur an additional exponential suppression compared to transitions to nearby vacua in field space. If new mechanisms enhance the tunneling rate to distant vacua, many vacua previously thought to be metastable could become unstable due to the larger number of possible decay channels, even if each of the decays is slow. Additionally, predictions in eternal inflation are sensitive to the transition rates between vacua, for most choices of measure. A thorough understanding of the quantum transitions between vacua is necessary to reliably compute probabilities of some types of events in an eternally inflating multiverse.

Dynamic effects could modify the cosmological constant problem presented above. If vacua with large vacuum energy density typically decay sufficiently quickly, then they may become irrelevant to cosmology, moderating the severity of the problem. We will present some progress on understanding quantum tunneling and occasionally comment on the relevance of our results to the issues discussed above.

1.3 Organization of this Dissertation

In Chapters 2 and 3 we present a novel tunneling mechanism, and discuss a way to test this mechanism in the laboratory. In Chapter 4 we discuss the relationship between quantum and thermal tunneling, and present some analytic results for thick-wall tunneling. In Chapter 5 we show how the Hawking-Moss tunneling rate is modified if the kinetic term takes a particular non-canonical form.

In Chapter 2 we show how the presence of an additional vacuum can exponentially enhance the tunneling rate in scalar quantum field theory without gravity. In the semi-classical limit, we use the functional Schrödinger method to map double-barrier tunneling in quantum field theory onto a one-dimensional time-independent quantum mechanics problem. We determine the conditions under which the absolute value of the exponent of the tunneling probability from one vacuum to second can be much smaller than the Euclidean action of the instanton interpolating between those two vacua. Surprisingly, this phenomenon can occur not only if the two vacua are separated by an intermediate vacuum in field space, but also if the two vacua are adjacent in field space.

In Chapter 3 we examine a possible way to test the resonant tunneling of Chapter 2 by experiments with superfluid Helium-3. Superfluid Helium-3 provides an excellent experimentally accessible model landscape for investigating vacuum transitions. In addition to being one of the most pure quantum systems observed, superfluid Helium-3 has a large number of metastable phases. In particular, the transition between the A and B phases of superfluid Helium-3 occurs exponentially faster than expected based on the measured values of the domain wall tension and free energy density difference between these two phases. We propose that this fast transition is due to the resonant tunneling phenomenon.

In Chapter 4 we study Coleman-de Luccia tunneling in detail. We show that, for a single scalar field potential with a true and a false vacuum, there are four types of tunneling, depending on the properties of the potential. A general tunneling process involves a combination of thermal (Gibbons-Hawking temperature) fluctuation part way up the barrier followed by quantum tunneling. The thin-wall approximation is a special limit of the case (of only quantum tun-

neling) where inside the nucleation bubble is the true vacuum while the outside reaches the false vacuum. Hawking-Moss tunneling is the (only thermal fluctuation) limit of the case where the inside of the bubble does not reach the true vacuum at the moment of its creation, and the outside is cut off by the de Sitter horizon before it reaches the false vacuum. We estimate the corrections to the Hawking-Moss formula, which can be large. In all cases, we see that the bounce of the Euclidean action decreases rapidly as the vacuum energy density increases, signaling that the tunneling is not exponentially suppressed. In some sense, this phenomenon may be interpreted as a finite temperature effect due to the Gibbons-Hawking temperature of the de Sitter space. As an application, we discuss the implication of this tunneling property to the cosmic landscape.

In Chapter 5 the Hawking-Moss tunneling rate for a field described by the Dirac-Born-Infeld action is calculated using a stochastic approach. We find that the effect of the non-trivial kinetic term is to enhance the tunneling rate, which can be exponentially significant. This result should be compared to the DBI enhancement found in the Coleman-de Luccia case.

CHAPTER 2

RESONANT TUNNELING IN SCALAR QUANTUM FIELD THEORY

2.1 Introduction

In quantum mechanics (QM) the tunneling probability (or the transmission coefficient) of a particle incident on a barrier is typically exponentially suppressed. Somewhat surprisingly the addition of a second barrier can increase the tunneling probability for specific values of the particle's energy. This enhancement in the tunneling probability, known as resonant tunneling, is due to constructive interference between different quantum paths of the particle through the barriers. Under the right conditions, the tunneling probability can reach unity. This is a very well understood phenomenon in quantum mechanics [12]. The first experimental verification of this phenomenon was the observation of negative differential resistance due to resonant tunneling in semiconductor heterostructures by [13]. In fact, this phenomenon has at least one industrial application in the form of resonant tunneling diodes [14].

Tunneling under a single barrier in quantum field theory (QFT) with a single scalar field is well understood, following the work of Coleman and others [15, 16]. Despite some arguments given in [17, 18], the issue of resonant tunneling in quantum field theory remains open [19, 20]. Recently, Sarangi, Shiu and Shlaer suggested that the functional Schrödinger method should allow one to study this resonant tunneling phenomenon [21]. In this chapter, we apply this approach to study resonant tunneling in QFT with a single scalar field. We show that resonant tunneling in quantum field theory does occur and describe its properties. Following Coleman, we shall work in the thin-wall approxima-

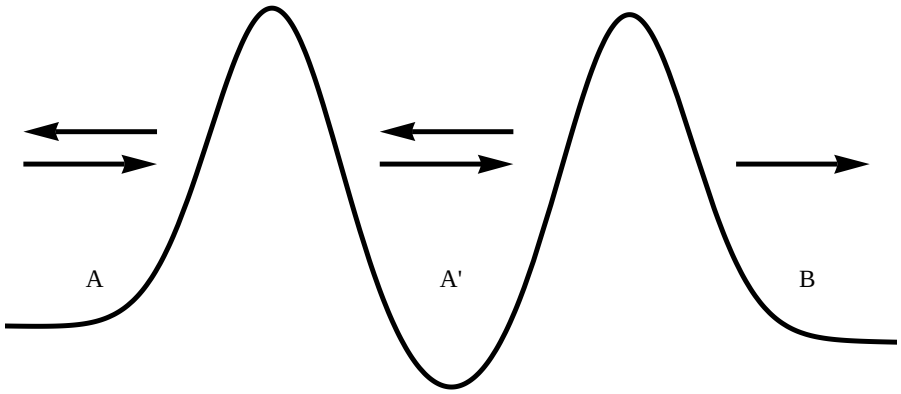

Figure 2.1: A one-dimensional potential in quantum mechanics with three local minima separated by two barriers. Consider an incoming particle from the left. The resonant tunneling effect can take place in the tunneling from $A \to B$ via A'. With the appropriate energy for the particle, the tunneling probability or transmission coefficient may be as large as unity.

tion.

Before going into any details, it is useful to give an intuitive argument why some effect like resonant tunneling should happen in QFT. Consider the following tunneling process for a potential shown in Figure 2.1. Let the tunneling rate from $A \to A'$ be $\Gamma_{A\to A'} = De^{-S}$, while its tunneling probability $P(A \to A') = Ke^{-S}$, which are taken to be exponentially small. The prefactor D or K is of order unity with the proper dimension. Here we shall focus on the exponential factor. Suppose the tunneling rate from $A' \to B$ is given by $\Gamma_{A'\to B}$, which is also exponentially suppressed. Both $P(A \to A')$ and $P(A' \to B)$ are evaluated using standard WKB method. A naive WKB analysis will suggest that the tunneling from $A \to B$ is doubly exponentially suppressed, i.e., $P(A \to B) \approx P(A \to A')P(A' \to B)$. However, this argument is not correct. Consider the typical time, namely $t_{A\to B}$,

it takes to go from $A \to B$. It should be the sum of the time it takes to go from $A \to A'$ plus the time it takes to go from $A' \to B$. Since the typical time is simply the tunneling (or decay) time, which is the inverse of the rate of tunneling, we have

$$\frac{1}{\Gamma_{A\to B}} = t_{A\to B} = t_{A\to A'} + t_{A'\to B} = \frac{1}{\Gamma_{A\to A'}} + \frac{1}{\Gamma_{A'\to B}} \tag{2.1}$$

So it follows that

$$P(A \to B) \approx \frac{P(A \to A')P(A' \to B)}{P(A \to A') + P(A' \to B)} \tag{2.2}$$

which is clearly not doubly suppressed. For the special case where $P = P(A \to A') = P(A' \to B)$, we see that $P(A \to B) \approx P/2$.

In QM, the exponential enhancement from $P(A \to B) \approx P^2$ to $P/2$ is due to the resonant tunneling effect. At the resonances, $P(A \to B) \approx 1$ while it is $\approx P^2$ off resonances. For a generic incoming wavefunction, with a spread in energy eigenvalues covering one or more resonances, this resonant effect yields $P(A \to B) \approx P/2$, so the resonances typically dominate the tunneling process $A \to B$. More generally, the relations (2.1) and (2.2) are reproduced [17, 18]. Since the argument for (2.1) is general, it should apply in QFT as well as in QM. This suggests that some phenomenon like resonant tunneling must take place in QFT. The challenge is to find and understand it.

The functional Schrödinger method was developed by Gervais and Sakita [22] and Bitar and Chang [23]. It starts with the idea that tunneling is dominated by the most probable escape path (MPEP) developed by Banks, Bender and Wu [24]. In QFT with a single scalar field ϕ, this path in the field space is described by $\phi_0(\mathbf{x}, \lambda)$, where $\mathbf{x}$ stands for the spatial coordinates and λ is a parameter that parametrizes the field configurations in the MPEP. In Coleman's Euclidean instanton approach, λ is chosen to be the Euclidean time τ, and the

$O(4)$ symmetry of the instanton simplifies the analysis. On the other hand, the functional Schrödinger method allows one to make a different choice of λ. In the leading order WKB approximation, a generic choice leads one to a simple time-independent Schrödinger equation. It is not surprising that the resulting WKB formula for a single barrier tunneling process reproduces that of the Euclidean instanton approach. We shall present a step-by-step comparison so the equivalence of the two approaches is transparent. It is also obviously clear that the functional Schrödinger method is cumbersome by comparison. However, this method has the great advantage of being immediately generalizable to the double (actually multiple) barrier case. The underlying reason is that the same real parameter λ parametrizes both the under barrier (Euclidean time τ) and the classically allowed (Lorentzian time t) regions.

For tunneling from vacuum A to vacuum B via the intermediate vacuum A' in scalar QFT, we consider the simultaneous nucleation of two bubbles, where the outside bubble separates A from A' and the inside one separates A' from B. The functional Schrödinger method reduces this problem, in the leading WKB approximation, to a one-dimensional time-independent QM problem with λ as the coordinate. The resulting double barrier potential in λ, namely $U(\lambda)$, allows us to borrow the QM analysis to show the existence of resonant tunneling. In the case when both bubbles grow classically after nucleation, the tunneling process from A to B will be completed. The tunneling rate is exponentially enhanced compared to the naive case. In the case where the inside bubble classically collapses back after its nucleation (because the bubble is too small for the difference in the vacuum energies to overcome the surface term due to the domain wall tension), only the tunneling from A to A' is completed. Still the tunneling rate from A to A' can be exponentially enhanced. To draw a distinction between

these two different phenomena, we call the second process catalyzed tunneling. For catalyzed tunneling, vacuum B plays the role of a catalyst.

The rest of this chapter is organized as follows. Resonant tunneling in quantum mechanics is reviewed in Section 2.2. This review follows that in [12, 17] . As we shall see, the functional Schrödinger method reduces the QFT problem to a QM problem, so the resonant tunneling formalism in QM presented here goes over directly. In Section 2.3, we briefly review Coleman's Euclidean action approach, following [15]. In Section 2.4, we present the functional Schrödinger method. Here, the discussion follows closely that given by Bitar and Chang [23, 25] and we need only the leading order WKB approximation. For the single-barrier tunneling process, we see how Coleman's result is reproduced. In Section 2.5, we discuss the double-barrier case. This is the main section of the chapter. Here we find that resonant tunneling can occur in two different ways. It can enhance the tunneling from vacuum A to vacuum B via the intermediate vacuum A', or it can enhance the tunneling from A to A' in the presence of B. Section 2.6 contains some remarks.

2.2 Resonant Tunneling in Quantum Mechanics

We first briefly review resonant tunneling in quantum mechanics. We consider a particle moving under the influence of a one-dimensional potential $V(x)$ with three vacua shown in Figure 2.1. Using the WKB approximation to solve the Schrödinger equation $H\psi = E\psi$ for the wavefunction of the particle $\psi(x)$ gives the linearly independent solutions

$$\psi_{L,R}(x) \approx \frac{1}{\sqrt{k(x)}} \exp\left(\pm i \int dx k(x) \right) \tag{2.3}$$

in the classically allowed region, where $k(x) = \sqrt{\frac{2m}{\hbar^2}(E - V(x))}$, and

$$\psi_{\pm}(x) \approx \frac{1}{\sqrt{\kappa(x)}} \exp\left(\pm \int dx \kappa(x) \right) \tag{2.4}$$

in the classically forbidden region, where $\kappa(x) = \sqrt{\frac{2m}{\hbar^2}(V(x) - E)}$. A complete solution is given by $\psi(x) = \alpha_L \psi_L(x) + \alpha_R \psi_R(x)$ in the classically allowed region and $\psi(x) = \alpha_+ \psi_+(x) + \alpha_- \psi_-(x)$ in the classically forbidden region. To find the tunneling probability from A to A' we need to determine the relationship between the coefficients $\alpha_{L,R}$ of the components $\psi_{L,R}$ in vacuum A and the coefficients $\beta_{L,R}$ in vacuum A'. The WKB connection formulae give

$$\begin{pmatrix} \alpha_R \\ \alpha_L \end{pmatrix} = \frac{1}{2} \begin{pmatrix} \Theta + \Theta^{-1} & i(\Theta - \Theta^{-1}) \\ -i(\Theta - \Theta^{-1}) & \Theta + \Theta^{-1} \end{pmatrix} \begin{pmatrix} \beta_R \\ \beta_L \end{pmatrix} \tag{2.5}$$

where Θ is given by

$$\Theta \simeq 2 \exp\left(\frac{1}{\hbar} \int_{x_1}^{x_2} dx \sqrt{2m(V(x) - E)} \right) , \tag{2.6}$$

and x_1 and x_2 are the classical turning points. Setting $\beta_L = 0$, the tunneling probablity is given by

$$P(A \to A') = |\frac{\beta_R}{\alpha_R}|^2 = 4 \left(\Theta + \frac{1}{\Theta} \right)^{-2} \simeq \frac{4}{\Theta^2} . \tag{2.7}$$

Since Θ is typically exponentially large, $P(A \to A')$ is exponentially small.

The same analysis gives the tunneling probability from A to B, via A', as [12, 17],

$$P(A \to B) = 4 \left(\left(\Theta\Phi + \frac{1}{\Theta\Phi} \right)^2 \cos^2 W + \left(\frac{\Theta}{\Phi} + \frac{\Phi}{\Theta} \right)^2 \sin^2 W \right)^{-1} , \tag{2.8}$$

where

$$\Phi \simeq 2 \exp\left(\frac{1}{\hbar} \int_{x_3}^{x_4} dx \sqrt{2m\,(V(x) - E)} \right) \tag{2.9}$$

and

$$W = \frac{1}{\hbar}\int_{x_2}^{x_3} dx\,\sqrt{2m(E - V(x))}\ , \tag{2.10}$$

with x_3 and x_4 the turning points on the barrier between B and C.

If $W = 0$, $P(A \to B)$ is very small,

$$P(A \to B) \simeq 4\Theta^{-2}\Phi^{-2} = P(A \to A')P(A' \to B)/4 \tag{2.11}$$

However, if W satisfies the quantization condition for the nth bound states in A',

$$W = (n + 1/2)\pi \tag{2.12}$$

then $\cos W = 0$, and the tunneling probability approaches a small but not necessarily exponentially small value

$$P(A \to B) = \frac{4}{(\Theta/\Phi + \Phi/\Theta)^2} \tag{2.13}$$

This is the resonance effect. If $P(A \to A')$ and $P(A' \to B)$ are very different, we see that $P(A \to B)$ is given by the smaller of the ratios between $P(A \to A')$ and $P(A' \to B)$. Suppose $P(A \to A') \to P(A' \to B)$. Following (2.13), we see that $P(A \to B) \to 1$ that is, the tunneling probability approaches unity. Notice that the existence of resonant tunneling effect here is independent of the detailed values of Θ, Φ, and W.

The above phenomenon is easy to understand in the Feynman path integral formalism. A typical tunneling path starts at A and tunnels to A'. It bounces back and forth k times, where $k = 0, 1, 2, ...\infty$, before tunneling to B. When the Bohr-Sommerfeld quantization condition (2.12) is satisfied, all these paths interfere coherently, leading to the resulting resonant tunneling. On the other hand, if we raise the energy of the local minimum at A' above the incoming energy E, then $W = 0$ and $P(A \to B) \sim P(A \to A')P(A' \to B)$ which is typically doubly exponentially suppressed.

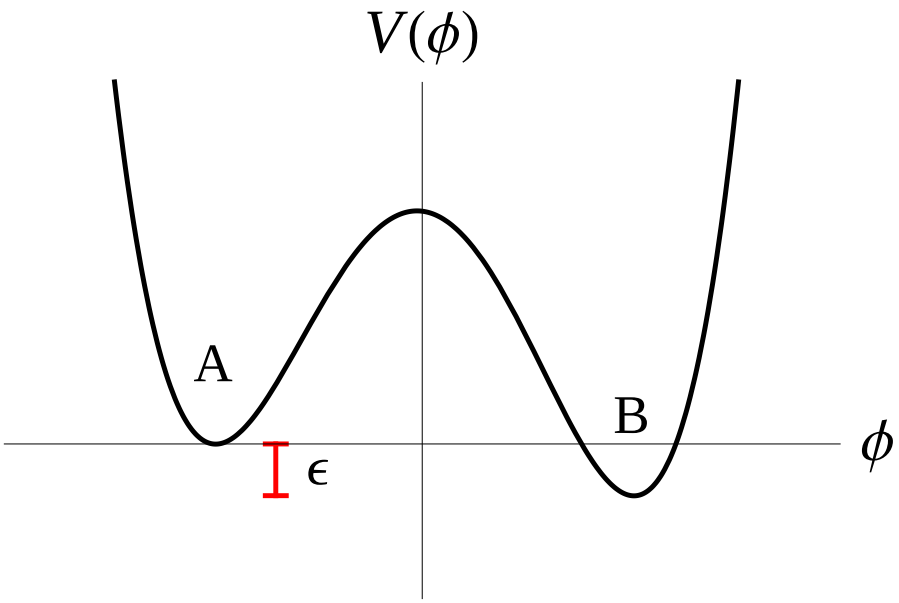

Figure 2.2: A typical effective potential $V(\phi)$ with a false vacuum (A) and a true vacuum (B). Here ϵ is the difference in vacuum energy density.

2.3 Coleman's Euclidean Instanton Method

Single-barrier tunneling in quantum field theory was studied by [15] using the Euclidean instanton method. For concreteness, we will focus on the (3 + 1)-dimensional scalar field theory in Minkowski space described by the Lagrangian

$$\mathcal{L} = \frac{1}{2}\dot{\phi}^2 - \frac{1}{2}(\nabla\phi)^2 - V(\phi) \tag{2.14}$$

with an asymmetric double well potential

$$V(\phi) = \frac{1}{4}g(\phi^2 - c^2)^2 - B(\phi + c) \tag{2.15}$$

with B a small symmetry-breaking parameter. The potential at the false vacuum at $\phi = -c$ is zero, while the potential at the true vacuum at $\phi = +c$ is $-\epsilon \approx -2Bc$ as shown in Figure 2.2. The energy density difference between the two minima,

namely ϵ, is assumed to be small so that we may confine our analysis of this potential to the thin-wall regime. In the under-barrier (i.e., classically forbidden) region, one starts with the Euclidean action $S_E(\phi(\tau, \mathbf{x}))$ where τ is the Euclidean time. Solving the resulting Euclidean equation of motion for ϕ (with appropriate boundary conditions) and substituting it back into $S_E(\phi(\tau, \mathbf{x}))$ yields S_E. In the semi-classical limit [15] showed that the tunneling rate per unit volume is

$$\Gamma/V = A \exp(-S_E/\hbar) \ , \tag{2.16}$$

where the subexponential prefactor A studied in [16] will be unimportant for our purposes. The solution $\phi(\tau, \mathbf{x}, R)$ to the Euclidean equation of motion is the familiar $O(4)$-symmetric domain-wall solution

$$\phi_{DW}(\tau, \mathbf{x}, R) = -c \tanh\left(\frac{\mu}{2}(r - R)\right) , \tag{2.17}$$

where μ measures the (inverse) thickness of the domain wall,

$$\mu = \sqrt{2gc^2} \tag{2.18}$$

so a relatively large μ (i.e., thin wall) is assumed. Here

$$r^2 = |\mathbf{x}|^2 + \tau^2, \tag{2.19}$$

and R is the radius of the bubble. The bubble wall sits at $r = R$, so $\phi = +c$ for $r \ll R$ and $\phi = -c$ for $r \gg R$. That is, the bubble is surrounded by the false vacuum. It is useful to introduce the tension σ of the domain wall,

$$\sigma = \int_{-c}^{c} d\phi \sqrt{2V(\phi)} \approx \int_{-c}^{c} d\phi \sqrt{\frac{g}{2}(\phi^2 - c^2)^2} = \frac{2}{3}\mu c^2 \tag{2.20}$$

so the Euclidean action of this solution is now given by

$$S_E = -\frac{1}{2}\pi^2 R^4 \epsilon + 2\pi^2 R^3 \sigma \ . \tag{2.21}$$

where the first term is the four-volume times the energy density difference ϵ while the second term is the contribution of the domain wall. Setting the variation of this S_E to zero yields

$$\mathcal{E} = -\frac{4}{3}\pi R^3 \epsilon + 4\pi R^2 \sigma = 0 \ . \tag{2.22}$$

So the action is stationary for

$$R = \lambda_c = 3\sigma/\epsilon, \tag{2.23}$$

which gives us

$$S_E = \frac{\pi^2}{2}\sigma\lambda_c^3 = \frac{27\pi^2}{2}\frac{\sigma^4}{\epsilon^3} \tag{2.24}$$

What happens to the bubble after nucleation? The bubble will behave in a way to decrease the energy $\mathcal{E}$, i.e., $d\mathcal{E}/dR < 0$. It is easy to see that the bubble prefers to grow (classically) as long as

$$R > 2\lambda_c/3 \tag{2.25}$$

which is the case here. So, once the bubble is created with radius λ_c, the domain wall starts at rest and moves (classically) outwards, eventually attaining relativistic speed. Notice that the condition (2.22) is simply the classical energy conservation equation: at the moment right after bubble nucleation, the total energy $\mathcal{E}$ of the bubble and its interior equals to that of the original false vacuum in the region, which is zero.

2.4 Functional Schrödinger Method

Now let us introduce the functional Schrödinger method and apply it to the single barrier tunneling process discussed above in the same scalar QFT. In the semi-classical regime, a discrete set of classical paths, namely the most probable

escape paths (MPEP) in configuration space give the dominant contributions to the vacuum tunneling rate [24, 22, 23]. Essentially this approximation allows us to reduce an infinite-dimensional quantum field theory calculation to a one-dimensional quantum mechanical computation. The effects of nearby paths can be included systematically in an $\hbar$ expansion, and were calculated to $O(\hbar^2)$ in [22, 23], but will not be relevant for the rest of our analysis.

The Hamiltonian for a scalar field $\phi(t, \mathbf{x})$ where $\mathbf{x}$ denotes the three spatial directions is

$$H = \int d^3\mathbf{x}\left(\frac{\dot{\phi}^2}{2} + \frac{1}{2}(\nabla\phi)^2 + V(\phi)\right). \tag{2.26}$$

where $V(\phi)$ is that given in (2.15). To quantize the field theory we use $[\dot{\phi}(\mathbf{x}), \phi(\mathbf{x}')] = i\hbar\delta^3(\mathbf{x} - \mathbf{x}')$ to replace $\dot{\phi}$ with $-i\hbar\delta/\delta\phi$. This replacement allows us to write the time-independent functional Schrödinger equation as

$$H\Psi(\phi(\mathbf{x})) = E\Psi(\phi(\mathbf{x})) \tag{2.27}$$

where

$$H = \int d^3\mathbf{x}\left(-\frac{\hbar^2}{2}\left(\frac{\delta}{\delta\phi(\mathbf{x})}\right)^2 + \frac{1}{2}(\nabla\phi)^2 + V(\phi)\right), \tag{2.28}$$

and the eigenvalue E is the energy of the system. As usual $\Psi(\phi(\mathbf{x}))$ is the amplitude that gives a measure of the likelihood of the occurrence of the field configuration $\phi(\mathbf{x})$.

With the ansatz $\Psi(\phi) = A\exp(-\frac{i}{\hbar}S(\phi))$ where A is constant, the functional Schrödinger equation (2.27) becomes

$$\int d^3\mathbf{x}\left(-\frac{\hbar^2}{2}\left[\frac{i}{\hbar}\frac{\delta^2 S(\phi)}{\delta\phi^2} - \frac{1}{\hbar^2}\left(\frac{\delta S(\phi)}{\delta\phi}\right)^2\right] + \frac{1}{2}(\nabla\phi)^2 + V(\phi)\right)e^{\frac{i}{\hbar}S(\phi)} = Ee^{\frac{i}{\hbar}S(\phi)}. \tag{2.29}$$

Expanding $S(\phi)$ in powers of $\hbar$, $S(\phi) = S_{(0)}(\phi) + \hbar S_{(1)}(\phi) + ...$, and comparing terms with equal powers of $\hbar$ the functional Schrödinger equation (2.29) yields

$$\int d^3\mathbf{x}\left[\frac{1}{2}\left(\frac{\delta S_{(0)}(\phi)}{\delta\phi}\right)^2 + \frac{1}{2}(\nabla\phi)^2 + V(\phi)\right] = E, \tag{2.30}$$

$$\int d^3\mathbf{x}\left[-i\frac{\delta^2 S_{(0)}(\phi)}{\delta\phi^2}+2\frac{\delta S_{(0)}(\phi)}{\delta\phi}\frac{\delta S_{(1)}(\phi)}{\delta\phi}\right]=0,$$

$$etc.$$

The infinite set of nonlinear equations (2.30) on an infinite-dimensional configuration space can be reduced to a one-dimensional equation in the leading approximation. For our purpose here, we shall focus on $S_{(0)}$ and ignore the higher-order corrections $S_{(1)}$, $S_{(2)}$, etc. The essential idea is that there is a trajectory in the configuration space of $\phi(\mathbf{x})$, known as the most probable escape path (MPEP), perpendicular to which the variation of $S_{(0)}$ vanishes, and along which the variation of $S_{(0)}$ is nonvanishing. We use λ to parametrize this path in the configuration space of $\phi(x)$, so the MPEP is $\phi(\mathbf{x},\lambda)$. This MPEP satisfies

$$\begin{aligned}\frac{\delta S_{(0)}}{\delta\phi_{\parallel}}\mid_{\phi_0(\mathbf{x},\lambda)} &= C(\lambda)\frac{\partial\phi_0}{\partial\lambda},\\ \frac{\delta S_{(0)}}{\delta\phi_{\perp}}\mid_{\phi_0(\mathbf{x},\lambda)} &= 0\ .\end{aligned}\tag{2.31}$$

Along the MPEP, we have

$$\frac{\partial S_{(0)}}{\partial\lambda}=\int d^3\mathbf{x}\frac{\partial\phi_0(\mathbf{x},\lambda)}{\partial\lambda}\frac{\delta S_{(0)}}{\delta\phi_{\parallel}}\mid_{\phi_0(\mathbf{x},\lambda)}\tag{2.32}$$

so $C(\lambda)$ is determined and we have

$$\frac{\delta S_{(0)}}{\delta\phi_{\parallel}}\mid_{\phi_0(\mathbf{x},\lambda)}=\frac{\partial S_{(0)}}{\partial\lambda}\left(\int d^3\mathbf{x}\left[\frac{\partial\phi_0(\mathbf{x},\lambda)}{\partial\lambda}\right]^2\right)^{-1}\frac{\partial\phi_0(\mathbf{x},\lambda)}{\partial\lambda},\tag{2.33}$$

We now define the effective potential $U(\lambda)=U(\phi(\mathbf{x},\lambda))$, so

$$U(\phi(\mathbf{x},\lambda))=\int d^3\mathbf{x}\left(\frac{1}{2}(\nabla\phi(\mathbf{x},\lambda))^2+V(\phi(\mathbf{x},\lambda))\right)\ ,\tag{2.34}$$

then the classically allowed regions have $U(\phi_0(\mathbf{x},\lambda))<E$ and the classically forbidden regions have $U(\phi_0(\mathbf{x},\lambda))>E$.

Using the zeroth-order equation in (2.30) with (2.33) we find the WKB equation

$$-\frac{1}{2}\left(\int d^3\mathbf{x}\left[\frac{\partial\phi_0}{\partial\lambda}\right]^2\right)^{-1}\left(\frac{\partial S_{(0)}}{\partial\lambda}\right)^2=U(\phi(\mathbf{x},\lambda))-E\ .\tag{2.35}$$

To find the WKB wavefunctional it is sometimes useful to rewrite (2.35) in terms of the path length ds in the configuration space. This path length is defined by

$$(ds)^2 = \int d^3\mathbf{x}(d\phi(\mathbf{x}))^2 = (d\lambda)^2 \int d^3\mathbf{x}\left(\frac{\partial\phi(\mathbf{x},\lambda)}{\partial\lambda}\right)^2 = (d\lambda)^2 m(\phi(\mathbf{x},\lambda)) \ . \tag{2.36}$$

That is, choosing s to parametrize the MPEP, (2.35) simplifies to

$$-\frac{1}{2}\left(\frac{\partial S_{(0)}}{\partial s}\right)^2 = U(\phi(\mathbf{x},s)) - E \ . \tag{2.37}$$

Now let us consider first the classically forbidden region, $U(\phi(\mathbf{x},s)) > E$. The solution to (2.37) is

$$S_{(0)} = i\int_0^s ds' \sqrt{2[U(\phi(\mathbf{x},s')) - E]} = i\int_{\lambda_{t1}}^{\lambda_{t2}} d\lambda\left(\frac{ds}{d\lambda}\right)\sqrt{2[U(\phi(\mathbf{x},\lambda)) - E]} \ . \tag{2.38}$$

where λ_{t1} and λ_{t2} are the turning points. Treating both $\frac{ds}{d\lambda}(\phi(\mathbf{x},\lambda))$ (2.36) and $U(\phi(\mathbf{x},\lambda))$ (2.34) as functionals of ϕ, the Euler-Lagrange equation for $\phi(\mathbf{x},\lambda)$ follows from setting the variation of $S_{(0)}$ to zero. It turns out that the resulting equation of motion derived from (2.38) simplifies considerably if we choose τ as the parameter where

$$\frac{ds}{d\tau} = \sqrt{2[U(\phi(\mathbf{x},\tau)) - E]} \ . \tag{2.39}$$

With τ as the parameter, setting the variation of (2.38) equal to zero now yields

$$\frac{\partial^2\phi(\mathbf{x},\tau)}{\partial\tau^2} + \nabla^2\phi(\mathbf{x},\tau) - \frac{\partial V(\phi(\mathbf{x},\tau))}{\partial\phi} = 0 \tag{2.40}$$

Here τ simply plays the role of Euclidean time, and (2.40) is simply the Euclidean equation of motion for $\phi(\mathbf{x},\tau)$. Once we obtain the solution for $\phi(\mathbf{x},\tau)$, we insert this solution into (2.38) to obtain the value S_0 for $S_{(0)}$. So we see that the functional Schrödinger method leads both to a determination of S_0 along the MPEP and an equation that determines MPEP, namely, $\phi_0(\mathbf{x},\tau)$ itself. The subscript "0" indicates that it is the MPEP in the leading WKB approximation.

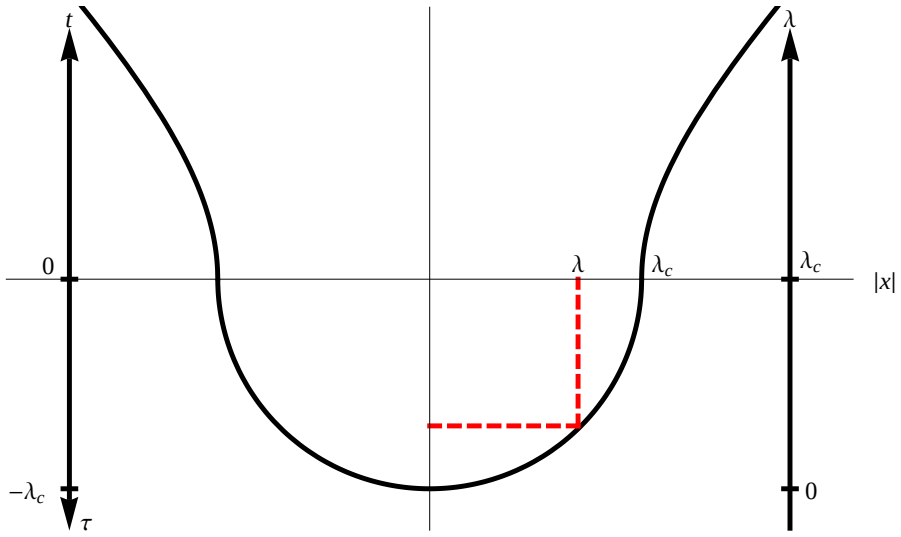

Figure 2.3: Spatial slices of the familiar domain-wall solution (2.43) can be parameterized by the spatial radius of the bubble of true vacuum, λ. Here λ is the length of the horizontal dashed line. The radius λ_c of the (bottom half) bubble is related to the Euclidean time τ via $\lambda_c^2 = \tau^2 + \lambda^2$. The choice of the λ parameter allows us to go smoothly from the classically forbidden region (below the x-axis) to the classically allowed region (above the x-axis).

The equation (2.40) has $O(4)$ symmetry, so it reproduces the familiar $O(4)$ symmetric domain-wall solution (2.17) in the thin-wall approximation (r is the four-dimensional radial coordinate, $r^2 = \tau^2 + |\mathbf{x}|^2$),

$$\phi_0(\mathbf{x}, \tau) = -c \tanh\left(\frac{\mu}{2}(r - \lambda_c)\right) \tag{2.41}$$

after imposing the boundary conditions, $\phi \to -c$ as $r \to \infty$ and $\phi \to +c$ as $r \to 0$ and $\frac{d\phi(0)}{dr} = 0$. Recall that λ_c is the critical radius of the bubble given by (2.23).

For our purpose, it is now convenient to introduce the parameter λ

$$\lambda = \sqrt{\lambda_c^2 - \tau^2} \tag{2.42}$$

which is the spatial radius of the bubble as shown in Figure 2.3. Here $\phi_0(\mathbf{x}, \lambda) = 0$ for $\lambda < 0$. For $\lambda_c > \lambda > 0$ and near the domain wall at $r = \sqrt{|\mathbf{x}|^2 + \tau^2}$, we

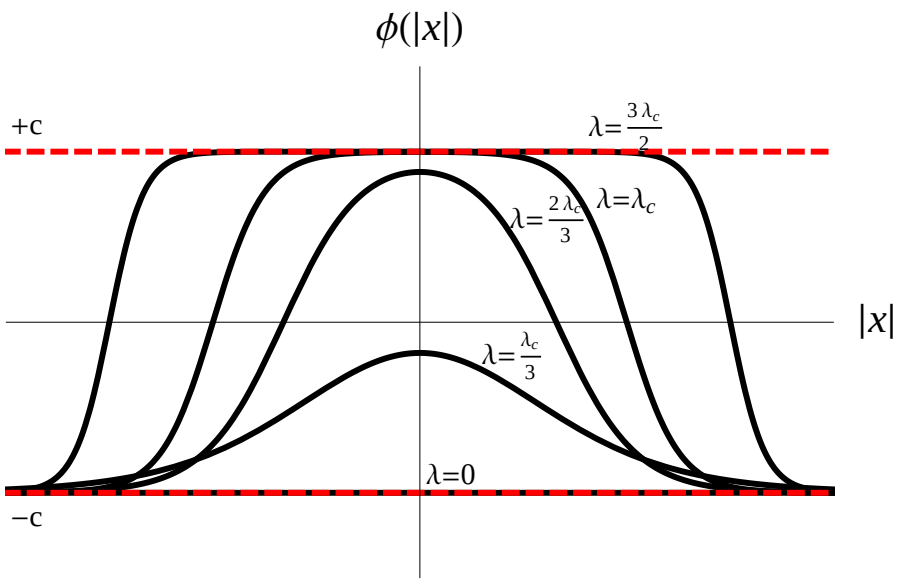

Figure 2.4: The MPEP is a path through field configuration space parameterized by λ. Here, x is the spatial radius, $\phi = -c$ is the false vacuum and $\phi = +c$ is the true vacuum. For the MPEP given by (2.43): $\lambda \leq 0$ corresponds to the false vacuum, $\lambda_c \geq \lambda > 0$ corresponds to the formation of the nucleation bubble during the tunneling process, $\lambda = \lambda_c$ corresponds to the completion of the nucleation of the bubble of true vacuum, and $\lambda \geq \lambda_c$ corresponds to the classical growth of the bubble.

have $r - \lambda_c \approx (|\mathbf{x}|^2 - \lambda^2)/(2\lambda_c) \approx (|\mathbf{x}| - \lambda)\lambda/\lambda_c$. The corrections introduced by this approximation are exponentially suppressed far from the domain wall, so we can express the $O(4)$ symmetric solution (2.41) as,

$$\phi_0(\mathbf{x}, \lambda) \approx -c \tanh\left(\frac{\mu}{2}(|\mathbf{x}| - \lambda)\frac{\lambda}{\lambda_c}\right), \tag{2.43}$$

This MPEP solution is plotted in Figure 2.4. (Slight care is needed for $\lambda \approx 0$, in which case, we simply go back to (2.41).) For $\lambda < 0$ the solution is the false vacuum $\phi_0(\mathbf{x}, \lambda) = -c$. As $\lambda > 0$ increases, quantum fluctuation tends to fluctuate towards the true vacuum. At $\lambda = \lambda_c$, the bubble is created, which then evolves classically for $\lambda > \lambda_c$.

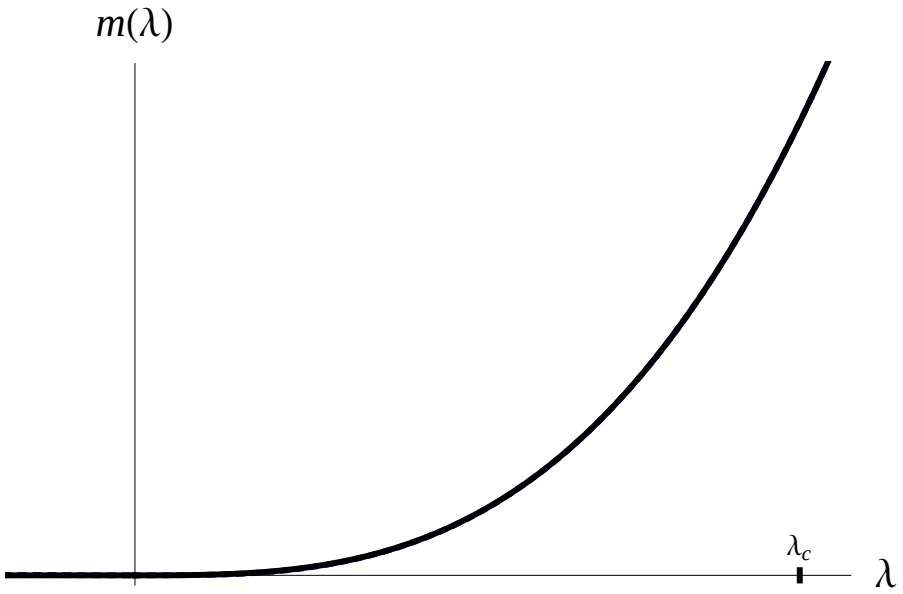

Figure 2.5: The position-dependent mass $m(\lambda)$ for $g = 1$, $c = 1.5$, and $B = 0.1$. The exact curve is indistinguishable from the approximate curve (2.45) in this plot.

We have effectively reduced the WKB wavefunctional in the classically forbidden region to a WKB wavefunction which can be written using (2.38) as

$$\Psi(\phi(\mathbf{x},\lambda)) = Ae^{iS_0/\hbar} = A\exp\left(-\frac{1}{\hbar}\left[\int_0^{\lambda_c} d\lambda\,\sqrt{2m(\lambda)[U(\lambda)-E]}\right]\right)\,, \tag{2.44}$$

where $m(\lambda)$ is obtained by substituting the MPEP $\phi_0(\mathbf{x},\lambda)$ (2.43) into $m(\phi(\mathbf{x},\lambda))$,

$$m(\lambda) \equiv \int d^3x\left(\frac{\partial\phi_0(\mathbf{x},\lambda)}{\partial\lambda}\right)^2 \approx 4\pi\sigma\frac{\lambda^3}{\lambda_c} \tag{2.45}$$

Here $m(\lambda)$ is the effective mass, which is manifestly positive, and the second equality is obtained in the thin-wall approximation.

This wavefunction (2.44) is the solution to the one-dimensional time-independent Schrödinger equation:

$$\left(-\frac{\hbar^2}{2}\frac{d^2}{d\lambda^2} + m(\lambda)U(\lambda)\right)\Psi_0(\lambda) = 0 \tag{2.46}$$

Given $V(\lambda) = m(\lambda)U(\lambda)$, Eq.(2.46) can be readily solved.

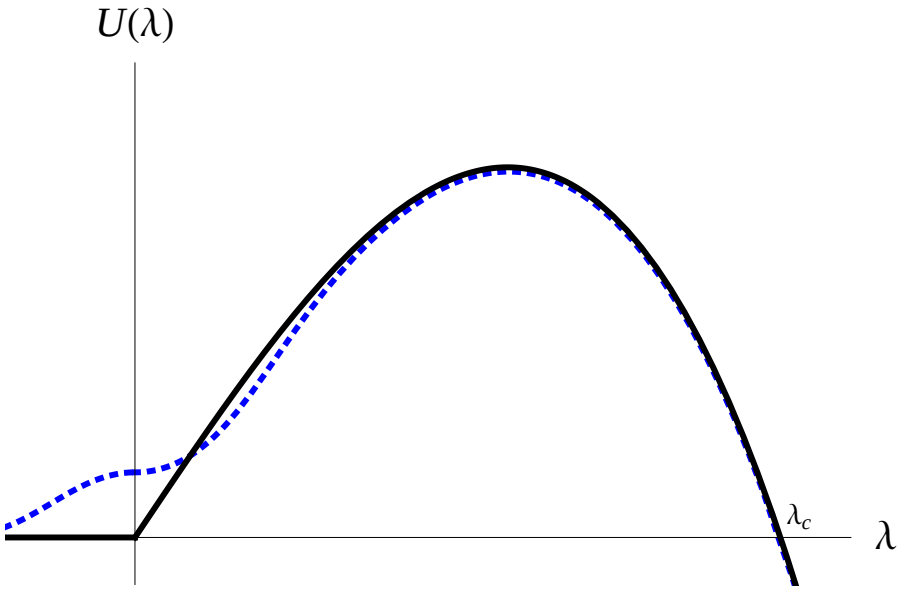

Figure 2.6: The effective tunneling potential $U(\lambda)$ for $g = 1$, $c = 1.5$, and $B = 0.1$. The black solid curve shows the approximate form of $U(\lambda)$ given in (2.47). The blue dotted curve shows the numerical result. The difference is not important for our analysis.

It is also straightforward to evaluate $U(\lambda)$ by substituting MPEP $\phi_0(\mathbf{x}, \lambda)$ (2.43) into $U(\phi(\mathbf{x}, \lambda))$ (2.34),

$$U(\lambda) \approx \frac{2\pi\sigma}{\lambda_c}\lambda(\lambda_c^2 - \lambda^2) \tag{2.47}$$

This approximation for $U(\lambda)$ is plotted in Figure 2.6. The classically forbidden region for zero-energy tunneling is $0 < \lambda < \lambda_c$. As mentioned above, $\phi_0(\mathbf{x}, \lambda)$ (2.43) needs correction for $\lambda \sim 0$. The more accurate $U(\lambda)$ (the blue dotted curve) is also shown in Figure 2.6. However, this difference is not important for our analysis here.

Given $m(\lambda)$ (2.45) and $U(\lambda)$ (2.47), the tunneling problem in QFT has been reduced to a one-dimensional time-independent QM problem. We can now perform the integral in the exponent in (2.44) and obtain, for $E = 0$,

$$-iS_0 = \frac{27\pi^2}{4}\frac{\sigma^4}{\epsilon^3} = S_E/2 \tag{2.48}$$

which reproduces (2.24). (The factor of two difference is because, here, we are evaluating the exponent of the tunneling amplitude instead of the tunneling rate.) This result is completely expected since the expression (2.24) is obtained by integrating the Langrangian density with the $O(4)$ symmetric solution (2.41) or (2.17) in polar coordinates while here we are performing the same integral, first in the spatial coordinates x and then in the λ (or equivalently in τ) coordinate. For an $O(4)$ symmetric solution, the latter approach is unnecessarily cumbersome.

So, before moving on, let us give a preview of the advantage of the functional Schrödinger method. This will also shed light on the underlying physics. In the classically allowed regions, similar arguments lead to the following $S_{(0)}$,

$$S_{(0)}(\phi(\mathbf{x},\lambda)) = \int d\lambda \sqrt{2m(\phi(\mathbf{x},\lambda))[E - U(\phi(\mathbf{x},\lambda))]} \tag{2.49}$$

Similar to the previous case, the Euler-Lagrange equation of motion for ϕ simplifies if we choose the parameter t such that

$$\frac{ds}{dt} = \sqrt{2[E - U(\phi(\mathbf{x},t))]} \ . \tag{2.50}$$

so setting the variation of $S_{(0)}$ with respect to $\phi(\mathbf{x},t)$ to zero leads to

$$\frac{\partial^2\phi(\mathbf{x},t)}{\partial t^2} - \nabla^2\phi(\mathbf{x},t) + \frac{\partial V(\phi(\mathbf{x},t))}{\partial\phi} = 0 \ , \tag{2.51}$$

where t is simply the normal time, and this is simply the equation of motion for $\phi(\mathbf{x},t)$ in Minkowski space, $t \geq 0$. Now, instead of t, let us choose λ as the parameter, where

$$\lambda = \sqrt{\lambda_c^2 + t^2} \tag{2.52}$$

which gives us ($\dot{\lambda} = d\lambda/dt$),

$$\frac{\lambda}{\lambda_c} = \frac{1}{\sqrt{1 - \dot{\lambda}^2}} \tag{2.53}$$

which is simply the Lorentz factor. Substituting this into the path (2.43), we obtain, for $\lambda > \lambda_c$,

$$\phi_0(\mathbf{x}, \lambda) = -c \tanh\left(\frac{\mu}{2}(|\mathbf{x}| - \lambda)\frac{\lambda}{\lambda_c}\right) = -c \tanh\left(\frac{\mu}{2}\frac{(|\mathbf{x}| - \lambda)}{\sqrt{1 - \dot{\lambda}^2}}\right), \tag{2.54}$$

so the classical path $\phi_0(\mathbf{x}, \lambda)$ now describes an expanding nucleation bubble, as its physical radius λ increases towards the limiting speed $\dot{\lambda} = 1$, with the proper Lorentz factor automatically included, and the effective tension now given by $\sigma/\sqrt{1 - \dot{\lambda}^2}$.

So we see that $\phi_0(\mathbf{x}, \lambda)$ for real λ spanning $\infty > \lambda > -\infty$ works equally well for classically allowed as well as classically forbidden regions. In summary, $\phi_0(\mathbf{x}, \lambda) = -c$ for $\lambda < 0$, when ϕ stays in the false vacuum. For $\lambda_c \geq \lambda > 0$, $\phi_0(\mathbf{x}, \lambda)$ describes the "averaged" quantum fluctuation that corresponds to the MPEP for the tunneling process under the potential barrier. The $|\mathbf{x}| < \lambda$ region has fluctuated to the true vacuum, which is separated from the false vacuum region by a domain wall at $|\mathbf{x}| = \lambda$. Finally, for $\lambda \geq \lambda_c$, $\phi_0(\mathbf{x}, \lambda)$ describes the classical propagation of the nucleation bubble. The advantage here is that a single real parameter describes the whole system. The problem has been reduced to that of a time-independent one-dimensional (i.e., the λ coordinate here) quantum mechanical system of a particle with position-dependent mass $m(\lambda)$ (2.45) and a potential $U(\lambda)$ (2.34) which has a barrier ($\lambda_c \geq \lambda > 0$) that separates the two classically allowed regions. In general, the position-dependent mass complicates the quantization of the position variable. However, at leading order in the WKB approximation, such a complication does not arise.

2.5 Resonant Tunneling in Scalar Quantum Field Theory

The above discussion introduces the functional Schrödinger method and its applications to the tunneling process at leading order in $\hbar$. It reduces the tunneling process in an infinite-dimensional field configuration space to a one-dimensional quantum mechanical tunneling problem. The essential difference between tunneling in field theory discussed in Section 2.4 and in quantum mechanics discussed in Section 2.2 is that in field theory one should first find the MPEP, namely $\phi_0(\mathbf{x}, \lambda)$, and then obtain the effective potential $U(\lambda)$ (2.34) and the effective mass $m(\lambda)$ (2.45). We have extended the MPEP to include regions where classical motion is allowed.

2.5.1 Setup

To examine resonant tunneling in QFT, let us consider the following potential shown in Figure 2.7,

$$V(\phi) = \begin{cases} \frac{1}{4}g_1((\phi + c_1)^2 - c_1^2)^2 - B_1\phi - 2B_1c_1 & \phi < 0 \\ \frac{1}{4}g_2((\phi - c_2)^2 - c_2^2)^2 - B_2\phi - 2B_1c_1 & \phi > 0 \end{cases} \tag{2.55}$$

where as before B_1 and B_2 are small. For this potential the false vacuum (vacuum A) at $\phi \approx -2c_1$ has zero energy density, the intermediate vacuum (vacuum A') at $\phi = 0$ has an energy density $-\epsilon_1 = -2B_1c_1$ and the true vacuum (vacuum B) at $\phi \approx 2c_2$ has an energy density $-\epsilon_1 - \epsilon_2 = -2B_1c_1 - 2B_2c_2$. We take both ϵ_1 and ϵ_2 to be small so that the thin-wall approximation is valid. Similar to the single barrier case, we introduce the inverse thickness $\mu_j = \sqrt{2g_jc_j^2}$ and the tension $\sigma^{(j)} = \frac{2}{3}\mu_jc_j$ for each of the two domain walls: $j = 1$ for the outside bubble and $j = 2$ for the inside bubble. Here $r_1 > r_2$. In the thin-wall approximation,

$\phi = -2c_1$ for $r \gg r_1$, $\phi = 0$ for $r_1 \gg r \gg r_2$, and $\phi = +2c_2$ for $r \ll r_2$. The six parameters of the potential $g_{1,2}$, $c_{1,2}$ and $B_{1,2}$ now become $\mu_{1,2}$, $\sigma_{1,2}$ and $\epsilon_{1,2}$. In the thin-wall approximation, the thicknesses $1/\mu_{1,2}$ of the domain walls drop out, simplifying the discussion.

We also assume that the $O(4)$-symmetric solution provides the dominant contribution to the vacuum decay rate. We note that the inside (half-)bubble does not have to be concentric with the outside (half-)bubble as long as the centers of the two bubbles lie on the same spatial slice. As we shall see, the analysis will go through without change as long as the two bubble walls are separated far enough, that is, much more than the combined thicknesses $1/\mu_1 + 1/\mu_2$. We expect the off-center bubble configurations to be subdominant if we include corrections to the thin-wall approximation. We focus here on the zero-energy (i.e., $E = 0$) case.

2.5.2 Ansatz

The MPEP involves ϕ in the two under-the-barrier regions as well as the classically allowed region between them. In the under-the-barrier regions, we can solve for $\phi(\mathbf{x}, \tau)$ using the Euclidean equation of motion (2.40), while in the classically allowed region, we can solve for $\phi(\mathbf{x}, t)$ using the equation of motion in Minkowski space (2.51). We can then convert them to $\phi_0(\mathbf{x}, \lambda)$.

However, in the thin-wall approximation, it is easier to simply write down the ansatz in the radial coordinate and then extract $\phi(\mathbf{x}, \lambda)$ from it. Here the tunneling process involves two concentric bubbles: an outside bubble whose domain wall separates A (outside) from A' and an inside bubble whose domain

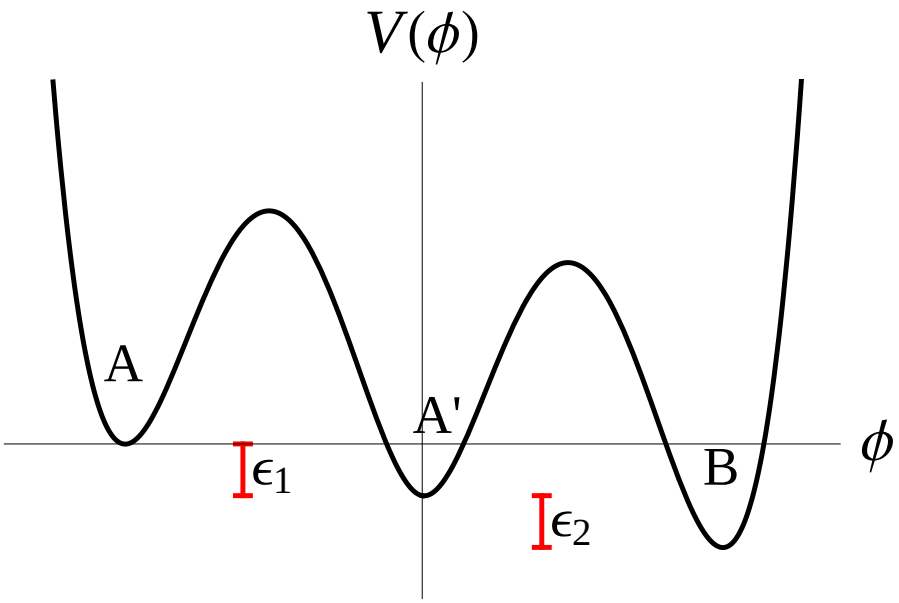

Figure 2.7: The potential $V(\phi)$ in (2.55). The vacuum A is at $\phi_A = -2c_1$, with $V(\phi_A) = 0$, the vacuum A' is at $\phi'_A = 0$, with $V(\phi'_A) = -\epsilon_1$, and the vacuum B is at $\phi_B = 2c_2$, with $V(\phi_B) = -\epsilon_1 - \epsilon_2$.

wall separates A' from B (inside). The radii of the two bubbles are r_1 and r_2 as shown in Figure 2.8. As a function of the four-dimensional radial coordinate r, we have the MPEP,

$$\phi(r) = -c_1 \tanh\left(\frac{\mu_1}{2}(r - r_1)\right) - c_2 \tanh\left(\frac{\mu_2}{2}(r - r_2)\right) + c_2 - c_1 \tag{2.56}$$

For appropriate r_1 and r_2, this solves the Euclidean equation of motion (2.40) (and the Lorentzian equation of motion (2.51) in the appropriate regions). However, here we shall use this ϕ (2.56) as an ansatz to find the resonant tunneling condition.

Now it is straightforward to extract $\phi(|\mathbf{x}|, \lambda)$ from $\phi(r)$ given by (2.56),

$$\phi_0(|\mathbf{x}|, \lambda) = -c_1 \tanh\left(\frac{\mu_1}{2}\frac{\lambda}{r_1}(|\mathbf{x}| - \lambda)\right) - c_2 \tanh\left(\frac{\mu_2}{2}\frac{\lambda'}{r_2}(|\mathbf{x}| - \lambda')\right) + c_2 - c_1 \tag{2.57}$$

where we use the same reparametrization as in the single-barrier case. Here Λ

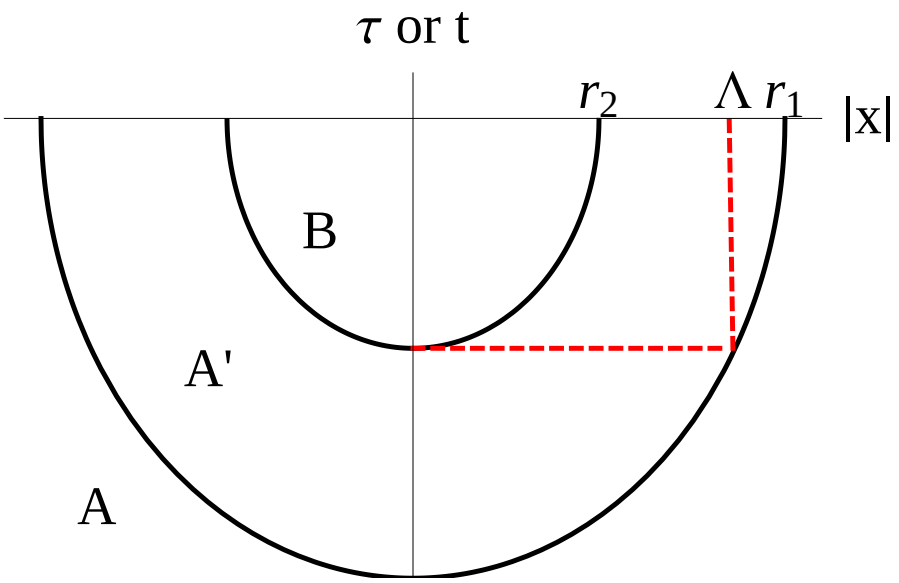

Figure 2.8: The tunneling process from A to B via A' leads to the formation of two bubbles: the outside bubble separates A' from A and the inside bubble separates B from A'. They are drawn as concentric bubbles here, though this is not the case in general as the inside bubble can shift sideways. Here Λ is the length of the horizontal dashed (red) line. We have $r_1 > \Lambda > r_2$.

is the value of λ at which the inside bubble has zero spatial extent,

$$\Lambda^2 = r_1^2 - r_2^2 \tag{2.58}$$

and as long as both bubbles are expanding

$$\lambda' = \begin{cases} \sqrt{\lambda^2 - \Lambda^2} & \Lambda < \lambda \\ 0 & \text{otherwise.} \end{cases} \tag{2.59}$$

This is shown in Figure 2.8. The equation (2.57) also implies that $\phi_0(|\mathbf{x}|, \lambda) = -2c_1$ for $\lambda < 0$. Note also that the sum of the second and third terms in (2.57) vanishes for $\lambda < \Lambda$. Substituting this MPEP $\phi_0(|\mathbf{x}|, \lambda)$ given by (2.57) into (2.34) now yields, after a straightforward calculation, the effective tunneling potential $U(\lambda) = U(\phi_0(|\mathbf{x}|, \lambda))$,

$$U(\lambda) = 2\pi\sigma_1\left(\frac{\lambda}{r_1} + \frac{r_1}{\lambda}\right)\lambda^2 - \frac{4\pi}{3}\epsilon_1\lambda^3 + 2\pi\sigma_2\left(\frac{\lambda'}{r_2} + \frac{r_2}{\lambda'}\right)(\lambda')^2 - \frac{4\pi}{3}\epsilon_2(\lambda')^3 \tag{2.60}$$

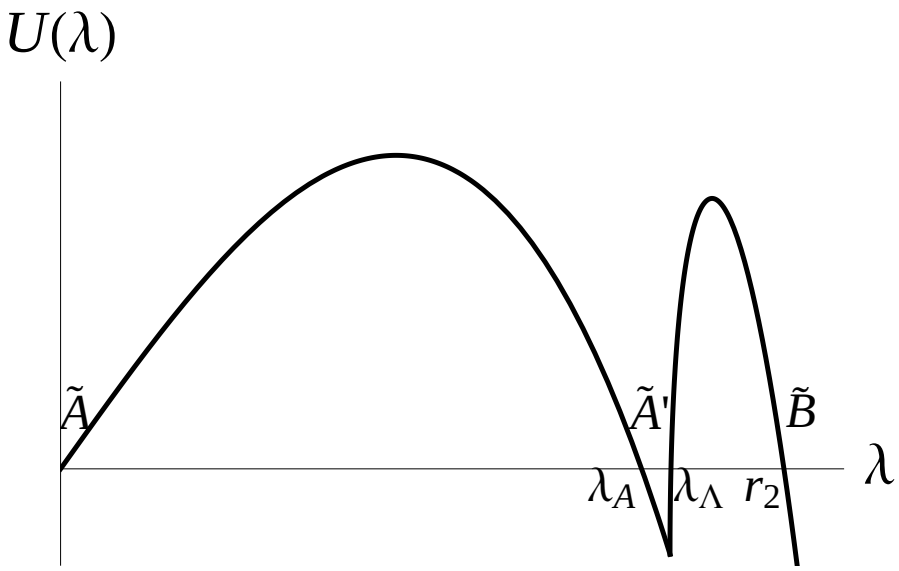

Figure 2.9: A typical effective tunneling potential $U(\lambda)$ (2.60) for double tunneling. The classical turning points for zero-energy tunneling are 0, λ_A, λ_Λ, and r_1. The discontinuity in the derivative of $U(\lambda)$ occurs at $\lambda = \Lambda$. If the negative part of $U(\lambda)$ (i.e., the classically allowed region) is not too deep, $\lambda_A \gtrsim \lambda_{1c} = 3\sigma_1/\epsilon_1$, and $\lambda_\Lambda \gtrsim \Lambda$. In appropriate units, the values plotted here are $\sigma_1 = 1$, $\sigma^2 = 1.4$, $\epsilon_1 = 0.25$, $\epsilon_2 = 8.4 \cdot 10^{-3}$, $r_2 = 14$ which gives $r_1 = 20$ and $\Lambda = 14.3$ using (2.58) and (2.63).

For appropriate parameter choices, we see that (2.60) has four zeros as shown in Figure 2.9. If the negative part of $U(\lambda)$ (i.e., the classically allowed region) is not too deep, $\lambda_\Lambda \gtrsim \Lambda$, and $\lambda_A \gtrsim \lambda_{1c} = 3\sigma_1/\epsilon_1$. We may take $U(\lambda) = 0$ for $\lambda < 0$. The discontinuity in the derivative of $U(\lambda)$ at Λ will be smoothed when the thickness of the bubble wall is taken into account.

It is also straightforward to evaluate the effective mass $m(\lambda)$ defined by (2.45) using $\phi_0(|\mathbf{x}|, \lambda)$ of (2.57), now given by

$$m(\lambda) = 4\pi\left(\frac{\sigma_1}{r_1}\lambda^2 + \frac{\sigma_2\lambda}{r_2\lambda'}(\lambda')^2\right)\lambda \ . \tag{2.61}$$

Note that, as expected, $m(\lambda) > 0$. Now we have a time-independent one-dimensional (with λ as its coordinate) QM problem with the double-barrier po-

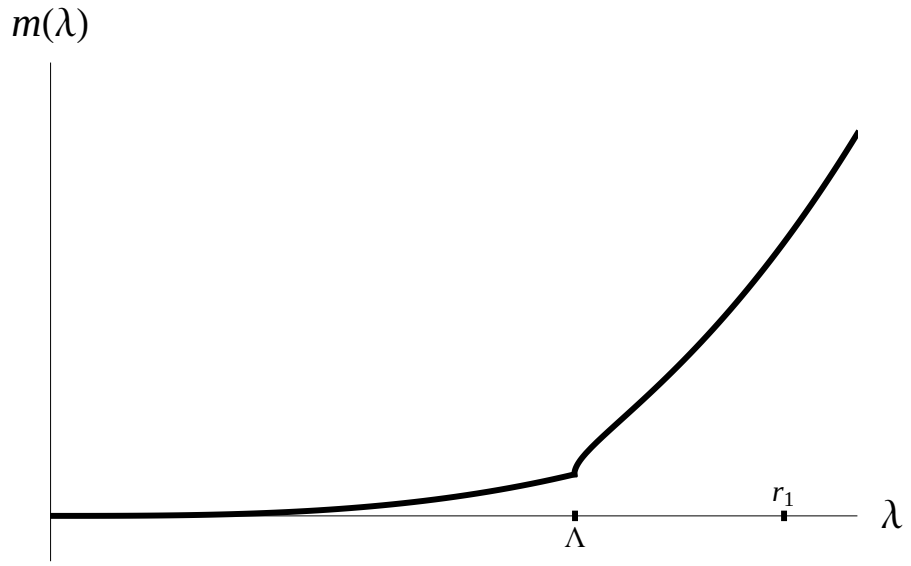

Figure 2.10: The position-dependent mass $m(\lambda)$ (2.61). In appropriate units, the values plotted here are $\sigma_1 = 1$, $\sigma_2 = 1.4$, $\epsilon_1 = 0.25$, $\epsilon_2 = 8.4 \cdot 10^{-3}$. The choice $r_2 = 14$ gives $r_1 = 20$ and $\Lambda = 14.3$ after solving the constraints (2.58) and (2.63).

tential $U(\lambda)$ (2.60) and mass $m(\lambda)$ (2.61), which is illustrated in Figure 2.10.

2.5.3 Constraints

We see that the existence of the classically allowed region $\tilde{A}'$ in $U(\lambda)$ will lead to resonant tunneling. We would like to see what properties of potential $V(\phi)$ (2.55) will yield resonant tunneling. It is important to emphasize that the existence of the classically allowed region $\tilde{A}'$ is not guaranteed. For $E = 0$ the existence of a double-barrier $U(\lambda)$ potential requires four distinct classical turning points satisfying

$$0 = U(0) = U(\lambda_A) = U(\lambda_\Lambda) = U(r_1) \ . \tag{2.62}$$

The radii of the two bubbles at the moment of nucleation are related via (2.58). Instead of finding the S_E that includes multiple passes through B, we use the the functional Schrödinger method to reduce the problem to a one-dimensional time-independent QM problem, which is then readily solved for $S_{(0)}$.

Once the simultaneous nucleation of the two bubbles is completed and just before they start to evolve classically, we are at $\lambda = r_1$, where $U(r_1) = 0$, and energy conservation gives

$$\mathcal{E}_{(2)} = U(r_1) = 4\pi(\sigma_1 - \frac{1}{3}r_1\epsilon_1)r_1^2 + 4\pi(\sigma_2 - \frac{1}{3}r_2\epsilon_2)r_2^2 = 0 \tag{2.63}$$

For the single-bubble case, the corresponding energy conservation condition (2.22) is equivalent to the minimization of the action. For the double-bubble case, the total energy $\mathcal{E}_{(2)}$ of the two bubbles at the moment of creation (at $\lambda = r_1$) must vanish. If we treat the region between the bubbles classically during the nucleation process, then the energy of the inside bubble, that is, the second term in the above condition (2.63) must vanish by itself (following from the condition (2.22)), in which case the first term vanishes as well. That is, $r_1 = \lambda_{1c} = 3\sigma_1/\epsilon_1$ and $r_2 = \lambda_{2c} = 3\sigma_2/\epsilon_2$. However, it is crucial that the classically allowed region receives a full quantum treatment. So we must treat the simultaneous nucleation of the two bubbles quantum mechanically and demand only $\mathcal{E}_{(2)} = 0$.

This is illustrated in Figure 2.11. The determination of the various approximate Euclidean/Lorentzian regions is possible only after we determine the MPEP. *A priori*, it is difficult to determine the existence of the classically allowed region and evaluate the sum of the set of coherent Feynman paths before the problem is reduced to a "time"-independent one-dimensional QM problem. This is why the functional Schrödinger method is very useful here, since it completely avoids the introduction of either Euclidean time or real time into the

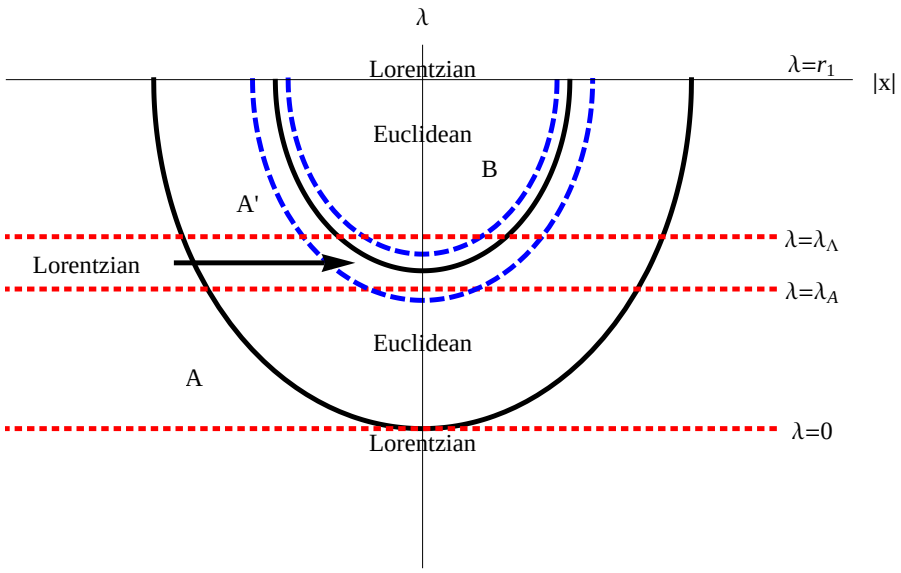

Figure 2.11: The various regions that can be described by Euclidean time or by Lorentzian time in the double bubble nucleation process. This figure corresponds to a case that permits resonant tunneling. The boundaries between these regions are the line $\lambda = r_1$, the outer bubble wall, and the region around the inner bubble wall enclosed by the two blue dashed lines. Of these boundaries, all but the line $\lambda = r_1$ are approximate. The actual (semi-circular) region of Lorentzian time description shrinks slightly as we approach $\lambda = r_1$. In the leading order approximation in the functional Schrödinger method, the boundaries between these regions are given by the red horizontal dotted lines and the line $\lambda = r_1$.

tunneling framework.

Note that the existence of a classically allowed region $\tilde{A}'$ implies that, $U(\lambda) < 0$ for $\Lambda > \lambda > \lambda_B$. Following (2.60), we obtain

$$\Lambda^2 > \lambda_A^2 = \frac{\lambda_{1c} r_1^2}{2r_1 - \lambda_{1c}} \tag{2.64}$$

from which it follows that ($\Lambda^2 = r_1^2 - r_2^2$)

$$\begin{aligned} r_1 &> r_2 \\ r_1 &> \lambda_A > \lambda_{1c} = 3\sigma_1/\epsilon_1 \end{aligned} \tag{2.65}$$

$$r_2 \quad < \quad \lambda_{2c} = 3\sigma_2/\epsilon_2 \ .$$

The existence of a second classically forbidden region requires $\lim_{\lambda \to r_1^-} dU/d\lambda|_\lambda < 0$ since $U(r_1) = 0$ is automatically satisfied. Equivalently

$$2(\sigma_1 + \sigma_2) < r_1\epsilon_1 + r_2\epsilon_2 \ . \tag{2.66}$$

The condition that at least one bubble must grow classically after nucleation is

$$\frac{\sigma_1}{r_1} + \frac{\sigma_2}{r_2} < \frac{2\epsilon_1}{3} + \frac{2\epsilon_2}{3} \ . \tag{2.67}$$

For some choices of σ_1, σ_2, ϵ_1, and ϵ_2, these conditions are incompatible and preclude any possibility of a resonance. In particular Eq.(2.64) and Eq.(2.67) rule out any possibility of a resonance effect for $\epsilon_1 < 0$ or $\epsilon_2 < 0$. These constraints are illustrated in Figure 2.12. We see that the simultaneous nucleation of two bubbles can now be parameterised by a single parameter, say r_2. When permitted, the sizes of the bubbles, namely r_1 and r_2, will be such that the resonance condition $W = (n + 1/2)\pi$ is satisfied.

The width of the classically allowed region $\Delta\lambda_{A'} \equiv \lambda_\Lambda - \lambda_A$ in $U(\lambda)$ decreases monotonically as r_2 increases. The classically allowed region is a point when $\Delta\lambda_{A'} = 0$ at some maximum value $r_{2,\max}$ of r_2 (when (2.64) is saturated). When $r_2 > r_{2,\max}$, there is no classically allowed region in $U(\lambda)$. Similarly the width of the second classically forbidden region $\Delta\lambda_{\text{barrier}} \equiv r_1 - \lambda_\Lambda$ increases monotonically as r_2 increases. At some minimum value $r_{2,\min}$ of r_2 (2.66) is saturated, and the second barrier in $U(\lambda)$ becomes a single point. The condition that $\Delta\lambda_{\text{barrier}} > 0$ is equivalent to the condition $\lim_{\lambda \to r_1^-} dU/d\lambda|_\lambda < 0$. Figure 2.13 shows a typical effective tunneling potential in each of these two cases.

After the simultaneous nucleation of the two bubbles quantum mechanically, the outside bubble will grow so the tunneling out of vacuum A will com-

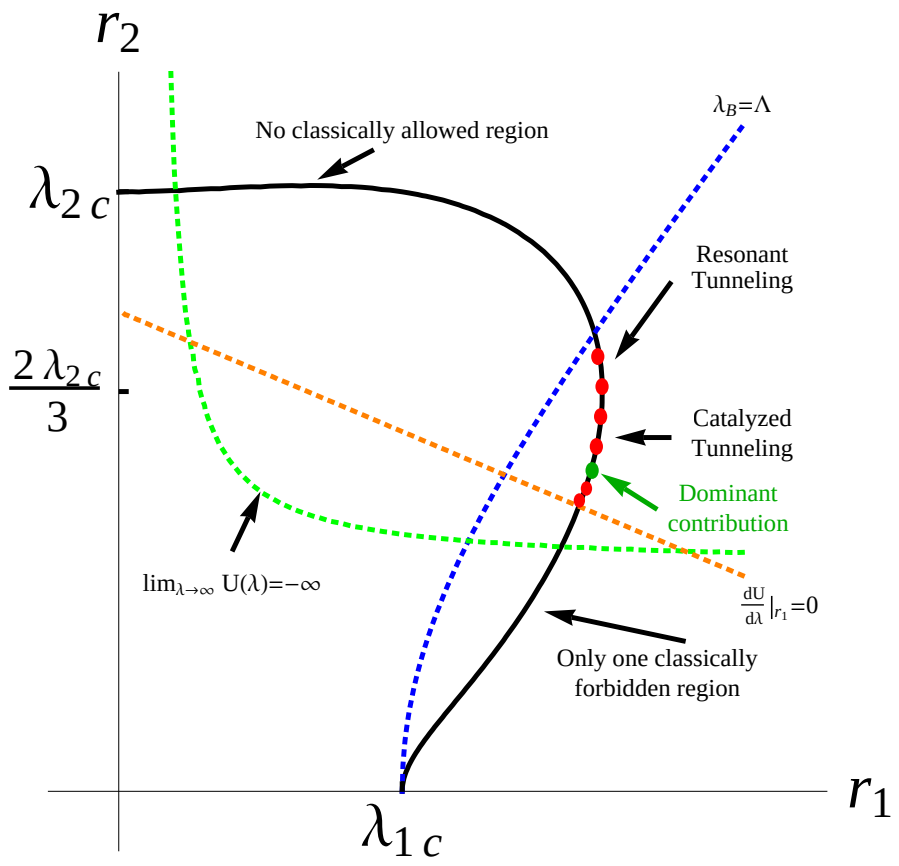

Figure 2.12: The allowed parameter region for resonant tunneling. In appropriate units, the values plotted here are $\sigma_1 = 1$, $\sigma_2 = 5$, $\epsilon_1 = 0.1$, $\epsilon_2 = 0.3$. The energy constraint (2.63) constrains r_1 and r_2 to lie on the black solid curve. The region to the left of the blue dotted curve labeled $\lambda_A = \Lambda$ is excluded since in this region $\tilde{A}'$ does not exist. The region below the blue dotted curve labeled $dU/d\lambda|_{r_1} = 0$ is excluded since in this region there is only one barrier in $U(\lambda)$. The red dots and green dot satisfy the Bohr-Sommerfeld quantization condition (2.12) in addition to satisfying the consistency conditions (2.63), (2.64), (2.65), and (2.66). The green dot with $r_2 \approx 0.54\lambda_{2c}$ provides the dominant contribution to the tunneling probability. Since this point lies below the orange dashed line, catalyzed tunneling occurs. The tunneling probability is $-\log P(A \to A') \approx 2.6 \cdot 10^4$, which is exponentially enhanced compared to the naive single-barrier tunneling probability $S_E^{A\to A'} \approx 1.3 \cdot 10^5$.

plete. Now there are two possibilities for the inside bubble, depending on whether it has the critical size (2.25) to grow or not (note that the binding energy of the two bubbles is expected to be negligible):

(1) $\lambda_{2c} > r_2 > 2\lambda_{2c}/3$, in which case the inside bubble will grow as well. Hence the tunneling from vacuum A to vacuum B will complete. This is the analogue of resonant tunneling in quantum mechanics, so we refer to this tunneling process from A to B via A' as resonant tunneling when $W = (n + 1/2)\pi$.

(2) $0 < r_2 < 2\lambda_{2c}/3$, in which case the inside bubble will collapse after nucleation, while the outside bubble will grow. In this case, the tunneling from A to A' will complete. At a later time, tunneling from A' to B will take place via a normal tunneling process. In this process, the presence of vacuum B can increase the tunneling rate from A to A' by an exponential factor compared to the naive rate given by (2.24). We refer to this tunneling process from A to A' in the presence of vacuum B as assisted or catalyzed tunneling, since B plays the role of a catalyst. Note that in this region (2.59) is modified for $\lambda > r_1$:

$$\lambda' = \begin{cases} \sqrt{\lambda^2 - \Lambda^2} & \Lambda < \lambda \leq r_1 \\ \sqrt{r_1^2 + r_2^2 - \lambda^2} & r_1 < \lambda < \sqrt{r_1^2 + r_2^2} \\ 0 & \text{otherwise.} \end{cases} \tag{2.68}$$

The inside bubble shrinks for $\lambda > r_1$ and disappears entirely when $\lambda = \sqrt{r_1^2 + r_2^2}$.

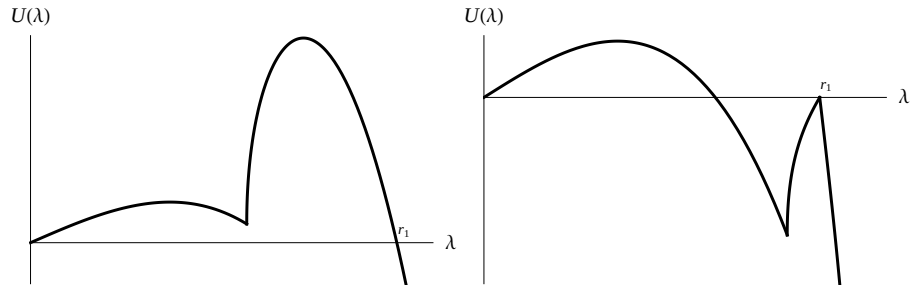

Figure 2.13: Two examples where resonant tunneling is absent. In appropriate units, the values plotted here are $\sigma_1 = 1$, $\sigma_2 = 5$, $\epsilon_1 = 0.1$, $\epsilon_2 = 0.3$. The left plot shows the effective tunneling potential $U(\lambda)$ for $r_2 = 0.8\lambda_{2c} > r_{2,\max}$. No classically allowed region exists for this potential. The right plot shows the effective tunneling potential for $r_2 = 0.4\lambda_{2c} < r_{2,\min}$. There is no second barrier for this potential. The discontinuities in the derivative of $U(\lambda)$ will be smoothed out when the thickness of the bubble walls are taken into account.

2.5.4 Tunneling Probability

Explicitly, as shown in Figure 2.9, the classical turning points (with $E = 0$) are 0, λ_B, λ_Λ and r_1. Then the single-barrier tunneling probability is given by

$$P(\tilde{A} \to \tilde{A}') \simeq \frac{4}{\Theta^2} \ , \tag{2.69}$$

where now

$$\Theta = 2\exp\left(\int_0^{\lambda_A} d\lambda \sqrt{2m(\lambda)U(\lambda)} \right) . \tag{2.70}$$

In the thin-wall limit with $E = 0$

$$\ln\left(\frac{\Theta}{2}\right) = \frac{\pi^2}{4}\lambda_A^3\sigma_1 \tag{2.71}$$

As before, the tunneling probability (2.7) calculated using the functional Schrödinger equation, with Θ given by (2.71), agrees with the result of the Euclidean instanton method, $\exp(-S_E/\hbar)$, where S_E is given by (2.24).

The tunneling probability from vacuum $\tilde{A}$ to vacuum $\tilde{B}$ via the intermediate

vacuum $\tilde{A}'$, is given by (2.8) where now W is given by

$$\begin{aligned} W &= \int_{\lambda_A}^{\lambda_\Lambda} d\lambda \sqrt{2m(\lambda)(-U(\lambda))} \\ &= \frac{\sigma_1 \lambda_\Lambda}{\lambda_A} \sqrt{\lambda_\Lambda^2 - \lambda_A^2} - \sigma_1 \lambda_A \log\left[\frac{\lambda_\Lambda + \sqrt{\lambda_\Lambda^2 - \lambda_A^2}}{\lambda_A}\right] \\ &\approx \frac{\sigma_1 \Lambda}{\lambda_{1c}} \sqrt{\Lambda^2 - \lambda_{1c}^2} - \sigma_1 \lambda_{1c} \log\left[\frac{\Lambda + \sqrt{\Lambda^2 - \lambda_{1c}^2}}{\lambda_{1c}}\right]. \end{aligned} \tag{2.72}$$

with the classical turning points shown in Figure 2.9. The third equality in (2.72) is valid if the classically allowed region is shallow. In this approximation, we also have, with $\lambda_\Lambda \approx \Lambda$,

$$\begin{aligned} \ln\left(\frac{\Phi}{2}\right) &= \int_{\lambda_\Lambda}^{r_1} d\lambda \sqrt{2m(\lambda)U(\lambda)} \\ &\approx \frac{{S_E}^{A\to B}}{2} - \frac{\pi^2}{4}\Lambda^3 \sigma_1 \end{aligned} \tag{2.73}$$

where $S_E^{A\to B} = 2\pi^2 r_1^3 \sigma_1 - \frac{\pi^2}{2}\epsilon_1(r_1^4 - r_2^4) + 2\pi^2 r_2^3 \sigma_2 - \frac{\pi^2}{2}(\epsilon_1 + \epsilon_2) r_2^4$ is the Euclidean action of the solution 2.56. Since Λ, r_1 and r_2 are related by (2.58) and (2.63), we may consider $\Theta(r_2)$, $W(r_2)$ and $\Phi(r_2)$ as functions of r_2 only.

The bubble sizes are dominated by the ones that satisfy the resonance condition (2.12), i.e., $W = (n + 1/2)\pi$ for the nth resonance. With r_2 satisfying this condition and the constraints shown in Figure 2.12, the resulting tunneling probability is now given by (2.13):

$$P(A \to B) = \frac{4}{(\Theta/\Phi + \Phi/\Theta)^2}$$

which can approach unity for suitably chosen potential (2.55).

Next let us consider catalyzed tunneling. This is the case when the inside bubble classically re-collapses after its creation. The normal probability $P(A \to A')$ has a bounce value $\hat{S}_E$ smaller than that given by (2.71), or

$$e^{-S_E^{A\to A'}} = e^{-\pi^2 \lambda_{1c}^3 \sigma_1/2} > 4/\Theta^2 \tag{2.74}$$

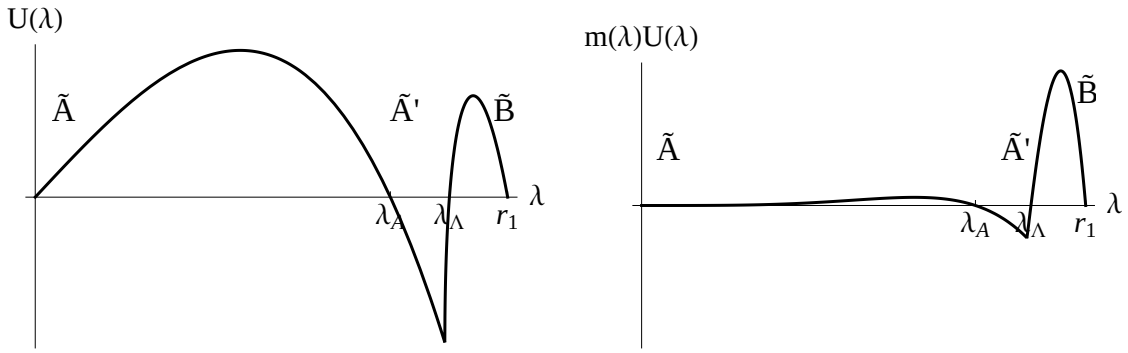

Figure 2.14: Left : $U(\lambda)$ for the double barrier potential $V(\phi)$ in Fig. 2.7. Here, $U(\lambda) = 0$ for $\lambda < 0$. Right : $V(\lambda) = m(\lambda)U(\lambda)$ for the same double barrier case.

where Θ is given by (2.71). The presence of vacuum B can lead to an enhanced tunneling probability,

$$P^{\text{res}}_{A\to A'} \approx \frac{4}{(\Theta/\Phi + \Phi/\Theta)^2}$$

which can be substantially bigger than $P^{\text{normal}}_{A\to A'}$ if $\Theta \sim \Phi$. Typical plots of $U(\lambda)$ and $V(\lambda)$ for which $\Theta \sim \Phi$ are shown in Figure 2.14. On the other hand, the catalytic effect is negligible if Φ is exponentially too big or too small when compared to Θ.

2.5.5 Condition for Resonant Tunneling

As noted in section 2.5.3, fixing the potential $V(\phi)$ and imposing energy conservation does not uniquely fix the size of the bubbles. A range $r_{2,\min} < r_2 < r_{2,\max}$ of bubble sizes is determined via energy conservation (2.62) and the constraints (2.64) and (2.67). Because r_2 is not fixed uniquely by these constraints, the tunneling probability $P(A \to B)$ (2.8) depends nontrivially on the parameters $\sigma_{1,2}$ and $\epsilon_{1,2}$.

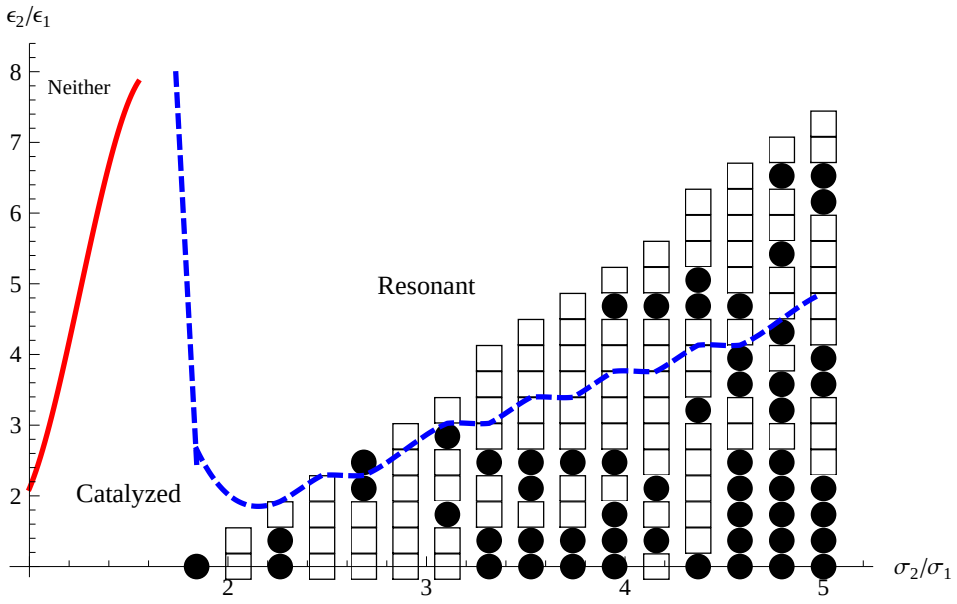

Figure 2.15: This plot illustrates for which regions in parameter space the resonant effect is important. Here $\epsilon_1 = 1.0 \cdot 10^{-4}\text{J/m}^3$ and $\sigma_1 = 2.5 \cdot 10^{-11}\text{J/m}^2$ are fixed (with $v_F = 55\text{m/s}$ so $S_E^{A\to A'}/\hbar \sim 8 \cdot 10^3$) and a linearly spaced grid of points are sampled. To the left of the red solid line, neither catalyzed nor resonant tunneling can occur. The blue dashed line divides the region in which catalyzed tunneling occurs from the region in which resonant tunneling occurs. Both lines are approximate and are based on numerical simulations. The centers of the squares indicate points at which $100 < -S_E^{A\to A'}/(\hbar \ln P) < 1000$ and the centers of the circles indicate points at which the tunneling is essentially unsuppressed: $1000 < -S_E^{A\to A'}/(\hbar \ln P)$, where P is $P(A \to B)$ in the resonant tunneling regions and P is $P(A \to A')$ in the catalyzed tunneling regions. In general the enhancement due to the resonance effect becomes more likely as ϵ_2/ϵ_1 decreases and as σ_2/σ_1 increases. The peaks in P are generally very narrow.

The smallest allowed $r_{2,\min}$ occurs where $\Phi = 0$ (2.73), and Φ increases monotonically with r_2 in the allowed region $r_{2,\min} < r_2 < r_{2,\max}$. If $\Phi(r_{2,\max}) > \Theta(r_{2,\max})$ (2.70), there must be some r_2^* for which $\Phi(r_2^*) = \Theta(r_2^*)$ because Θ is always positive. If $W(r_2^*) = (n + 1/2)\pi$ (2.72), then the tunneling probability will be approximately unity. Generically the dominant contribution to the tunneling probability will come from either the closest point above r_2^* or the closest point below r_2^* on the energy conservation curve that satisfies $W = (n + 1/2)\pi$. Alternatively if $\Phi(r_{2,\max}) \ll \Theta(r_{2,\max})$, then there is no possibility of a large enhancement.

In the allowed region $W(r_2)$ decreases monotonically. Holding ϵ_1/ϵ_2 and σ_1/σ_2 fixed, the range of W increases as the single barrier instanton action $S_E^{\mathrm{A}\to\mathrm{A}'} = \frac{27\pi^2}{2}\sigma_1^4/(\epsilon_1^3)$ increases. The shape of the curves in Figure 2.12 do not change as $S_E^{\mathrm{A}\to\mathrm{A}'}$ is increased, but as the range of W increases it becomes more likely for a point satisfying $W = (n + 1/2)\pi$ to occur very close to r_2^*. Thus the probability of a large enhancement due to resonance effects tends to increase as single-barrier tunneling becomes more unlikely.

Let us now determine for which potentials $V(\phi)$ the resonant effect is important:

- We can use the quantity $-S_E^{A\to A'}/(\hbar \ln P)$ where P is $P(A \to B)$ if resonant tunneling occurs and P is $P(A \to A')$ if catalyzed tunneling occurs to estimate the presence of the resonant effect. In the total absence of the resonant effect,
$$-S_E^{A\to A'}/(\hbar \ln P) \simeq \frac{S_E^{A\to A'}}{S_E^{A\to A'} + S_E^{A'\to B}} < 1 \tag{2.75}$$
while $-S_E^{A\to A'}/(\hbar \ln P) > 1000$ when the resonant effect begins to eliminate the exponential suppression factor in the tunneling rate. This is shown in Fig. 2.15. The center of each black dot or circle satisfies $-S_E^{A\to A'}/(\hbar \ln P) >$

1000, i.e., each black dot contains a region with $-S_E^{A\to A'}/(\hbar \ln P) > 1000$.

- Within each dot, there may be points where the resonant effect is significantly more pronounced and $P \sim 1$.
- If we enlarge the plot (Fig. 2.15) to a three-dimensional plot, with $S_E^{A\to A'}$ as the third axis, we expect that there are points within each three-dimensional cluster of dots and each isolated dot where $P \sim 1$. If there are a number of intermediate A' vacua available, nature will automatically pick the one with the fastest tunneling rate for the $A \to B$ transition.
- As is clear from Fig 2.15, the resonant tunneling phenomenon persists in the region where both σ_2/σ_1 and ϵ_2/ϵ_1 increase. Keeping the $A' - B$ tension σ_2 and $A' - B$ energy density difference ϵ_2 fixed, the resonant effect will be present (keeping the ratio σ_1^4/ϵ_1^3 large enough to stay above the blue dashed line in Fig. 2.15) as both the $A - A'$ tension σ_1 and the $A - A'$ energy density difference ϵ_1 approach zero. Although the thin-wall approximation breaks down before we reach the limit, this does suggest that the resonant effect will remain in this limit under some appropriate conditions. Physically, it will mean that the coherence now comes from the sum of paths in the degenerate or almost degenerate $A - A'$ vacua.
- In a physical system, as the barrier between A and A' disappears, the tunneling probability from A to B must approach the tunneling probability from A' to B. That is, the system will simply roll from A to A' and then tunnel to B. If the barrier is too small for a system at finite temperature, we expect that thermal effects will smear the resonant phenomenon.

2.5.6 Generic Situation

For large Θ and Φ, so that the penetration through the barriers is strongly suppressed, the tunneling probability has sharp narrow resonance peaks at the values in (2.12). If we allow the possibility of a non-zero inital energy E that is small compared to all other relevant mass scales, we introduce an extra variable without introducing any additional constraints, although (2.62) and (2.63) will be slightly modified. Treating the resonance shape as a function of energy E, the resonance has a width Γ_E. Expanding around the resonance at $E = E_R$, we have

$$\cos W = \pm \left(\frac{\partial W}{\partial E} \right) \Big|_{E_R} (E - E_R), \qquad \sin W = 1 \tag{2.76}$$

and

$$P(A \to B) \propto \frac{1}{(E - E_R)^2 + (\Gamma_E/2)^2} \tag{2.77}$$

so this yields, for large Θ and Φ,

$$\Gamma_E = \frac{2}{\Theta\Phi(\frac{\partial W}{\partial E})} \left(\frac{\Theta}{\Phi} + \frac{\Phi}{\Theta} \right) \tag{2.78}$$

Next, let the separation between neighboring resonances be ΔE, where

$$\Delta E \simeq \frac{\pi}{(\frac{\partial W}{\partial E})} \tag{2.79}$$

Then a good estimate of the probability of hitting a resonance is given by

$$P(\text{resonance}) = \frac{\Gamma_{\text{E}}}{\Delta \text{E}} \simeq \frac{2}{\pi\Theta\Phi} \left(\frac{\Theta}{\Phi} + \frac{\Phi}{\Theta} \right) = \frac{1}{2\pi} \left(\text{P(A} \to \text{A}') + \text{P(A}' \to \text{B)} \right) \tag{2.80}$$

We see that the probability of hitting a resonance is given by the larger of the two decay probabilities, $P(A \to A')$ or $P(A' \to B)$, and the average tunneling probability is given by

$$< P(A \to B) >= P(\text{resonance}) \text{P(A} \to \text{B)} \sim \frac{\text{P(A} \to \text{A}')\text{P(A}' \to \text{B)}}{\text{P(A} \to \text{A}') + \text{P(A}' \to \text{B)}} \tag{2.81}$$

which is essentially given by the smaller of the two tunneling probabilities. This is a derivation of Eq.(2.2). Following the argument for (2.1), the generalization to tunneling with multiple barriers is straightforward.

2.6 Remarks

Our results do not conflict with the no-go theorem of [19] since the assumptions are inapplicable as anticipated by [21]. (Note that in [19] the term MPEP is used exclusively to refer to the path in the classically forbidden region; our more inclusive definition will be used in the discussion here.) In particular one of the assumptions is that the MPEP is everywhere stationary $\frac{\partial \phi_0}{\partial \tau} = 0$ or $\frac{\partial \phi_0}{\partial t} = 0$ at the boundary between the classically allowed region and the classically forbidden region, i.e. for $\lambda = \lambda_B$ and $\lambda = \lambda_\Lambda$. This condition is clearly violated by our MPEP (2.57) which is only stationary everywhere for $\lambda \leq 0$ and $\lambda = r_1$. The exact solution (2.56) also violates this condition.

In [20] it was shown how a bubble of vacuum A surrounded by vacuum B could produce a bubble of vacuum C with probability of order unity under certain conditions. It was assumed that the vacuum energy density of vacuum C was greater than the vacuum energy density of vacuum A or vacuum B. The inhomogeneous initial state violates one of the conditions of the no-go theorem. The physics is quite different because the asymptotic false vacuum is intermediate in field space. Since our analysis applies only in the double thin-wall approximation, it is possible that the oscillons or its quantized version may play an important role in a different setup.

We apply the functional Schrödinger method to show how resonant tunnel-

ing takes place in quantum field theory with a single scalar field. Our analysis is carried out in the double thin-wall approximation. The double-barrier potential problem in QFT is reduced to a double-barrier potential problem in a time-independent one-dimensional QM problem, so the quantum mechanical analysis can be applied.

The relevance of resonant tunneling is obvious if the potential has many local minima, as is the case of the cosmic landscape in string theory. So resonant tunneling in the presence of gravity is a very important question to be addressed.

What happens if the conditions (2.63), (2.64), (2.65), and (2.66) cannot be satisfied? Generically, the double thin-wall approximation breaks down and a more careful analysis is needed. Based on the analysis of (2.1), we are led to believe that the resonant tunneling phenomenon will continue to happen. So it is interesting to study more general cases to obtain a complete picture.

CHAPTER 3

RESONANT TUNNELING IN SUPERFLUID HELIUM-3

3.1 Introduction

It is well known that superfluid He-3 has a very rich phase structure [26]. Its superfluidity properties allow a typical sample to be treated as a pure quantum system devoid of impurities. A number of its phases have been well studied, in particular the A phase and the B phase. They are well described by the so-called mean field theory. Their properties (such as free energy density difference, critical temperature and domain wall tension [27, 28]) are well understood and measured so the $A \to B$ phase transition rate can be reliably calculated. At low enough temperature, B phase has a lower free energy density than that of the A phase. In the nucleation theory for a supercooled A phase sample, the $A \to B$ first order phase transition can go via thermal fluctuations or via quantum tunneling. The characteristic time for a typical sample in A phase (the false ground state) to thermally fluctuate over the barrier is [29, 30]

$$T \sim 10^{1,470,000}\,\mathrm{s} \tag{3.1}$$

(Note that choosing the units in years instead of seconds leads to a tiny error in the exponent, well within the uncertainties of the estimate.) If it goes via quantum tunneling at zero temperature, one obtains, in the usual WKB approximation [31],

$$T \sim 10^{20,000}\,\mathrm{s} \tag{3.2}$$

This estimate at zero temperature is too optimistic for the actual situation. At higher temperatures where the transition has been observed, the quantum tunneling time is estimated to be longer (the exponent is bigger by at least an order

of magnitude). These estimates imply that the transition should never have happened. Yet, it is a well known fact that this transition actually happens very rapidly, in hours if not in seconds. This very rapid transition allows experimentalists to reach and study the B phase by supercooling the superfluid He-3 in the A phase (which is in turn usually reached via the A_1 phase). The discrepancy between theory and experiments is huge : the above exponents are too big by four to five orders of magnitude.

Superfluid He-3 is one of the most pure quantum systems accessible in the laboratory. Any impurity will self separate (e.g., He-4 will sink to the bottom). So superfluid He-3 is an excellent quantum system to study. It is intuitively clear that impurities can provide seeds of nucleation bubbles for the transition. Since superfluid He-3 has no impurities, external beams such as cosmic rays may provide the necessary seeds of nucleation, thus exponentially speed up the phase transition process. This is the "Baked Alaska" model [32]. Although we agree that external interference (e.g., shooting neutron beams or cosmic rays on the sample) can surely speed up the transition process [29], a direct search of cosmic ray effect detected no such correlation in a superfluid He-3 sample [33, 34]. So this observed superfast phase transition remains an outstanding puzzle. Here, we propose to explain this rapid phase transition as a natural consequence of the resonant tunneling phenomenon.

If our explanation is correct, there is at least a plausible, qualitative but very distinctive prediction that may be readily checked experimentally. Resonant tunneling phenomenon happens only under some fine-tuned conditions. This feature predicts the existence of peaks in the $A \rightarrow B$ transition rate for certain values of the temperature, pressure, and external magnetic field. Away

from these peaks, the transition simply will not happen. These high probability regions may take the form of isolated peaks, or lines or surfaces in the three-dimensional space with temperature, pressure, and magnetic field as the three coordinates. The locations and shapes of such regions should also depend on the container geometry as well as the properties of the container surface.

Experiments in Ref.[34, 35] have shown that, for fixed pressure, magnetic field and geometry, the B phase nucleation takes place at a specific temperature. For example, Ref.[35] finds that, for pressure at 29.3 bar and magnetic field $H = 28.4$ mT, B phase nucleation takes place at temperature $T = 0.67T_c$ with a full width of about $0.02T_c$ (where T_c is the superfluid transition temperature) when the sample is slowly cooled, i.e., there is a peak in the plot of transition event number vs T. This is what our proposal expects : the resonant tunneling condition is satisfied only when the properties of the He-3 sample are just right. This happens at a specific temperature when other conditions are fixed. Now, the resonant condition is simply the Bohr-Sommerfeld quantization condition (2.12), which has multiple solutions. This allows the possibility that there is more than one nucleation temperature. In the three-dimensional space with pressure, magnetic field and temperature as the three coordinates, there are isolated regions where the $A \rightarrow B$ transition is fast enough to be observed. This also suggests the following two possibilities to Ref.[35] :

(1) The resonant peak in the event number (of B phase transition) versus temperature is actually an unresolved collection of two or more extremely narrow peaks.

(2) The width may be due to the spread caused by the finite temperature and experimental setup resolution limit. Depending on the details, there may be other critical nucleation temperatures besides the one observed. A simple search of

additional nucleation temperatures below $T = 0.67T_c$ will be very interesting. If they exist, we expect their widths to be narrower as well.

In the previous chapter, we showed how resonant tunneling occurs in quantum field theory. To identify this resonant tunneling phenomenon in nature, we need a quantum system with multiple false vacua with appropriate properties. In this chapter, we present arguments that this resonant tunneling phenomenon has already been observed in superfluid He-3.

The properties of the A and B phases are among the best understood, both theoretical and experimental, qualitative and quantitative, in condensed matter physics. The He-3 pairing is in p-wave spin $S = 1$ state. Here the order parameter (a 3×3 complex matrix $\mathbf{\Delta}(\mathbf{r}, t)$) describes the properties of various phases and the real scalar field ϕ we have in mind is the interpolating field among the specific phases the particular transition is taking place. Although the calculated thermal fluctuation time (3.1) is faster than single-barrier quantum tunneling time at the temperatures at which the transition is observed, under appropriate conditions the resonant tunneling effect can reduce the exponent in Eq.(3.2) by orders of magnitude, reversing the inequality. (Pre-factors will be ignored throughout.)

In this chapter, we propose how resonant tunneling may occur in the $A \to B$ phase transition. It is well accepted that both the A phase and the B phase actually consist of multiple distinct local classically metastable minima of the free energy functional, which we shall refer to as A sub-phases and B sub-phases. To avoid confusion with the A_1 phase, we shall refer to these as A^i sub-phases (similarly for the B sub-phases). The barrier and the free energy density difference between any two A sub-phases are small compared to that between an A

sub-phase and a B sub-phase (similarly for the B sub-phases). Here, we start with this qualitative property and show that the $A^i \to A^j \to B$ transition can easily be enhanced by the resonant tunneling effect. This enhancement can be particularly strong for a specific B^k sub-phase, so the $A^i \to A^j \to B^k$ transition will dominate. Even though we may not know the actual sub-phases involved in a specific sample, we argue that this phenomenon is quite generic in He-3. As supercooling is taking place, the detailed properties of the sub-phases are slowly changing accordingly, increasing the probability of hitting the resonance condition at certain point, and so a typical transition can be quite fast.

Our analysis further suggests that the resonant tunneling effect may remain as both the A^i–A^j tension σ_1 and the A^i–A^j energy density difference ϵ_1 approach zero while keeping the ratio $\sigma_1^4/(\epsilon_1^3 v_F \hbar)$ large but fixed (where v_F is the Fermi velocity). This suggests that the resonant effect may remain when we have a degenerate or an almost degenerate A phase. Here the resonant tunneling effect probably follows from the coherence of the infinite sum of Feynman paths in the degenerate $A = A^i - A^j$ phase. Further study will be important in finding the necessary condition for resonant tunneling in this case.

We shall also compare this resonant tunneling scenario to other proposed explanations to this fast transition puzzle and discuss some possible ways to test this proposal.

Our original motivation to study resonant tunneling is its possible implication in string theory and cosmology [17, 18]. String theory suggests a multi-dimensional "landscape" with numerous (if not infinite number of) classically stable local vacua (i.e., phases) [37]. Tunneling between possible vacua in this cosmic landscape is an outstanding problem under investigation. A better un-

derstanding of the first order phase transition processes in superfluid He-3 will certainly help, since the actual tunneling processes are rather complicated, so it is truly useful that one can do experiments to test the model calculations. In this sense, this is another way to realize the connection of He-3 to cosmology [38]. It will be very useful to find other systems in the laboratory that exhibit the resonant tunneling phenomenon.

The rest of the chapter contains the following sections. In Sec. 3.2, we review some of the properties of phase transitions in superfluid He-3 that are relevant to the above estimates of the transition rates (3.1,3.2). This brings out clearly the puzzle. In Sec. 3.3, we study the conditions for resonant tunneling and identify the tunneling $A^i \to A^j \to B^k$ to be most likely, as compared to other transitions that involve an intermediate B sub-phase. *A priori*, other tunneling paths, say those involving other possible phases in superfluid He-3, may be potential candidates too. In Sec. 3.4 we discuss some possible ways to test this proposal. Sec. 3.5 contains some remarks.

3.2 Thermal and Quantum Tunneling

The features of superfluid He-3 physics is well described by the mean field theory. Both the A-phase and the B-phase are continuously degenerate. These degeneracies are typically lifted by the presence of external magnetic field, which interacts with the spin and the orbital waves, the container wall effect, as well as the wall surface irregularities etc.. Let us ignore these effects for the moment and consider the tunneling between the A-phase and the B-phase. Here we like to review the inputs that go into the estimates (3.1, 3.2) and show that these

estimates of the exponents are reasonable within the present context.

A He-3 atom has spin one-half and the He-3 pairing happens in the spin $S = 1$ p-wave state. So the order parameter is a 3×3 matrix $\Delta_{\alpha i}$, where $\alpha \in (x, y, z)$ is the spin index and $i \in (x, y, z)$ is the index for the $l = 1$ p-wave orbital. Ignoring small corrections, the Ginzburg-Landau free energy functional takes the form [26, 31]

$$\mathcal{L} = \mathcal{L}_{\text{cond}} + \mathcal{L}_{\text{grad}} + \mathcal{L}_{\text{kin}} \tag{3.3}$$

where

$$\mathcal{L}_{\text{cond}} = \frac{1}{2}\frac{\text{dn}}{\text{d}\epsilon}[(T - T_c)/T_c]\Delta^*_{\alpha i}\Delta_{\alpha i} + \beta_1\Delta^*_{\alpha i}\Delta^*_{\alpha i}\Delta_{\beta j}\Delta_{\beta j} + \beta_2\Delta^*_{\alpha i}\Delta_{\alpha i}\Delta^*_{\beta j}\Delta_{\beta j} + \beta_3\Delta^*_{\alpha i}\Delta^*_{\beta i}\Delta_{\alpha j}\Delta_{\beta j} + \beta_4\Delta^*_{\alpha i}\Delta_{\beta i}\Delta^*_{\beta j}\Delta_{\alpha j} + \beta_5\Delta^*_{\alpha i}\Delta_{\beta i}\Delta_{\beta j}\Delta^*_{\alpha j} \tag{3.4}$$

$$\mathcal{L}_{\text{grad}} = K_L\partial_i\Delta^*_{\alpha i}\partial_j\Delta_{\alpha j} + K_T\epsilon_{ijk}\partial_j\Delta^*_{\alpha k}\epsilon_{ilm}\partial_l\Delta_{\alpha m} \tag{3.5}$$

and

$$\mathcal{L}_{\text{kin}} = \frac{1}{32T_c^2}\frac{dn}{d\epsilon}\partial_t\Delta^*_{\alpha i}\partial_t\Delta_{\alpha i} \tag{3.6}$$

where $\frac{\text{dn}}{\text{d}\epsilon}$ is the density of states. Assuming that the order parameter takes the shortest path in field space from the A-phase to the B-phase, the order parameter takes form

$$\Delta_{\alpha i} = \frac{\Delta(A)}{\sqrt{2}}(1-\zeta)\begin{pmatrix} 1 & i & 0 \\ 0 & 0 & 0 \\ 0 & 0 & 0 \end{pmatrix} + \frac{\Delta(B)}{\sqrt{3}}\zeta\begin{pmatrix} 1 & 0 & 0 \\ 0 & 1 & 0 \\ 0 & 0 & 1 \end{pmatrix} \tag{3.7}$$

for the configuration of interest. The false ground state, namely the A phase, is at $\zeta = 0$ and the true ground state, namely the B phase, is at $\zeta = 1$. Up to a normalization factor, ζ is simply the interpolating field ϕ.

Although we shall not go into any details, it is important to point out the following key point. It is obvious from the form of the A phase matrix that it is highly degenerate. For example, instead of putting the non-zero values in the xx and xy entries, we can rotate them into other entries. Besides $\mathcal{L}$(3.3), there are many other interaction terms that will contribute to the free energy density [26]. Some examples include interactions with the external magnetic field and the container wall. Magnetic field effects are generally small, but container wall (which typically can have some irregularities on its surface) effects can be very strong for He-3 close to the wall. There are texture and topological properties, as well as current properties. In general, these effects tend to lift (or reduce) the large degeneracy of the A phase, leading to many A sub-phases. A similar situation happens for the B phase. This fact will play a crucial role in our proposal.

The critical temperature depends on the pressure and the magnetic field. Here we shall use the typical value $T_c \approx 2.5$mK. The measured value of the domain wall tension between the A and B phases at melting pressure is $\sigma \simeq 9.3 \times 10^{-9}\mathrm{J/m}^2$ [27] while the calculated value using the path (3.7) is within 10% of the measured value [28]. At $T = 0.7T_c$ (a typical temperature in the experiments), the free energy density difference is $\epsilon = 0.013\mathrm{J/m}^3$ [26, 29]. Note that both σ and ϵ are temperature dependent.

The decay width of the A phase to the B phase is given by, ignoring the prefactor,

$$\Gamma \simeq e^{-S/\hbar} \tag{3.8}$$

Using the above values for σ and ϵ (at $T = 0.7T_c$), the exponent S for the pure quantum tunneling decay process in the thin-wall approximation is given by

[36, 15]

$$S_{\text{quantum}} = \frac{27\pi^2}{2}\frac{\sigma^4}{\epsilon^3}\frac{1}{v_F} = 8.2 \times 10^7 \hbar \tag{3.9}$$

if the Fermi velocity v_F is about 55m/s. The difference between this estimate and the estimate (3.2) is in the values of σ and ϵ used. The estimate (3.2) uses instead the values of σ and ϵ at $T = 0$ while the actual temperatures in the experiments are closer to the value ($T = 0.7T_c$) we use.

As a simple estimate of the validity of the thin-wall approximation, we can compute the ratio of the radius of the bubble at nucleation λ_c to the thickness of the domain wall $1/\mu$. For a symmetric double well potential (ignoring the small ϵ term), $\mu \approx \sqrt{2}mv_F/\hbar$, where m is the mass of the scalar field in the false vacuum. The correlation length ξ_0 is of order $\hbar/mv_F$, and $\xi_0 = (\frac{7\zeta(3)}{48\pi^2})^{1/2}\frac{\hbar v_F}{kT_c}$ implies $\xi_0 \approx 15$nm, so $1/\mu \sim 10$nm. In the thin-wall limit, $\lambda_c = 3\sigma/\epsilon \approx 2000$nm, so the radius of the bubble is $O(100)$ times the thickness of the domain wall, and the approximation is consistent.

The simplest estimate one could do for the pure thermal activation exponent simply uses the Boltzmann factor:

$$S_{\text{thermal}} = \frac{16\pi}{3}\frac{\sigma^3}{\epsilon^2}\frac{1}{k_B T} = 3.3 \times 10^6 \hbar \tag{3.10}$$

The actual tunneling takes place via a combination of quantum and thermal processes. In a scalar quantum field theory with a false vacuum and a true vacuum, tunneling starts from the bottom of the false vacuum in the potential. At finite temperature, tunneling does not need to occur from the bottom of the false potential well. Instead, tunneling proceeds by a combination of thermal excitation part way up the barrier followed by quantum tunneling through the barrier.

Taking the finite temperature effect into account, the quantum tunneling rate is determined by [31]:

$$\begin{aligned} S_{\text{quantum}} &= C \int_{-\beta/2\beta_0}^{\beta/2\beta_0} d\tau \int d^3\mathbf{x} \mathcal{L}(\alpha) \\ &= C \frac{24\pi^2}{25} \frac{A^2}{\eta^3} \frac{T_c}{T_c - T} \end{aligned} \tag{3.11}$$

where $A \approx 3.3$, $\eta \approx 0.36(1 - T/T_c)$. Here α (which is simply ϕ up to a normalization factor) is the $O(4)$ symmetric instanton. Note that C is a model-dependent constant that is roughly temperature independent. Estimates of C depend on the interpolation between A and B and range from roughly $25\hbar$ in [31] to $250\hbar$ in [29]. The temperature dependence in Eq.(3.11) arises solely because of the temperature dependence of the potential.

The thermal tunneling rate is determined by [31]:

$$\begin{aligned} S_{\text{thermal}} &= C \int_{-\beta/2\beta_0}^{\beta/2\beta_0} d\tau \int d^3\mathbf{x} \mathcal{L}(\tilde{\alpha}) \\ &= C \frac{512\pi}{3} \left(\frac{T_c}{T_c - T} \right)^{1/2} \frac{\beta}{2\beta_0 \eta^2} \left(\frac{A}{30} \right)^{3/2} \end{aligned} \tag{3.12}$$

where $\tilde{\alpha}$ is the $O(3)$ symmetric thermal critical bubble (the rotationally symmetric configuration of the order parameter).

In any case, although the actual estimate of S may vary somewhat, no reasonable theoretical argument can push the value of S substantially below that of Eq.(3.2), which implies that the $A \to B$ phase transition should never have happened. This is the puzzle we are facing.

3.3 Condition for Resonant Tunneling in Superfluid Helium-3

Now we are ready to find the condition for the resonant tunneling phenomenon. As is well known, the mean field theory allows many possible phases for superfluid He-3. So far only the normal, the A_1, the A and the B phases have been observed, where the last three are superfluids. The $A_1 \to A$ phase transition is second order, while the transition from A to B is first order. As we have mentioned in Section 3.2, theoretical calculations argues that the A to B transition should never have happened, which is frequently contradicted by experiments. In a normal condensed matter system, impurities are typically present and they can provide seeds of bubble nucleation. However, since He-3 is devoid of impurities, the answer should lie somewhere else. It is possible that cosmic rays hitting the sample may play a role, as proposed in the "Baked Alaska" model [32, 30]. Showering beams of particles or ionizing radiation should certainly enhance the transition rate [29]. However, there is strong evidence that the transition rate is puzzlingly fast even in the absence of any such external disturbances. We believe the fast transition is a resonant tunneling phenomenon.

To apply the resonant tunneling phenomenon to the $A \to B$ transition, there are *a priori* two possibilities : via catalyzed tunneling or resonant tunneling. In both cases, a third phase besides A and B must be present in the phase diagram. At first sight, one may consider one of the predicted but as yet not discovered phases of He-3. However, none of them seems to have the right properties. Our analysis shows that resonant tunneling is the likely scenario and that requires a phase between the A and the B phases but very close to the A phase; that is, both the domain wall tension σ_1 and the free energy density difference ϵ_1 between that phase and the A phase should be small compared to that (σ_2 and

ϵ_2) between that phase and the B phase. How can we find such a phase?

As is well known, both the A phase and the B phase in a superfluid He-3 model are degenerate. These degeneracies are typically weakly lifted by the presence of an external magnetic field, and by the spin-orbit interaction. Furthermore, container wall effect has a large impact on the ground states of superfluid He-3 close to the wall. So both the A phase and the B phase are actually a collection of phases. Some of these phases have rich intricate properties; they are well studied, both theoretically and experimentally. Depending on the experimental setup and conditions, the initial A phase is actually in one of these sub-phases. Let us call it the A^i phase. If there is another A sub-phase which has a lower free energy density than that of A^i, then we are in business. We call this sub-phase the A^j phase.

With resonant tunneling, the decay rate of $A^i \to A^j \to B$ will be substantially enhanced. However, even with resonant tunneling, this decay rate is typically still exponentially suppressed (see Eq.(2.13)). For example, even if the exponent in Eq.(3.2) is reduced by a factor of 100, the decay time is probably still far too long. Here, the presence of B sub-phases should help. Again the various B sub-phases have slightly different free energy densities and the domain wall tension σ_2 between A^j and a B sub-phase varies a little from one B sub-phase to another. That is, nature will pick the particular B sub-phase, called the B^k sub-phase, that has the fastest tunneling rate. That is, the choice of a specific B sub-phase provides a fine-tuning to enhance further the tunneling rate. Again, this enhancement is in the exponent for the $A^i \to A^j \to B^k$ transition.

As shown in Fig. 2.15, large enhancements in the tunneling probability due to resonant effects can only occur in certain regions of the $(\sigma_1, \sigma_2, \epsilon_1, \epsilon_2)$ parame-

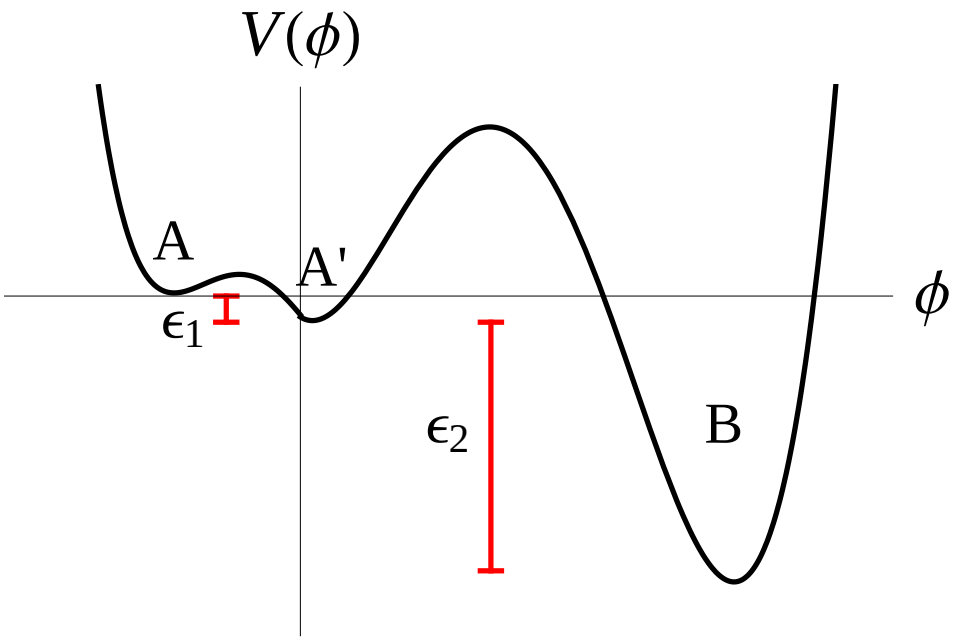

Figure 3.1: Plot of the potential for superfluid Helium-3 as a function of the interpolating field ϕ. The detailed form of the potential is not important to resonant tunneling explanation of the fast A to B transition. The only property that we require is that the domain wall tension and energy density difference should be larger between the A and B phases than between the A subphases. We neglect finite temperature effects for now, and comment on their role in Section 3.5.

ter space. Of particular interest is the $\epsilon_2 \gg \epsilon_1$, $\sigma_2 \gg \sigma_1$ limit, as this region supports resonant tunneling, has the possibility of a large enhancement in the tunneling probability, and describes superfluid Helium-3 near the transition temperature. If $\epsilon_2 \gg \epsilon_1$, $\sigma_2 \gg \sigma_1$, and $r_2 \sim r_1$, then $r_{2,\max}$ approaches λ_{2c}. Using (2.71) and (2.73) we see that in this limit $\Phi(r_{2,\max}) \gtrsim \Theta(r_{2,\max})$ only if

$$\frac{(\sigma_2)^8}{\epsilon_2^6} \gtrsim (\sigma_1)^2\Big[\frac{(\sigma_1)^2}{\epsilon_1^2} - \frac{(\sigma_2)^2}{\epsilon_2^2}\Big]. \tag{3.13}$$

Qualitatively the potential should be similar to the one shown in Figure 3.1.

3.4 Some Predictions

Let us first briefly review existing proposals to the fast $A \rightarrow B$ transition puzzle and then propose how our explanation may be tested. Although the predictions are very qualitative in nature, they are very distinctive. Some of the experiments proposed should be readily performed.

3.4.1 Comparison to Other Explanations

The best known explanation of the rapid $A \rightarrow B$ transition is the "Baked Alaska" model [32, 30]. It proposes that the fast transition is triggered by cosmic rays, which provide the seeds of B phase bubble nucleation. We do agree that showering ionizing radiation or shooting beams of external particles to a sample of A phase superfluid He-3 can trigger the formation of B phase nucleation bubbles, thus leading to a fast $A \rightarrow B$ transition [29]. The "Baked Alaska" model explains how the external particle beam causes the fast transition, though there are alternative explanation of the mechanism by which it occurs [39]. Here we are not concerned with the precise mechanism caused by external disturbances.

As pointed out in Ref.[33], no correlation has been detected between nucleation events and coincidence counts from the cosmic ray detectors. Even though the cosmic ray detectors apparently do not cover all angles, this experiment strongly indicates that the fast $A \rightarrow B$ transition happens even in the absence of cosmic rays. That is the puzzle.

Another experiment [34] shows that the nucleation temperature (about $0.67T_c$) depends on pressure and the geometry of the sample, again suggesting

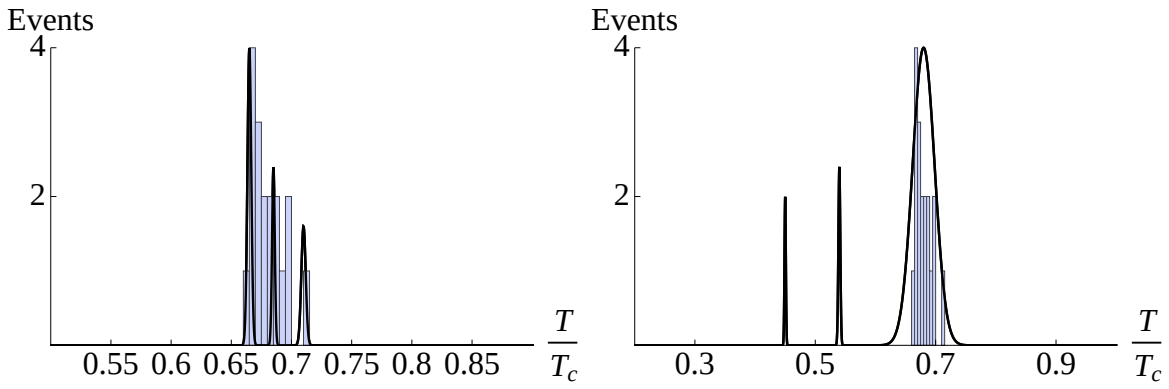

Figure 3.2: The number of $A \rightarrow B$ transition events in a ^{3}He-A sample as the temperature is slowly decreased. In the left figure, we illustrate the possibility that the broad resonant peak in Ref.[35] is actually a collection of three unresolved narrow peaks at three nearby nucleation temperatures around $T = 0.67T_c$. The right figure assumes the broad peak at $T = 0.67T_c$ is a single resonant peak (its breadth due to finite temperature effect) and there are additional peaks at nucleation temperatures below $T = 0.67T_c$. These two features are not mutually exclusive. Note that the expected number of events at a given temperature in this experiment is not proportional to $P(A \rightarrow B)$ at that temperature, because only a fraction of the trials reach the lower temperatures. In both figures the bars indicate the number of observed A to B transitions in Ref.[35].

that cosmic rays are not the cause of the fast $A \rightarrow B$ transition.

These two experiments are in accord with our explanation, which has nothing to do with external disturbances. One can certainly extend the cosmic ray detection to all angles to improve the experiment of Ref.[33] to rule out with certainty that cosmic rays are not the reason for the fast $A \rightarrow B$ transition.

Vortex nucleation experiments in superfluid He-3 do not provide any direct test of our proposal because vortices are defects and hence the analysis of Chapter 2, which relied on the formation of bubbles, is not readily applicable to the

nucleation of vortices. Vortex nucleation can occur in one of three ways: when the barrier disappears [40], when the sample is stimulated by external radiation [41], or when shear instability occurs at the A-B interface [42]. The second of these explanations, if applied to B phase nucleation, is the "Baked Alaska" model described above. If the first or third of these explanations can be applied to B phase nucleation, the experimental signatures will be distinct from those we describe in the following section.

3.4.2 A Plausible Prediction

The nucleation temperature is simply the temperature that the $A \to B$ transition takes place. In our scenario, that means the nucleation temperature satisfies the resonant condition. Slightly away from the resonant condition, the transition time becomes exponentially long. Since the resonant tunneling phenomenon requires the satisfaction of a fine tuned condition, $A \to B$ transition happens only at specific values of pressure, temperature and magnetic field. Move slightly away from those values and the transition simply will not happen. Viewed another way, a small change in geometry, external magnetic field or pressure will certainly shift the properties of the various He-3 phases, so the nucleation temperature will be shifted accordingly. This seems to be the case in Ref.[34, 35].

Consider the nucleation temperature already seen in Ref.[34, 35]. For example, Ref.[35] finds that, for a ^{3}He-A sample with pressure at 29.3 bar and magnetic field $H = 28.4$ mT, B phase nucleation takes place at temperature $T = 0.67T_c$ with a (full) width of about $0.02T_c$ when the sample is slowly cooled, at a rate of 5μK per minute to 29μK per minute. At this magnetic field and pressure, the A

and B phases have equal free energy density at a temperature $T_{AB} = 0.85T_c$. In the event number (of $A \to B$ transitions) versus temperature plot (collected over a number of these temperature sweeps), the event number shows up as a resonance peak at $T = 0.67T_c$. The dependence of the transition probability $P(A \to B)$ on temperature can be inferred from the number of observed transitions at each temperature and the cooling rate, although not from either individually. Such a resonance peak is in accordance with our expectations. One can perform a more detailed data collection in the three-dimensional plot of the pressure, magnetic field and temperature to find the regions where the $A \to B$ transition happens. We expect multiple isolated regions. These regions may take the form of isolated peaks, or lines or surfaces in the 3-dimensional space with temperature, pressure, and magnetic field as the 3 coordinates.

Since the resonant condition is simply the Bohr-Sommerfeld quantization condition (2.12) and there are multiple solutions to this condition, there should be more than a single nucleation temperature. That is, for fixed pressure and magnetic field, there may be additional nucleation temperatures. In Fig. 3.2, we present two plausible scenarios of multiple nucleation temperatures :

- The peak in the event number (of B phase transition) versus temperature in Ref.[35] is actually an unresolved collection of two or more very narrow peaks. This is illustrated in the left panel of Fig. 3.2. To resolve them and to determine their actual widths, one may have to use a slower rate in the temperature sweep and collect more data. If the finite temperature effects are small, then the width of each individual peak can easily be much less than 1μK. Since the width of the unresolved peak is about 50μK, sitting at a random fixed temperature within this broad width is unlikely to

encounter an $A \rightarrow B$ transition (once off the peak, the transition probability becomes exponentially small). This agrees with the observation of Ref.[35], that a ^{3}He-A sample can sit at a stable temperature in that temperature range for hours.

- The width of the peak may be due to the spread caused by the finite temperature and other effects. In this case, there can be other critical nucleation temperatures besides the one observed. This is illustrated in the right panel of Fig. 3.2. A simple search of additional nucleation temperatures below $T = 0.67T_c$ will be very interesting. If they exist, we expect their widths to be narrower as well.

Although we do not know enough about the detailed structure of the free energy functional to find the positions or shapes of the additional resonances, we can still make some comments here :

- Our prediction only states that we expect more than a single nucleation temperature or a single resonance peak. That is, we predict the existence of narrow peaks in the transition rate, between which the transition is completely absent. The positions and shapes of the narrow resonance peaks shown in Fig. 3.2 are not predictions, and are shown for illustrative purposes only.
- It is entirely possible that the actual scenario incorporates both features of narrow peaks just described.
- Ref.[35] sees the nucleation temperature only during cooling down, not during warmup. This suggests that the warmup nucleation temperature may be shifted outside the temperature range studied. Another possibility

may be the tunneling probability is still too low even when hitting the resonance condition. As pointed out in Ref.[35], this difference between cooling down and warmup may be due to the continuous vortices induced by rotation in the sample of ^{3}He-A.

- It is possible that the additional resonances show up more readily if one adjust slightly the pressure and/or the magnetic field.
- Although we generically expect to have multiple resonances with different quantization number in the quantization condition (2.12), it is possible that variation of temperature, pressure, or magnetic field leads to variations of the effective potential $V(\phi)$ (in Fig. 3.1) for the interpolating field ϕ. This in turn leads to corresponding variations in $V(\lambda)$ (in Fig. 2.14) and so Θ, Φ and W in (2.70, 2.72, 2.73) in a way such that two or more distinct resonances appear at the same quantization number. We cannot rule out the possibility of such a coincidence.

3.4.3 Growth of Bubbles

Suppose for a particular choice of parameters, resonant tunneling occurs. After nucleation, both bubbles will grow classically. By symmetry, the radii $|\mathbf{x_1}|$ and $|\mathbf{x_2}|$ of the two bubbles satisfy

$$r_i^2 = |\mathbf{x_i}|^2 - \mathbf{t}^2 \tag{3.14}$$

where $i = 1, 2$ assuming both bubble walls have zero velocity at $t = 0$. Thus

$$\frac{|\mathbf{x_2}|^2}{|\mathbf{x_1}|^2} = \frac{r_2^2 + t^2}{r_1^2 + t^2} \tag{3.15}$$

which implies that smaller bubble always grows faster, since this ratio is monotonic in $t > 0$, and approaches unity at future infinity. In a physical system,

the bubble walls will interact, and once they are close enough they will merge. In superfluid He-3, energy dissipation could complicate this simple treatment, but should not alter the conclusion that the separation between the two bubble walls is initially decreasing.

The distance between the two walls at nucleation could be much larger than the thickness of either individual wall. If it were possible to observe the nucleation of the bubbles without sufficient resolution to separate the double walls, they will appear as a single thick wall. Then we expect to see that "thick wall" becomes thinner as the bubble grows.

3.5 Discussion and Remarks

Now, we like to summarize the scenario we envision. In a typical experiment trying to reach the B phase of superfluid He-3, the sample starts at the A phase, say, the A^i sub-phase. One reaches this phase via either the normal or the A_1 phase, where the $A_1 \to A$ transition is second order. As the temperature is lowered to supercool the A^i sub-phase, fast tunneling requires the presence of a A^j sub-phase slightly below the A^i phase.

As the temperature of the sample is being lowered (in some experiments, adjustment of pressure and/or external magnetic field may also take place), all the properties (say $\sigma_{1,2}$ and $\epsilon_{1,2}$) will be varying slowly. This fine sweeping of the parameters of the system (as well as the choices of A^j and B^k) offers a good chance that resonant tunneling with vanishing (or almost vanishing) exponent will be hit at certain point for specific choices of the A^j and B^k sub-phases., enabling tunneling with little or no exponential suppression. This scenario clearly

requires the existence of the A^j sub-phase.

Note that we are not concerned with tunneling from the B phase back to the A phase. Presumably, even in the B phase, some regions adjacent to the container walls will remain in the A phase, so that when the temperature is raised so that the A phase becomes the true ground state, those A phase regions will simply grow and take over the sample.

3.5.1 Some Subtleties

Notice that our analysis assumes homogeneity and isotropy of the medium. However, many sub-phases are not homogeneous and/or isotropic. Explicit calculations of the tunneling in such situations will be much more complicated. However, one may convince oneself that resonant tunneling is a generic phenomenon, independent of the details, as long as some constraints are satisfied; that is, the presence of a classically allowed region that allows the Bohr-Sommerfeld quantization condition (i.e., the coherent sum of Feynmann paths) to be satisfied. As we have seen, this is not a very tight constraint when the A^j sub-phase is present. Experimentally and/or theoretically, one has to check that such a sub-phase is actually present. This is a qualitative prediction.

Additionally our analysis neglects thermal fluctuations. On general grounds we expect thermal effects to broaden the resonances, but if $S_E^{A\to A'}/\hbar$ is sufficiently large these effects are likely negligible.

3.5.2 Cosmic Landscape

In superstring theory, we believe there are classically stable local vacua, described by many "parameters and variables" known as moduli. They number in the dozens to hundreds. In superfluid He-3, we have a complex 3×3 matrix as the order parameter plus many interaction parameters. (Here, tiny interaction terms can be important in reaching the sweet spots of resonant tunneling.) Not surprisingly, both systems have many solutions : classically stable local vacua in string theory, collectively known as the cosmic landscape, or phases in He-3. That a phase transition in He-3 is much much faster than naively expected is a pleasant surprise for experimentalists. This phenomenon should be fully understood so we can decide whether the same phenomenon should happen in the cosmic landscape. Here we speculate that, due to the resonant tunneling effect, the tunneling transitions in the cosmic landscape may happen surprisingly fast. In fact, the transitions may simply become exponentially faster as the number of vacua becomes more numerous.

3.5.3 Eternal Inflation

In particular resonant tunneling may modify the standard argument for eternal inflation (see [8] for a review) in at least one important way. Eternal inflation can either be of the random walk type or of the false vacuum type. Chaotic eternal inflation [43], [44] occurs when quantum fluctuations of the inflaton up the potential compete successfully with the classical evolution so that in an increasing physical volume the inflaton does not move closer to the nearest local minimum of the potential. This type of eternal inflation car require large field values, and

it can be challenging to construct potentials controlled over the entire field range that lead to chaotic eternal inflation. Eternal inflation can also occur if inflaton is at a local maximum of potential, and the time it takes for the inflaton to move away from the local maximum is longer than the Hubble time. For a single scalar field this type of eternal inflation may be generic, but as the number of scalar fields increases it becomes at least modestly more difficult to satisfy the condition for eternal inflation of this type. Resonant tunneling does not change any of the standard arguments for random walk eternal inflation. Finally eternal inflation arises if the inflaton is stuck in metastable de Sitter vacuum, and the characteristic decay rate per unit volume of that vacuum is smaller than H^4, where H is the Hubble parameter. If the decay is dominated by Coleman-de Luccia or Hawking-Moss tunneling, then the decay rate per unit volume is generally much smaller than H^4. However it is plausible that if there are a sufficiently large number of vacua resonant and catalyzed tunneling could make this last type of eternal inflation unlikely. The implication of this phenomenon on the behavior of the universe cannot be understated. It is interesting that He-3 experiments may help clarify some outstanding theoretical issues in cosmology.

CHAPTER 4

COLEMAN-DE LUCCIA TUNNELING AND THE GIBBONS-HAWKING TEMPERATURE

4.1 Introduction

Tunneling in the presence of gravity was first beautifully analyzed by Coleman and de Luccia (CDL) [6]. This problem emerges in the study of the early universe in relation to the inflationary epoch, and more recently, in relation to the cosmic landscape as suggested by superstring theory. However, there are properties of the CDL tunneling that remain to be better understood.

Consider a simplified theory of a single scalar field with potential $V(\phi)$ and a canonical kinetic term in the presence of gravity. The potential $V(\phi)$ has a false vacuum V_+ at ϕ_+ and a true vacuum V_- at ϕ_-, so the energy density difference between them is $\epsilon = V_+ - V_- > 0$. The potential barrier between these two local minima has height V_T, as shown in Figure 4.1.

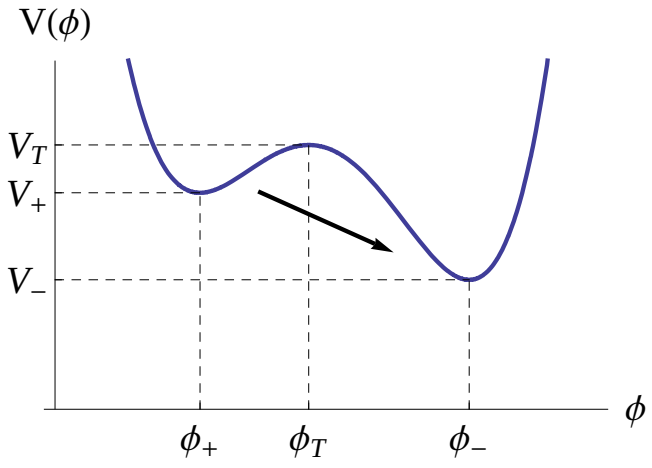

Figure 4.1: Potential $V(\phi)$.

In the semiclassical approximation, the tunneling rate per unit volume is given by

$$\Gamma \simeq Ae^{-B}, \tag{4.1}$$

$$B = S_E(\phi) - S_E(\phi_+) \tag{4.2}$$

where $S_E(\phi)$ is the Euclidean action for the bounce solution and $S_E(\phi_+)$ is the Euclidean action evaluated at the false vacuum at ϕ_+. In the thin-wall approximation ($\epsilon \to 0$), when the vacuum energy density is negligible compared to the Planck scale, B recovers the result in the absence of gravity [15], as expected. On the other hand, as we increase $V_+ \gtrsim V_-$, while still in the thin-wall approximation [45], B takes a different form,

$$B \simeq \frac{27\pi^2\sigma^4}{2\epsilon^3} \to \frac{2\pi^2\sigma}{H^3} \tag{4.3}$$

where σ is the domain wall tension and the Hubble constant is given by $H^2 = 8\pi G_N V_+/3 = V_+/3M_p^2$. Note that the first form (when V_+ is small) is independent of V_+ while the second form is independent of $\epsilon = V_+ - V_-$. We see that, for fixed σ, B decreases rapidly as H increases. It seems that we can easily have a situation where $B \ll 1$, in which case, the tunneling is not exponentially suppressed at all (and the evaluation of the prefactor A in (4.1) as well as subdominant contributions to Γ becomes important).

A similar phenomenon seems to be happening in the Hawking-Moss (HM) tunneling [7],

$$B_{HM} = 24\pi^2 M_p^4\left(\frac{1}{V_+} - \frac{1}{V_T}\right) = 24\pi^2 M_p^4 \frac{\Delta V_+}{V_T V_+} \sim \frac{8\pi\Delta V_+}{3H^4} \tag{4.4}$$

where $\Delta V_+ = V_T - V_+$. Note that if we move $V(\phi)$ up without changing its shape, that is, keeping ϵ, σ and ΔV_+ fixed, B decreases like H^{-3} or H^{-4}, depending on which formula (i.e., thin wall or HM) is applicable. In this chapter, we will see if

and under what conditions this phenomenon is real. More precisely, we examine the CDL tunneling more generally to see when the thin-wall approximation or the HM formula (4.4) is valid.

CDL tunneling concerns quantum fluctuations in the false vacuum of a nucleation bubble which subsequently grows classically. The following picture emerges. Depending on the properties of $V(\phi)$, there are four regions in the parameter space, yielding four different situations how the nucleation bubble is created :

(I) The center of the nucleation bubble is in the true vacuum V_- while the outside of the bubble reaches the false vacuum V_+. The thin-wall approximation is a special limit ($\epsilon \to 0$) in this case.

(II) The outside of the bubble reaches the false vacuum V_+ but the inside of the nucleation bubble never reaches the true vacuum V_- in the Euclidean solution. After the creation of the bubble, its inside falls towards the true vacuum V_- as the bubble grows.

(III) The inside of the bubble reaches V_-, but the outside of the bubble does not reach the false vacuum in the Euclidean action, due to the presence of the de Sitter horizon.

(IV) Not only does the inside of the bubble not reach V_-, the outside of the bubble does not reach the false vacuum in the Euclidean action, due to the presence of the de Sitter horizon. HM tunneling is a special limit in this case.

In the absence of gravity, regions far away from the bubble are by definition in the false vacuum, so we have only case (I) and (II). In the presence of gravity,

the de Sitter horizon cut off the scalar field ϕ as it tries to reach the false vacuum at large distance from the nucleation bubble [46]. That is why case (III) and (IV) are possible. This phenomenon of cases (III) and (IV) may be interpreted as a Gibbons-Hawking (GH) temperature $T_H = H/2\pi$ effect. This point was recently made by Brown and Weinberg [47], who show that tunneling in the presence of gravity may be interpreted as a combination of thermal (Gibbons-Hawking temperature) fluctuation plus quantum tunneling. We agree with this picture. That is, ϕ thermally fluctuates from the false vacuum at ϕ_+ part way up the potential (to ϕ_{f+}) before quantum tunneling to the other side of the barrier. In the Hawking-Moss limit, it fluctuates all the way to the top of the barrier at V_T. Here, our explicit calculations (in particular, the determination of ϕ_{f+}) allow us to estimate in some detail, for a given potential, the individual contribution of the thermal fluctuation versus that of the quantum tunneling in the tunneling rate. We also evaluate the back-reaction effect on the background geometry and show that it can be very important.

There are a few other properties that are worth mentioning here.

• The thin-wall approximation is valid only when the tunneling belongs to case (I). In addition to the case (I) conditions (to be specified), we see that $M_P^4 \gg V_T \gg \Delta V_+ \gg \epsilon$. As we increase V_T with a generic fixed shape of $V(\phi)$ (with $\epsilon > 0$), the tunneling goes over to case (IV) via case (II) and/or case (III).

• For large V_T and $\epsilon > 0$, case (IV) is generic, where HM tunneling is a special limit. Here we estimate the accuracy of the HM formula (4.4) and its correction. We see that the HM formula for B is an over-estimate, by as much as a factor of three. That is, the actual decay is a combination of thermal tunneling and quantum tunneling, whose rate can be much faster.

• Another interesting point is that tunneling in the absence of gravity is always downwards, while gravitational effects allow tunneling upwards.

• With an overall picture, we see that the fast drop off of B as H increases is real. This is illustrated in Figure 4.2, where case (III) does not appear due to the particular choice of the potential used.

• Strictly speaking, for a "general" smooth potential with varying parameters, the above four cases may reduce to case (IV) only. However, within case (IV), it contains regions that resemble the various cases discussed above. The triangular potential has four different cases so it actually demonstrates the change from thin wall to HM case more dramatically (but does not change the physics qualitatively.)

• As B decreases, multi-nucleation bubbles will form and the phase transition involves bubble collisions. Once B is small (say $B \lesssim 1$), Eq.(4.1) is no longer valid. The prefactor and sub-leading terms will become important. All we can say is that tunneling is no longer exponentially suppressed. The rate of transition depends on the details. We do expect that O(4) nucleation bubbles no longer dominate. That is, bubbles of other shapes as well as bubble collisions become important. The transition can be complicated and is at a fast time scale. Something analogous to spinodal decomposition may happen.

In terms of pure thermal (Gibbons-Hawking (GH) temperature) tunneling the suppression of the tunneling is interpreted as due to the Boltzmann factor, where the bubble is a 3-sphere and the inverse temperature is treated as an imaginary time with period $1/T_H$. In case (I) and (II), we see that the quantum tunneling is dominant (i.e., has a smaller value) due to the $O(4)$ symmetry that is

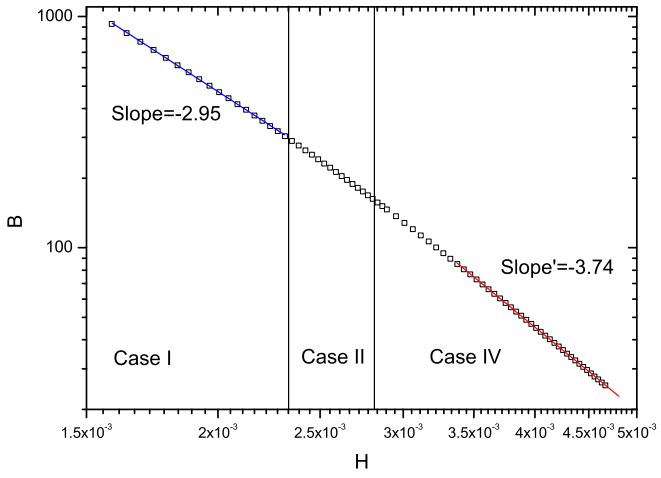

Figure 4.2: The log-log plot of the tunneling exponent B as a function of the Hubble parameter H for a fixed potential $V(\phi)$ except for its overall height as measured by H. ($G \equiv 1$). The three cases are separated by the two solid vertical lines. As $H \sim \sqrt{V_T}$ increases, the tunneling behavior goes from case (I) to case (IV) via case (II); that is, it goes from the CDL thin-wall approximation (to the left in case (I), with slope ~ -3 as given by Eq.(4.3)), to the HM tunneling (to the right of case (IV), with slope ~ -4 as given by Eq.(4.4)). For this particular potential, the slope case (IV) (~ -3.74) never quite reaches the HM value due to corrections. The specific potential used here is described in Sec. 6. Case (III) does not appear for this potential.

lacking in the finite temperature effect. So strictly speaking, the enhancement of the tunneling rate due to a large vacuum energy density is a pure gravitational effect. In de Sitter-like vacua, we may interpret this as a GH temperature effect in the presence of an enhanced (here $O(4)$) symmetry. In case (III) and (IV), the GH temperature starts to play a more prominent role.

The same GH temperature will also contribute to the finite temperature effect on the potential $V(\phi) \to V(\phi, T_H)$ [48, 49]. This contribution is perturbative

in the couplings while its effect in tunneling is non-perturbative. In the finite temperature formalism, this leads to a term of the form $T_H^2\phi^2$ into the finite temperature potential. In the gravity perspective, this is simply a coupling of the form $R\phi^2$, where R is the Ricci scalar. One an also interpret this as a finite volume effect, due to Gauss's law, $H^2\phi^2$, where H^{-1} is the horizon size. The overall picture is self-consistent and clear.

We shall comment on the impact of the GH temperature on the cosmic landscape, both on the shape of the effective potential of the landscape and on the tunneling rate. Because of fast tunneling when the wavefunction of the universe is high up in the landscape, it is likely that the universe is quite mobile there.

For a general potential $V(\phi)$, the coupled equations of $\phi(\xi)$ and the cosmic scale factor $r(\xi)$ are too complicated to solve even in the absence of the gravity except in the thin-wall approximation. However, for some special potentials, say, the triangular potential $V(\phi)$ (Figure 4.3), the bounce B can be obtained analytically [50]. So it is natural to consider the tunneling rates for such a potential in the presence of gravity. Unlike Ref.[50], we cannot get an exact analytic formula for B in the presence of gravity, but the resulting analytic study gives a very good approximation and does simplify enough for us to see the overall picture. Here the absolute height of the potential, which corresponds to the vacuum energy density, is important for tunneling with gravity. To be specific, we shall adopt this triangular potential in this chapter.

The rest of the chapter is organized as follows. In Sec. 4.2, we briefly review the overall framework of tunneling in de Sitter space. This framework is the CDL tunneling formalism. In Sec. 4.3, we go back to tunneling in the absence of gravity. In particular, we review the special case of tunneling in a triangular

potential studied by Duncan and Jensen [50]. Here we emphasize the formulation that is suitable in the extension of their analysis to include gravity. Sec. 4.4 presents the setup for tunneling in de Sitter space, again using the triangular potential. As ϕ varies, the tunneling is not happening in pure de Sitter space and the back-reacrtion is estimated. Sec. 4.5 presents the main result of this chapter. The above four cases and their conditions are discussed. The meaning and implications of the results are discussed in Sec. 4.6. We then discuss thermal tunneling in Sec. 4.7. Here we are referring to the treatment of the de Sitter horizon effect as a Gibbons-Hawking temperature effect. In Sec. 4.8, we point out that the Gibbons-Hawking temperature should also modify the potential via finite temperature effect on potentials. We then consider the implication of the Gibbons-Hawking temperature on the cosmic landscape. Sec. 4.9 contains the summary and some remarks.

4.2 Coleman-de Luccia Tunneling

Let us consider the theory of a single scalar field ϕ with a potential $V(\phi)$ in the presence of gravity, given by

$$S = \int d^4x \sqrt{-g}\left[\frac{1}{2}g^{\mu\nu}\partial_\mu\phi\partial_\nu\phi - V(\phi) - \frac{R}{2}\kappa\right], \tag{4.5}$$

where $\kappa = 8\pi G = 1/M_p^2$.

The potential $V(\phi)$ has a false vacuum V_+ at ϕ_+ and a true vacuum V_- at ϕ_-. There is a potential barrier between these two local minima, as shown in Figure 4.1. Let the height of the barrier at ϕ_T be V_T. We have chosen $\phi_- > \phi_T > \phi_+$. Let the energy density difference between the false and the true vacua be $\epsilon = V_+ - V_- > 0$.

In the presence of gravity, the CDL tunneling rate per unit volume is given by Eq. (4.1,4.2), in term of the coefficient $B = S_E(\phi) - S_E(\phi_+)$, where $S_E(\phi)$ is the Euclidean action for the bounce solution and $S_E(\phi_+)$ is the Euclidean action evaluated at the false vacuum. Since a Euclidean solution with a $O(4)$ symmetry has an etremum action, B is in general dominated by the "bounce" solution with $O(4)$ symmetry. This solution has the Euclidean metric,

$$ds^2 = d\xi^2 + r(\xi)^2 d\Omega_s^2, \tag{4.6}$$

where $d\Omega_s^2$ is the metric of a unit 3-sphere. The Euclidean equation for the "bounce" solution is determined by the minimum value of the Euclidean action,

$$\phi'' + \frac{3r'}{r}\phi' = \frac{dV}{d\phi} \tag{4.7}$$

$$r'^2 = 1 + \frac{r^2}{3M_p^2}\left(\frac{1}{2}\phi'^2 - V\right). \tag{4.8}$$

where the prime is derivative with respect to ξ. Here the Einstein equation yields one non-trivial equation, since the equation of motion for $r(\xi)$ follows from Eqs. (4.7,4.8). We can choose $r(0) = 0$. Using Eq.(4.8) to simplify the Euclidean action, one obtains

$$S_E = 4\pi^2 \int d\xi \left[r^3 V - \frac{3r}{\kappa}\right] \tag{4.9}$$

The CDL instanton is a unique solution with the topology of a four sphere S^4 in Euclidean space [51]. The geometry after bubble nucleation is described by the analytic continuation of the CDL instanton to Lorentzian signature. The radial coordinate ξ is continued to $\xi = it$ and the metric in Lorentzian frame is

$$-ds^2 = -dt^2 + r^2(it) d\Omega_{H^3}^2, \tag{4.10}$$

here the metric is multiplied by an overall minus sign and $d\Omega_{H^3}$ is the element of length for a unit hyperboloid with timelike normal. The metric within the spherical bubble describes a spatially open Friedmann-Robertson-Walker Universe.

As we shall see, a qualitative picture emerges: depending on the properties of the potential, there are four different cases how the nucleation bubble is created :

(I) The center of the nucleation bubble reaches the true vacuum V_- while the outside of the bubble reaches the false vacuum V_+. The thin-wall approximation is a special limit ($\epsilon \to 0$) in this case.

(II) The outside of the bubble reaches the false vacuum V_+ but the inside of the nucleation bubble never reaches the true vacuum V_- in the Euclidean solution. After the creation of the bubble, its inside will fall towards the true vacuum V_- as the bubble grows.

(III) The inside of the bubble reaches V_-, but the outside of the bubble does not reach the false vacuum V_+ in the Euclidean action, due to the presence of the de Sitter horizon. This case and the next case never happen in the absence of gravity, since we start with the false vacuum everywhere. Far from the bubble, ϕ approaches the false vacuum by definition. However, when the vacuum energy is not negligible, there is a de Sitter horizon so it is possible that ϕ hits the horizon before it reaches the false vacuum.

(IV) Not only does the inside of the bubble not reach V_-, the outside of the bubble does not reach the false vacuum in the Euclidean action. The HM tunneling is the limit in this case. Here we are able to estimate the accuracy of the

Hawking-Moss formula and its correction, which can be substantial.

For a general potential $V(\phi)$, the coupled equations (4.7, 4.8) are complicated to solve. In the absence of the gravity, for some simple potentials, say, the triangular potential $V(\phi)$ (Figure 4.3), the bounce B can be obtained analytically [50]. Then it is natural to consider the tunneling rates for such potentials in the presence of the gravity. Unlike Ref.[50], we cannot get an analytical formula for B in the presence of gravity, but the analysis does simplify enough for us to see the overall picture. Here the absolute height of the potential, which corresponds to the vacuum energy density, is important for tunneling with gravity. To be specific, we shall adopt this triangular potential in this chapter.

The triangular potential may be parametrized in the following way. Let the height of the barrier of $V(\phi)$ at ϕ_T be V_T, which also provides a measure of the overall vacuum energy density. Let $\Delta V_\pm = (V_T - V_\pm)$. Both $\Delta\phi_+ = \phi_T - \phi_+$ and $\Delta\phi_- = \phi_- - \phi_T$ are defined to be positive so the slopes (gradients) $\pm\lambda_\pm$ of $V(\phi)$ are given by

$$\lambda_\pm = \frac{\Delta V_\pm}{\Delta\phi_\pm} \tag{4.11}$$

Note that, in general, $\lambda_+ \neq \lambda_-$. Since the $\epsilon = \Delta V_- - \Delta V_+ > 0$, we have

$$\eta = \sqrt{\frac{\Delta V_+}{\Delta V_-}} = \frac{1}{\sqrt{1 + \epsilon/\Delta V_-}} < 1 \tag{4.12}$$

$\Delta\phi_+$, $\Delta\phi_-$ and λ. Here, to simplify the solution, we set $\lambda_L = \lambda_R = \lambda$.

4.3 Tunneling Without Gravity

When gravity is negligible, Eq. (4.8) reduces to $r' = 1$. This happens if we set $\kappa = 0$. Alternatively, this is a very good approximation when the overall height

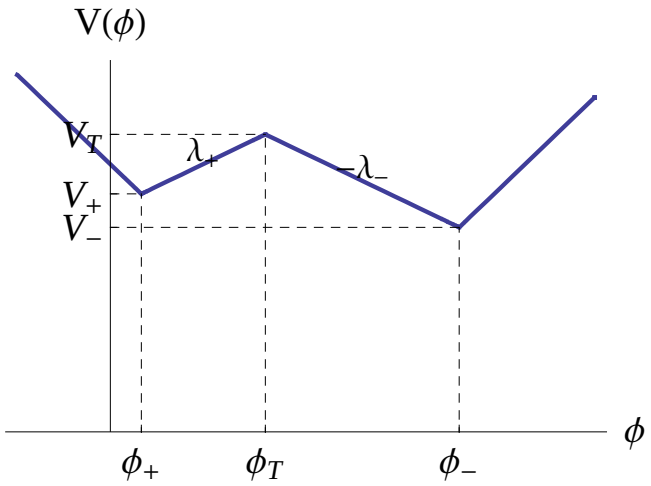

Figure 4.3: Triangular potential $V(\phi)$. The false vacuum is at $V_+ = V(\phi_+)$ and the true vacuum is at $V_- = V(\phi_-)$, with the top of the barrier at $V_T = V(\phi_T)$. Here λ_+ and $-\lambda_-$ are the gradients.

of the potential is much smaller than the Planck scale.

With $r(\xi = 0) = 0$, we have $r = \xi$, so tunneling reduces to the simple case without gravity. The solution must satisfy the boundary condition,

$$\phi'(0) = 0 \tag{4.13}$$

which is necessary for ϕ to make sense at the center of the nucleation bubble. At large radius, we expect

$$\phi \to \phi_+, \qquad \xi \to \infty \tag{4.14}$$

As we shall see, this condition may be modified when gravity is important.

Let us first review the solution to the triangular potential without gravity, the case worked out by Duncan and Jenson [50]. For $\phi_+ \le \phi \le \phi_-$, Eq.(4.7) becomes

$$\phi'' + \frac{3}{\xi}\phi' = \frac{dV}{d\phi} = \pm\lambda_\pm \tag{4.15}$$

The general solution is

$$\phi(\xi) = a + b/\xi^2 \pm \lambda_\pm \xi^2/8 \tag{4.16}$$

where the constant a and b are determined by the boundary conditions and by matching the field values and their derivatives at the top of the barrier, which occurs at some radius ξ_T to be determined.

It is easy to see that ϕ will reach its false vacuum value at finite radius ξ_+ (to be determined) and then stay there. The above boundary condition (4.14) is replaced by

$$\begin{cases} \phi(\xi_+) = \phi_+ \\ \phi'(\xi_+) = 0 \end{cases} \tag{4.17}$$

while there are two possibilities to satisfy the condition (4.13). The first case, namely case (I), is when ϕ stays close to ϕ_- until at radius ξ_- when ϕ starts to decrease under Eq.(4.15). The boundary conditions in this case are

$$\begin{cases} \phi(\xi) = \phi_- \qquad 0 \le \xi \le \xi_- \\ \phi'(\xi_-) = 0 \end{cases} \tag{4.18}$$

The other possibility, namely case (II), happens when, at the time of creation, the inside of the bubble never reaches the true vacuum. In this case, the boundary conditions are

$$\begin{cases} \phi(0) = \phi_0 \\ \phi'(0) = 0 \end{cases} \tag{4.19}$$

where the initial value ϕ_0 is to be determined. This case only happens if ϕ_0 is to the right side of the barrier (i.e., near ϕ_-) and $\phi_0 \le \phi_-$. Also, we expect $V_+ \ge V(\phi_0) \ge V_-$.

4.3.1 Case (II)

Let us consider case (II) first. On the right and left sides of the barrier, we have

$$\begin{cases} \phi_R(\xi) = \phi_0 - \frac{\lambda_-}{8}\xi^2 & 0 \le \xi \le \xi_T \\ \phi_L(\xi) = \phi_+ + \frac{\lambda_+}{8\xi^2}(\xi^2 - \xi_+^2)^2 & \xi_T \le \xi \le \xi_+ \end{cases} \tag{4.20}$$

Matching the derivatives of the two solutions (4.20) at ξ_T,

$$\xi_+^4 = (1+c)\xi_T^4 \tag{4.21}$$

where $c = \lambda_-/\lambda_+$. Matching the field values at ξ_T yields

$$\begin{cases} \phi_0 = \phi_T + \frac{\lambda_-}{8}\xi_T^2 \\ \Delta\phi_+ = \phi_T - \phi_+ = \frac{\lambda_+}{8}\left(\sqrt{1+c} - 1\right)^2 \xi_T^2 \end{cases} \tag{4.22}$$

Now that the unknowns ξ_T, ξ_+ and ϕ_0 are determined in terms of properties of the potential $V(\phi)$, we simply insert the solution (4.20) into the Euclidean action and integrate it from $\xi = 0$ to $\xi = \xi_+$. The bounce (4.2) is given by

$$B = \frac{32\pi^2}{3}\frac{1+c}{(\sqrt{1+c}-1)^4}\frac{(\Delta\phi_+)^4}{\Delta V_+} \tag{4.23}$$

Let $\Delta V_0 = V_T - V_0 = V_T - V(\phi_0)$ so, using Eq.(4.22),

$$\frac{\Delta V_+}{\Delta V_-} < \frac{\Delta V_+}{\Delta V_0} = \frac{\left(\sqrt{1+c}-1\right)^2}{c^2} \tag{4.24}$$

which implies that tunneling is always downward, and $\Delta V_+/\Delta V_0 \le 1/4$.

Recall that case (II) holds only if $V_0 > V_-$, or $\phi_0 \le \phi_-$, which translates to the above condition (4.24). or equivalently, $\beta > 1$, where

$$\beta = \sqrt{\frac{\Delta V_-}{\Delta V_+}}\frac{\Delta\phi_- - \Delta\phi_+}{2\Delta\phi_-} \tag{4.25}$$

In general, β is semi-positive. If $\beta = 1$, then $\phi_0 = \phi_-$ and one can rewrite the bounce (4.23) in the following form

$$B = \frac{2\pi^2}{3}\frac{(\Delta\phi_-^2 - \Delta\phi_+^2)^2}{\Delta V_+} \tag{4.26}$$

4.3.2 Case (I)

If $\beta < 1$, the inside of the bubble reaches the true vacuum V_-, that is, $\phi(0) = \phi_-$. At certain radius ξ_-, ϕ begins to decrease until it reaches ϕ_+ at radius ξ_+. The region for $\xi > \xi_+$ stays at the false vacuum. Now, the solution $\phi(\xi)$ contains four pieces,

$$\phi(\xi) = \begin{cases} \phi_- & x \in [0, \xi_-] \\ \phi_1(\xi) = \phi_- - \frac{\lambda_-}{8\xi^2}(\xi^2 - \xi_-^2)^2 & x \in [\xi_-, \xi_T] \\ \phi_2(\xi) = \phi_+ + \frac{\lambda_+}{8\xi^2}(\xi^2 - \xi_+^2)^2 & x \in [\xi_T, \xi_+] \\ \phi_+ & x \geq \xi_+ \end{cases} \tag{4.27}$$

where $\phi_- \geq \phi_1(\xi) \geq \phi_T$ and $\phi_+ \leq \phi_2(\xi) \leq \phi_T$. Now we have three unknowns : ξ_T, ξ_- and ξ_+. Matching the derivatives as well as the field values at ξ_T yields

$$\begin{cases} \xi_+^4 - \xi_T^4 = c(\xi_T^4 - \xi_-^4) \\ \Delta\phi_+ = \frac{\lambda_+}{8\xi_T^2}\left(\xi_T^2 - \xi_-^2\right)^2 \\ \Delta\phi_- = \frac{\lambda_-}{8\xi_T^2}\left(\xi_T^2 - \xi_-^2\right)^2 \end{cases} \tag{4.28}$$

so ξ_T, ξ_- and ξ_+ can be solved in terms of the properties of $V(\phi)$. Once again, one can insert these solutions of the parameters into the ϕ solution (4.27) and evaluate the bounce. We find that it is convenient to introduce the tension to be

$$\sigma = \sigma_+ + \sigma_- \tag{4.29}$$

$$\sigma_\pm = \pm \int_{\phi_\pm}^{\phi_T} d\phi \, \sqrt{2[V(\phi) - V_\pm]} = \frac{2}{3}\sqrt{2\Delta V_\pm}\Delta\phi_\pm \tag{4.30}$$

After some algebra, B can be written in terms of these values

$$B = \frac{27\pi^2}{32\epsilon^3}[\sigma_+(1 + 1/\eta) + \sigma_-(1 + \eta)]^3[\sigma_+(3/\eta - 1) + \sigma_-(3\eta - 1)] \tag{4.31}$$

where $\epsilon = V_+ - V_-$ and $\eta^2 = \Delta V_+/\Delta V_- < 1$ (4.12). In the limit $\beta \to 1$, B in (4.31) reduces to B in (4.26), that is, it agrees with B in case (II).

Here $\sigma_\pm$ in Eq. (4.30) should be treated as a convenient definition. The value of σ as defined should be very close to the actual domain wall tension. For more general potentials, the coefficient 2/3 in Eq. (4.30) will have order one variations. Note that $\epsilon/\Delta V_- = 1 - \eta^2$. In the thin-wall approximation, $\eta \to 1$ as $\epsilon/\Delta V_-$ becomes small, and B reduces to the usual thin-wall formula for B,

$$B \to \frac{27\pi^2}{2\epsilon^3}\sigma^4 \tag{4.32}$$

So we see that the thin-wall approximation is inside the region of case (I). Comparing the small $\epsilon/\Delta V_-$ case to that in case (I) Eq.(4.24), we see that there is a sizable parameter region where the thin-wall approximation is not valid. For case (II), since the inside of the bubble never reaches the true vacuum value ϕ_-, the wall tension does not carry much physical significance here. The non thin-wall approximation has also been studied in Ref.[52].

In summary, the regions (I) and (II) are divided by the value of β (4.25): case (I) if $0 \le \beta < 1$ and case (II) ($\phi(0) = \phi_0 < \phi_-$) if $\beta > 1$. For $\beta = 1$, only the center of the bubble reaches the true vacuum.

In the absence of gravity, the overall height of the potential is not important, so the triangular potential is parameterized by a set of four parameters, namely ($\Delta V_\pm$, $\Delta\lambda_\pm$). This set can be replaced by an equivalent set ($\Delta V_\pm$, $\Delta\phi_+$, c). The bounce B in Eq.(4.23) is expressed in terms of this set, where we see that ΔV_- does not enter, since the inside of the bubble never reaches V_-. In Eq.(4.31), we express B in terms of an equivalent set ($\sigma_\pm$, ϵ, η), which is more convenient when we want to take the thin-wall limit. Here, we also see how B behaves as we move away from the triangular potential: the leading order correction is automatically incorporated into the two tension components $\sigma_\pm$ by varying appropriately the 2/3 coefficient in Eq.(4.30).

If $\lambda_- = \lambda_+$, we see that β simplifies somewhat,

$$\beta = \frac{(1-\eta)}{2\sqrt{\eta}} \tag{4.33}$$

where $0 < \eta < 1$ is given in Eq.(4.12); so the dividing point is at $\eta_c = (\sqrt{2}-1)^2 \approx 0.17$. Often times in our analysis below, we shall restrict ourselves to this special case.

4.4 Turning on Gravity

Let us now turn on gravity [6], so the triangular potential has five parameters, namely $(\Delta V_\pm, \Delta\lambda_\pm, V_T)$. As noted above, at times, it may be convenient to choose an alternative but equivalent set of parameters.

To emphasize the effect of gravity, let us consider the situation where

$$V_T \gg \Delta V_- = V_T - V_- \tag{4.34}$$

where $V_T/M_P^4 \ll 1$ so gravitational effects can be important for the tunneling while the semi-classical approximation is still valid.

The equation (4.7) now reads,

$$r'^2 = 1 + \frac{r^2}{3M_p^2}(L - V_T), \tag{4.35}$$

where $L = \phi'^2/2 - V + V_T$ is the (shifted) Euclidean energy. By (4.34), for large V_T, we use the approximation

$$r'^2 \sim 1 - \frac{r^2}{3M_p^2}V_T = 1 - H^2 r^2. \tag{4.36}$$

where

$$H^2 = V_T/3M_p^2 \tag{4.37}$$

is the Hubble constant of the de Sitter space with vacuum energy V_T. So we have

$$r(\xi) = H^{-1}\sin(H\xi) \tag{4.38}$$

where $r(0) = r(\pi/H) = 0$. That is, the range of ξ is bounded, $0 \le \xi \le \pi/H$.

It is easy to check that this approximation is self-consistent, i.e., $|L(\xi)| \ll V_T$. For a tunneling solution, $\phi(\xi) \in [\phi_-, \phi_+]$, so

$$L \ge 0. \tag{4.39}$$

Using Eq.(4.7),

$$L' = \left(\frac{1}{2}\phi'^2 - V(\phi)\right)' = -3\frac{r'}{r}\phi'^2 \sim -3H\cot(H\xi)\phi'^2 \tag{4.40}$$

When $\xi \in [0, \pi/2H)$, $L' \le 0$ and if $\xi \in (\pi/2H, \pi/H]$, $L' \ge 0$. Therefore $\max L = \max\{L(0), L(\pi/H)\} \le \Delta V_-$. So $|L| \ll V_T$, and Eq.(4.38) is valid to the leading order in $\Delta V_-/V_T$. For later purposes, we note that

$$S_E(\phi_+) = -\frac{24\pi^2 M_p^4}{V_+} \tag{4.41}$$

The equations (4.7, 4.8) are now decoupled, and

$$\phi'' + 3H\cot(H\xi)\phi' = \frac{dV}{d\phi}. \tag{4.42}$$

and can be solved with appropriate boundary conditions. This we shall do in the next section.

The bounce solution $\phi(\xi)$ will modify the geometric background used, i.e., $r(\xi)$ in (4.38). As we shall see, it is important to include this back-reaction. Inserting $\phi(\xi)$ back into Eq.(4.35), we get a first-order differential equation of the leading-order correction of r, namely $\delta r(\xi)$,

$$\cos(H\xi)\delta r' = -H\sin(H\xi)\delta r + \frac{L(\xi)}{2V_T}\sin^2(H\xi). \tag{4.43}$$

The formal solution for δr is,

$$\delta r(\xi) = \cos(H\xi) \cdot \int_0^{\xi} d\eta \tan^2(H\eta) \frac{L(\eta)}{2V_T}, \tag{4.44}$$

where the superficial singularity at $\eta = \pi/(2H)$ can be regularized as

$$\begin{aligned} \delta r(\xi) &= \cos(H\xi) \cdot \int_0^{\xi} d\eta \tan^2(H\eta) \frac{L(\eta) - L(\frac{\pi}{2H})}{2V_T} \\ &+ \frac{H^{-1}\sin(H\xi) - \xi\cos(H\xi)}{2V_T} \cdot L\Big(\frac{\pi}{2H}\Big). \end{aligned} \tag{4.45}$$

Notice that by (4.40), $L'(\pi/2H) = 0$ and the integral is well defined. Now we can consider the Euclidean action for this solution, to the leading order of $\Delta V_-/V_T$,

$$\begin{aligned} S_E &= 4\pi^2 \int_0^{\xi_{max}} d\xi \Big((r+\delta r)^3 V(\xi) - 3(r+\delta r) M_p^2 \Big) \\ &= 4\pi^2 \int_0^{\pi/H} d\xi \Big(r^3 V_T - 3 r M_p^2 \Big) && (4.46) \\ &+ 4\pi^2 \int_0^{\pi/H} d\xi \Big(\delta r (3r^2 V_T - 3M_p^2) + r^3 (V(\xi) - V_T) \Big) && (4.47) \\ &+ O\Big(\frac{\Delta V_-^2}{V_T^2}\Big) && (4.48) \end{aligned}$$

We separate the result into three parts. The first part (4.46) is $-24\pi^2 M_p^4/V_T$, the de-Sitter space Euclidean action. The second part (4.47) is suppressed by a small factor $\Delta V_-/V_T$ comparing with the first part, because by (4.45) the magnitude of δr is of $H^{-1}\Delta V_-/V_T$, and the magnitude $V(\xi) - V_T$ is at most ΔV_-. We will explicitly see that the two terms in the second part, which correspond to δr and ϕ contribution are of the same order and therefore the computation of $\delta r(\xi)$ in Eq. (4.45) is important. The last part represents all the high order terms of $\Delta V_-/V_T$. Notice that by the perturbation δr, ξ_{max} is no longer π/H. However, the action change induced by $(\xi_{max} - \frac{\pi}{H})$ is of the second order of the $\Delta V_-/V_T$ and hence is included in (4.48).

In conclusion, if we can get the analytic solution of (4.42) then the leading order of r is immediately given by the integral in (4.45). It then follows that

(4.46) and (4.47) give the leading order Euclidean action. Subtracting $S_E(\phi_+)$ given by(4.41) from it, we get the factor B.

4.5 The Four Scenarios of Tunneling in de Sitter Space

In general, Eq. (4.42) is still too difficult to solve in a way that the physics is transparent. However, for the triangle potential, we can solve (4.42) analytically. For the different choices of the five parameters V_T, $\Delta\phi_+$, $\Delta\phi_-$, $\lambda_\pm$, we find here are four different kinds of Euclidean solutions for ϕ (shown in Figure 4.4) :

- Case (I) $\phi(\xi)$ reaches both ϕ_+ and ϕ_-. This happens when $\alpha\lambda/H^2\Delta\phi_+ \geq 1$ and $(\lambda/H^2)I(H^2\Delta\phi_+/\lambda) \geq \Delta\phi_-$ where $\alpha \sim 0.4$ and $I(x)$ is a monotonic function shown in Figure 4.6.
- Case (II) $\phi(\xi)$ reaches ϕ_+ but not ϕ_-. That is, $\phi(\xi)$ reaches ϕ_+ and ϕ_{t-}, where $\phi_T \leq \phi_{t-} < \phi_-$. This happens when both $\alpha\lambda/H^2\Delta\phi_+ \geq 1$ and $(\lambda/H^2)I(H^2\Delta\phi_+/\lambda) < \Delta\phi_-$ are satisfied.
- Case (III). $\phi(\xi)$ reaches ϕ_- but not ϕ_+. That is, $\phi(\xi)$ reaches ϕ_{f+}, where $\phi_T \geq \phi_{f+} > \phi_+$. This case can happen only when the gradient towards the true vacuum is steeper than that towards the false vacuum.
- Case (IV). $\phi(\xi)$ reaches neither ϕ_+ nor ϕ_-. That is, $\phi(\xi)$ reaches only ϕ_{f+} and ϕ_{t-}. This case happens when $\alpha\lambda/H^2\Delta\phi_+ < 1$ is satisfied.

In the absence of gravity, the triangle potential just has two kinds of bounce solutions [50], the cases (I) and (II). Here, including gravity, we have a new bounce solution, either case (III) or case (IV), because here there is a cut-off ξ_{max} of the radius coordination ξ due to the Hubble radius of de Sitter space. So

in the finite range $0 \leq \xi \leq \pi/H$, the bounce solution may reach neither ϕ_+ nor ϕ_-. We will see that case (IV) is like HM tunneling, the case (I) is like thin-wall CDL tunneling, and case (II) is an intermediate case between the two limits. By adjusting the five parameters of the potential, we get a transition from HM tunneling to thin-wall CDL tunneling.

For the triangular potential $V(\phi)$ shown in Figure 4.3, we have, for large V_T,

$$\phi'' + 3H\cot(H\xi)\phi' = \frac{dV}{d\phi} = \pm\lambda_\pm \tag{4.49}$$

whose general solution is given by

$$\phi(\xi) = a_1 \pm \frac{\lambda_\pm}{H^2}\left[f_1(H\xi) + b_1 f_2(H\xi)\right] \tag{4.50}$$

where $f_1(H\xi)$ is the special solution and f_2 is the homogeneous solution.

$$\begin{aligned} f_1(x) &= \frac{3}{8}\cot^2 x - \frac{1}{24}\csc^2 x - \frac{1}{3}\ln(\sin x), \\ f_2(x) &= -\frac{1}{8}\csc^2\left(\frac{x}{2}\right) + \frac{1}{2}\ln\left(\tan\left(\frac{x}{2}\right)\right) + \frac{1}{8}\sec^2\left(\frac{x}{2}\right). \end{aligned} \tag{4.51}$$

Note that $f_2'(H\xi) = H/\sin^3(H\xi)$. The constants a_1 and b_1 are to be determined by the boundary and matching conditions. We begin our discussion with case (IV) since it is new and its limiting case corresponds to HM tunneling.

4.5.1 Case (IV)

For case (IV), the bounce solution of (4.49) contains two pieces, which correspond to the ϕ_- side and the ϕ_+ side,

$$\phi(\xi) = \begin{cases} \phi_R(\xi) & \xi \in [0, \xi_T] \\ \phi_L(\xi) & \xi \in [\xi_T, \pi/H] \end{cases} \tag{4.52}$$

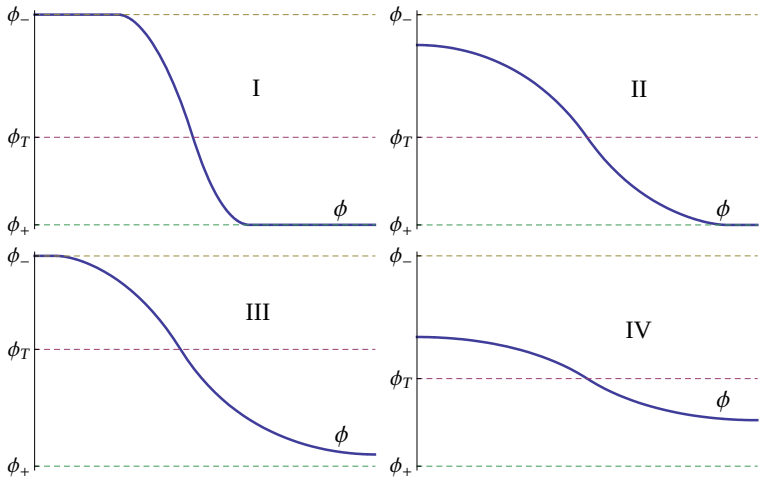

Figure 4.4: The Euclidean bounce solution of $\phi(\xi)$ as a function of $\xi = [0, \pi/H]$ in the four cases: (I) ϕ reaches the true vacuum at ϕ_- inside the nucleation bubble and the false vacuum at ϕ_+ away from the outside of the bubble, (II) ϕ reaches ϕ_+ but not ϕ_-, (III) ϕ reaches ϕ_- but not ϕ_+ and (IV) ϕ reaches neither ϕ_- nor ϕ_+; here the bounce starts at $\phi(0) = \phi_{t-} < \phi_-$ and ends at $\phi(\xi_{max} = \pi/H) = \phi_{f+} > \phi_+$. Case (I) and (II) can happen in the absence of gravity. Case (III) and (IV) can happen due to the presence of the de Sitter horizon. The thin-wall approximation is valid when the transition from ϕ_- to ϕ_+ in case (I) is rapid. The HM formula is a good approximation when the variation of ϕ deviates little from ϕ_T in case (IV).

where $\phi_- > \phi_{t-} \geq \phi_R(\xi) \geq \phi_T$ and $\phi_+ < \phi_{f+} \leq \phi_L(\xi) \leq \phi_T$, whose general form can be obtained analytically. The boundary and matching conditions are

$$\begin{cases} \phi_R'(0) = 0 \\ \phi_R(\xi_T) = \phi_L(\xi_T) = \phi_T \\ \phi_R'(\xi_T) = \phi_L'(\xi_T) \\ \phi_L'(\pi/H) = 0 \end{cases} \tag{4.53}$$

The first and last conditions require the specific combination $f_1 + 2f_2/3$ in the solutions (4.50). Imposing the boundary conditions at ξ_T, we have,

$$\phi_R(\xi) \quad = \quad \phi_T - \frac{\lambda_-}{H^2}(f(H\xi) - f(H\xi_T))$$

$$\phi_L(\xi) \;=\; \phi_T + \frac{\lambda_+}{H^2}(f(\pi - H\xi) - f(\pi - H\xi_T)), \tag{4.54}$$

where

$$f(x) = f_1(x) + \frac{2}{3}f_2(x) = \frac{1}{24}\left(4\sec\left(\frac{x}{2}\right)^2 - 8\ln\left(2\cos\left(\frac{x}{2}\right)^2\right) - 9\right). \tag{4.55}$$

where we note that $f(\pi - x) = f_1(x) - 2f_2(x)/3$. Matching the derivative at ξ_T determines ξ_T,

$$c = \frac{\lambda_-}{\lambda_+} = \frac{f'(\pi - H\xi_T)}{f'(H\xi_T)} \tag{4.56}$$

so all parameters are now fixed.

To simplify the discussion, let us first consider the symmetric case $\lambda = \lambda_+ = \lambda_-$, so the analytical solution has a symmetry about $\xi = \pi/(2H)$, and the solution is particularly simple: $\xi_T = \pi/(2H)$. It is easy to check that $\phi(\xi)$ is a monotonic decreasing function. For this case (IV), we require that $\phi(\xi)$ does not reach ϕ_+ or ϕ_-; in terms of the solution (4.54),

$$\phi_{f+} = \phi_L(\pi/H) > \phi_+, \tag{4.57}$$

Introducing a useful dimensionless parameter

$$\gamma = \frac{\lambda}{H^2\Delta\phi_+} \tag{4.58}$$

the above condition means

$$\alpha\gamma = \frac{\alpha\lambda}{H^2\Delta\phi_+} < 1 \tag{4.59}$$

where

$$\alpha = f(\pi/2) - f(0) = -\frac{1}{24} + \left(\frac{5}{24} + \frac{\ln 2}{3}\right) \sim 0.398 \tag{4.60}$$

is a numerical constant. The similar condition $\phi_R(0) < \phi_-$ is satisfied automatically since $\Delta\phi_- > \Delta\phi_+$. In conclusion, if the parameters of the potential satisfy (4.59), then the bounce solution is case (IV).

Before computing δr and $S_E(\phi)$, we estimate the magnitude of $\phi(\xi)$. By (4.54),

$$|\phi(\xi) - \phi_T| \sim \frac{\lambda}{H^2}. \tag{4.61}$$

When λ is small and H is large, $\phi(\xi)$ is confined in a small region which centers at ϕ_T. Because $\phi \equiv \phi_T$ is the Hawking-Moss bounce solution, case (IV) tunneling is like a fluctuation around HM tunneling and will approach the Hawking-Moss solution when λ/H^2 is small.

Further, for the (shifted) Euclidean energy L,

$$\frac{1}{2}\phi'^2 \sim \frac{\lambda^2}{H^2},\ |V - V_T| \sim \frac{\lambda^2}{H^2} \tag{4.62}$$

Hence $L/V_T \sim \lambda^2 H^{-2}/V_T$. By the condition (4.34) and (4.59), the ratio $\lambda^2/(H^2 V_T) \ll 1$ and hence $L/V_T \ll 1$ and the expansion (4.45) and (4.47) works for case (IV). The only new issue is that for case (IV), the small expansion factor is $\lambda^2/H^2 V_T$ not $\Delta V_-/V_T$, simply because the bounce solution (4.54) does not "feel" ϕ_-. The integral (4.45) is carried out analytically, and by (4.46),(4.47) and (4.48), we find that the two terms in the leading order correction have the same form,

$$S_E(\phi) = \frac{24\pi^2 M_p^4}{V_T} - C\frac{\lambda^2 M_p^6}{V_T^3} + O\Big(\frac{\lambda^4 M_p^8}{V_T^5}\Big). \tag{4.63}$$

where $C = C_1 + C_2 \sim 65.49$ is a positive constant. $C_1 \sim -196.47$ corresponds to the $\delta r(\xi)$ contribution and $C_2 \sim 261.96$ is from $\phi(\xi)$. So we see explicitly that the two terms in Eq. (4.47) are comparable. That is, the back-reaction is important. The above result has a simple interpretation that we shall describe in Sec. 6.

Since the Hawking-Moss scenario is a special limit in this case, let us treat this decay as a HM transition, with a correction to the HM formula that can be explicitly evaluated. So B is given by

$$B = S_E(\phi) - S(\phi_+) \quad = \quad 24\pi^2 M_p^4\Big(\frac{1}{V_+} - \frac{1}{V_T}\Big) - C\frac{\lambda^2 M_p^6}{V_T^3} + O\Big(\frac{\lambda^4 M_p^8}{V_T^5}\Big). \tag{4.64}$$

The first term is just the Hawking-Moss bounce B_{HM} (4.4). while the second term, correction from this bounce solution, lowers B and therefore the actual tunneling rate is larger than that given by the HM formula.

For $V_T \gtrsim V_+$, the first term in the bounce (4.63) is largely cancelled by $S(\phi_+)$, so the corrections can be important. Rewriting the bounce formula as

$$B = B_{HM}\left(1 - \frac{C}{72\pi^2}\gamma\left(\frac{V_+}{V_T}\right) + ...\right) = B_{HM}\left(1 - 0.2317(\alpha\gamma)\left(\frac{V_+}{V_T}\right) + ...\right) \tag{4.65}$$

Since both $\alpha\gamma < 1$ (4.59) and $V_+/V_T < 1$, we see that the correction to the HM formula is at most 23%. [1]

The picture of case (IV) is consistent with the interpretation proposed in [53], [54], [55]. HM tunneling should be interpreted as a quantum fluctuation up the potential barrier. Here we see that the field will thermally fluctuate from V_+ at ϕ_+ up to $V(\phi_L(\pi/H)) < V_T$ at $\phi_L(\pi/H) > \phi_+$, tunnel to $\phi_R(0) < \phi_-$ and then classically roll down to ϕ_-. In the limit where $\gamma\Delta V_+/V_T \to 0$, V_T is simply reached via the thermal fluctuations alone. Here, we see that the correction is typically not very big and the HM formula is quite good in general. On the other hand, as $\gamma \to 1/\alpha = 2.51$, $\phi_L(\pi/H) \to \phi_+$; the outside of the bubble can reach the false vacuum within the horizon. When this happens, the HM formula is no longer accurate.

Now let us consider the more general case where $c = \lambda_-/\lambda_+ \neq 1$. The solution of ξ_T should be determined by

$$c\left(-f_1'(\xi_T) - \frac{2}{3}f_2'(\xi_T)\right) = f_1'(\xi_T) - \frac{2}{3}f_2'(\xi_T) \tag{4.66}$$

[1]Notice that the perturbation series (4.47), (4.47) and (4.48) start from the de-Sitter space Euclidean action, not the HM tunneling exponential factor B_{HM}. So the correction, though large compared to B_{HM}, is still much smaller than the zero order, de-Sitter space Euclidean action. Hence the leading correction yields a very good approximation here. That is, the last term in Eq.(4.63) or (4.64) is negligible.

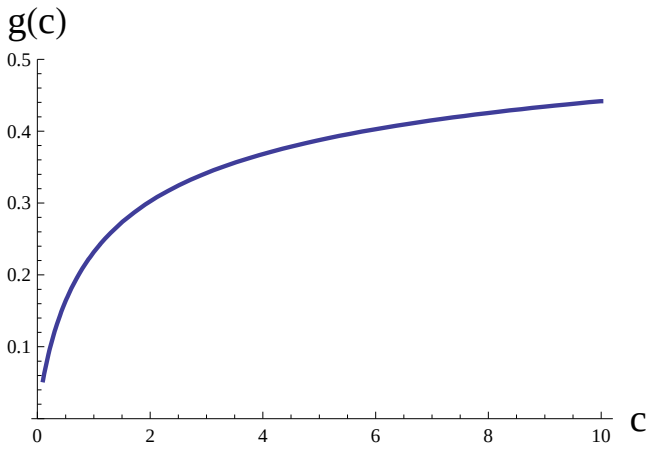

Figure 4.5: The function g(c).

which can be solved numerically. For large c, the solution of ξ_T is determined by series expansion, $\xi_T \sim \sqrt[4]{16/(3c)}$. The condition of the case (IV) is now

$$\alpha(c)\gamma < 1, \tag{4.67}$$

where $\alpha(c) = (f_1(\xi_T) - \frac{2}{3}f_2(\xi_T)) - (f_1(\pi) - \frac{2}{3}f_2(\pi))$, where $\alpha(1) = \alpha \sim 0.398$. For large c, by the asymptotic form of ξ_T, $\alpha(c) \sim \sqrt{C(c)/12}$. We can integrate the solution to get δr and B,

$$\begin{aligned} B &= 24\pi^2 M_p^4\Big(\frac{1}{V_+} - \frac{1}{V_T}\Big) - C(c)\frac{\lambda_+^2 M_P^6}{V_T^3} + O\Big(\frac{\lambda^4 M_P^8}{V_T^5}\Big), &(4.68)\\ &= B_{HM}\Big(1 - \frac{C(c)}{72\pi^2}\gamma\frac{V_+}{V_T}\Big) = B_{HM}\Big(1 - \frac{C(c)}{72\pi^2\alpha(c)}\alpha(c)\gamma\frac{V_+}{V_T}\Big) \\ &\equiv B_{HM}\Big(1 - g(c)(\alpha(c)\gamma)\frac{V_+}{V_T}\Big). &(4.69)\end{aligned}$$

As before, both $\alpha(c)\gamma < 1$ and $V_+/V_T < 1$. The function $g(c)$ is plotted in Figure 4.5, When C is large, $C(c)$ grows as $\sqrt{c}$ and numerically the proportional coefficient is ~ 131. Hence, by the asymptotic form of $\alpha(c)$,

$$g(c) \to 0.64, \qquad \text{when} \quad c \to \infty. \tag{4.70}$$

which means that the leading order correction is at most about 64%. We see that

the HM formula is an over estimate of the value of B, by as much as a factor of three.

4.5.2 Case (III)

Here we shall simply show that this case, where $\phi(\xi)$ reaches ϕ_- but not ϕ_+ in the Euclidean solution, exists for some choice of the potential. Following the above solution (4.54), we have

$$\begin{aligned} \Delta\phi_R = \phi_R(0) - \phi_T &= \frac{\lambda_-}{H^2}(f(H\xi_T) - f(0)) \leq \Delta\phi_- \\ \Delta\phi_L = \phi_T - \phi_L(\pi/H) &= \frac{\lambda_+}{H^2}(f(\pi - H\xi_T) - f(\pi)) \leq \Delta\phi_+ \end{aligned} \tag{4.71}$$

Let $\Delta V_R = V_T - V(\phi_R(0)) \leq \Delta V_-$ and $\Delta V_L = V_T - V(\phi_L(\pi/H)) \leq \Delta V_+$. Case (IV) corresponds to

$$\Delta V_R < \Delta V_-, \qquad \Delta V_L < \Delta V_+ \tag{4.72}$$

while case (III) would be reached if

$$\Delta V_R = \Delta V_-, \qquad \Delta V_L < \Delta V_+. \tag{4.73}$$

Using Eq.(4.55), Eq.(4.56) can be rewritten as

$$c = \frac{\lambda_-}{\lambda_+} = \frac{2\cos^2(H\xi_T/2) + \cot^2(H\xi_T/2)}{2\sin^2(H\xi_T/2) + \tan^2(H\xi_T/2)} \tag{4.74}$$

Moving slightly away from the symmetric case, we have, from the above equation (4.74), for small deviations,

$$H\xi_T \simeq \pi/2 - \frac{1}{3}(c-1). \tag{4.75}$$

so we have

$$\frac{\Delta V_R}{\Delta V_L} = \frac{c\Delta\phi_R}{\Delta\phi_L} \simeq c^2\frac{9\alpha - 2(c-1)}{9\alpha + 2(c-1)} \simeq 1 + (2 - \frac{4}{9\alpha})(c-1) \tag{4.76}$$

Hence for $c > 1$, we have

$$\Delta V_R > \Delta V_L \tag{4.77}$$

For $\Delta V_- > \Delta V_R$ and $\Delta V_+ > \Delta V_L$, we have still have the case (IV). Now we can consider potentials where

$$\Delta V_R \geq \Delta V_- > \Delta V_+ > \Delta V_L \tag{4.78}$$

(decreasing $\Delta\phi_-$ while keeping other parameters fixed) which belongs to case (III). This demonstrates that case (III) exists for some types of potential. Here is an explicit example: when $\Delta\phi_+ = 0.005$, $\Delta\phi_- = 0.004$, $\lambda_- = 1 \times 10^{-7}$, $\lambda_+ = 0.5 \times 10^{-7}$, $V_T = 0.77 \times 10^{-6}$, the bounce solution, which is plotted in Figure.4.4, does reach ϕ_- but not ϕ_+.

On the other hand, for $c < 1$ (that is, when the gradient towards the false vacuum is steeper than that towards the true vacuum), the Euclidean solution has $\Delta V_R < \Delta V_L$. This means the tunneling is from $V_L = V_T - \Delta V_L$ going up to $V_R = V_T - \Delta V_R$. As noted earlier, this tunneling up phenomenon does not happen in the absence of gravity. So this possibility is a gravitational effect. This phenomenon has been studied in [56].

Note that this case which reaches ϕ_- but not ϕ_+ does not exist for the symmetric ($\lambda = \lambda_+ = \lambda_-$) case. In this case, $c = 1$ so that $\Delta V_R = \Delta V_L$ and the above condition (4.78) cannot be satisfied unless $\Delta V_R = \Delta V_+ = \Delta V_L$, which means that ϕ does reach the false vacuum value. This corresponds to the cases we shall now turn to in the next subsection.

4.5.3 Case (II)

To see the existence of this case, we may restrict ourselves to the symmetric ($\lambda_+ = \lambda_-$) case. Since $\Delta\phi_- > \Delta\phi_+$we can have the situation where

$$\Delta\phi_- > \frac{\alpha\lambda}{H^2} \geq \Delta\phi_+ \tag{4.79}$$

That is, the condition (4.59) does not hold. Instead, we now have

$$\alpha\gamma = \alpha\frac{\lambda}{H^2\Delta\phi_+} \geq 1. \tag{4.80}$$

In this case, $\phi(\xi)$ reaches the false vacuum V_+ at ϕ_+ outside the bubble within the horizon but the bubble inside never reaches the true vacuum V_- at ϕ_- at the moment of creation. In this case, the solution of (4.49) contains three pieces.

$$\phi(\xi) = \begin{cases} \phi_1(\xi) & x \in [0, \xi_T] \\ \phi_2(\xi) & x \in [\xi_T, \xi_+] \\ \phi_+ & x \in [\xi_+, \pi/H] \end{cases} \tag{4.81}$$

where $\phi_1(\xi) \geq \phi_T$ and $\phi_2(\xi) \leq \phi_T$. The general solution for $\phi_1(\xi)$ and $\phi_2(\xi)$, which satisfies $\phi_1'(0) = 0$, is

$$\begin{aligned} \phi_1(\xi) &= \frac{\lambda}{H^2}\Big(C_1 - f_1(H\xi) - \frac{2}{3}f_2(H\xi)\Big) \\ \phi_2(\xi) &= \frac{\lambda}{H^2}\Big(C_2 + f_1(H\xi) + Af_2(H\xi)\Big), \end{aligned} \tag{4.82}$$

where f_1 and f_2 are given by Eq.(4.51). The remaining boundary and matching conditions are,

$$\begin{cases} \phi_1(\xi_T) = \phi_2(\xi_T) = \phi_T \\ \phi_1'(\xi_T) = \phi_2'(\xi_T) \\ \phi_2(\xi_+) = \phi_+,\ \phi_2'(\xi_+) = 0. \end{cases} \tag{4.83}$$

We have five parameters to determine, $C_1, C_2, A, \xi_T, \xi_+$, and also five equation from (4.83). It is helpful to rewrite (4.83) as three equations only in A, ξ_T, ξ_+

$$\begin{cases} f_1(H\xi_T) - f_1(H\xi_+) + A(f_2(H\xi_T) - f_2(H\xi_+)) = H^2\Delta\phi_+/\lambda = 1/\gamma \\ f_1'(H\xi_T) + (A/2 + 1/3)f_2'(H\xi_T) = 0 \\ f_1'(H\xi_+) + Af_2'(H\xi_+) = 0 \end{cases} \tag{4.84}$$

Because the functions f_1 and f_2 contain only pure number coefficients, the dimensionless parameters $A, H\xi_T, H\xi_+$ are determined just by the combination $\gamma = \lambda/H^2\Delta\phi_+$. So we may rewrite them as functions of $1/\gamma$ which can be obtained numerically. Then we can insert $A, H\xi_T, H\xi_+$ back into (4.83), we will get all the parameters.

For case (II), $\phi(\xi)$ does not reach ϕ_-, or

$$\phi_1(0) - \phi_T < \Delta\phi_-, \tag{4.85}$$

or

$$f_1(H\xi_T) + \frac{2}{3}f_2(H\xi_T) - f_1(0) - \frac{2}{3}f_2(0) \equiv I(1/\gamma) < \frac{H^2\Delta\phi_-}{\lambda}. \tag{4.86}$$

Notice that the left hand side is just a function of $1/\gamma = H^2\Delta\phi_+/\lambda$, which we call $I(1/\lambda)$. So we need,

$$\frac{\lambda}{H^2}I\left(\frac{H^2\Delta\phi_+}{\lambda}\right) < \Delta\phi_-. \tag{4.87}$$

Equation (4.87), together with (4.80), is the condition for case (II). The function $I(x)$ is a monotonic function which is plotted in Figure.4.6. Notice that $I(x) > x$, therefore,

$$\phi(0) - \phi_T > \Delta\phi_+ \tag{4.88}$$

which means the quantum tunneling is from the false vacuum V_+ to someplace lower than V_+ but not exactly at V_-. After the realization of quantum tunneling,

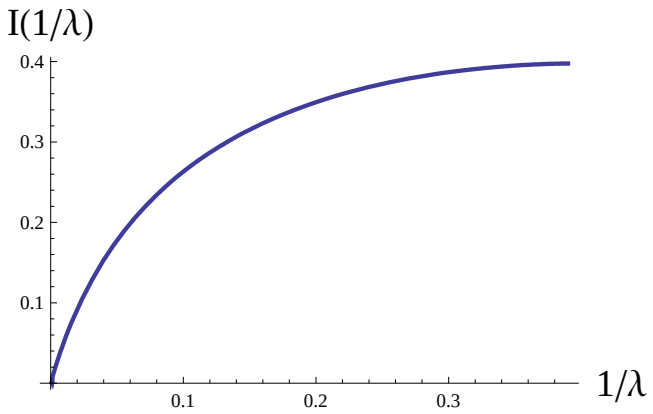

Figure 4.6: The function $I(1/\gamma)$. Note that $1/\gamma < \alpha = 0.398$.

V will continue to drop classically until reaching V_-, the true vacuum. After getting the solution ϕ, one uses the formulae (4.45), (4.46) and (4.47) to get the factor B for the case (II). Notice here ϕ does not reach ϕ_-, so actually, the small expansion factor is not $\Delta V_-/V_T$ but an even smaller factor $\Delta V_+/V_T$.

4.5.4 Case (I)

In the this case, $\phi(\xi)$ reaches both ϕ_+ and ϕ_-. Therefore the condition is

$$\begin{aligned} \alpha\gamma = \alpha\frac{\lambda}{H^2\Delta\phi_+} &\geq 1 \\ \frac{\lambda}{H^2} I\left(\frac{H^2\Delta\phi_+}{\lambda}\right) &\geq \Delta\phi_-. \end{aligned} \tag{4.89}$$

$\phi(\xi)$ contains four pieces,

$$\phi(\xi) = \begin{cases} \phi_- & x \in [0, \xi_-] \\ \phi_1(\xi) & x \in [\xi_-, \xi_T] \\ \phi_2(\xi) & x \in [\xi_T, \xi_+] \\ \phi_+ & x \in [\xi_+, \pi/H] \end{cases} \tag{4.90}$$

where $\phi_1(\xi) \geq \phi_T$ and $\phi_2(\xi) \leq \phi_T$. The general solution for $\phi_1(\xi)$ and $\phi_2(\xi)$ is,

$$\begin{aligned}\phi_1(\xi) &= \frac{\lambda}{H^2}\Big(C_1 - f_1(H\xi) + A_1 f_2(H\xi)\Big) \\ \phi_2(\xi) &= \frac{\lambda}{H^2}\Big(C_2 + f_1(H\xi) + A_2 f_2(H\xi)\Big),\end{aligned} \tag{4.91}$$

where f_1 and f_2 are defined in (4.51). The boundary conditions are,

$$\begin{cases} \phi_1(\xi_-) = \phi_-,\ \phi_1'(\xi_-) = 0 \\ \phi_1(\xi_T) = \phi_2(\xi_T) = \phi_T \\ \phi_1'(\xi_T) = \phi_2'(\xi_T) \\ \phi_2(\xi_+) = \phi_+,\ \phi_2'(\xi_+) = 0. \end{cases} \tag{4.92}$$

So we have seven parameters to determine, $C_1, C_2, A_1, A_2, \xi_-, \xi_T, \xi_+$, and also seven equations from (4.92). Like case (II), we can reduce the number of both the parameters and the equations and then solve it. The solution looks like the thin-wall tunneling solution in [6]. The reason is, by the condition (4.89), $\Delta\phi_+$ cannot be very small comparing with $\Delta\phi_-$, so the energy difference of the two vacua $\epsilon = V_+ - V_-$ cannot be large and the thin-wall approximation may apply. Again, after getting the solution of $\phi(\xi)$, we can get the Euclidean action and B by (4.45), (4.46) and (4.47).

It is clear that the thin-wall approximation belongs to case (I), since the inside of the bubble reaches ϕ_- while the outside reaches ϕ_+ (see Figure 4.4). The thin-wall approximation requires a rapid transition of ϕ from ϕ_- to ϕ_+. This case has been analyzed in Ref.[45], [57], [58]. For the sake of completeness, let us review the basic result following [45]. In the thin-wall approximation ($\epsilon \to 0$), we may divide the integration for the bounce B into three parts. Outside the bubble, $\phi = \phi_+$ and thus

$$B_{out} = 0. \tag{4.93}$$

In the wall, we have

$$B_{wall} = 2\pi^2 r^3 \sigma, \tag{4.94}$$

where r is the bubble size and σ is the tension of the wall which is decided by the barrier between the false and true vacua,

$$\sigma \simeq \int_{\phi_-}^{\phi_+} d\phi \sqrt{2[V(\phi) - V(\phi_+)]} \tag{4.95}$$

Inside the bubble, $\phi = \phi_-$ is a constant and Eq.(4.8) becomes

$$d\xi = dr(1 - \kappa r^2 V/3)^{-1/2}. \tag{4.96}$$

Hence

$$S_{E,in}(\phi) = -\frac{12\pi^2}{\kappa} \int_0^r \tilde{r} d\tilde{r} (1 - \kappa V(\phi)\tilde{r}^2/3)^{1/2}. \tag{4.97}$$

Summing the three parts of B, we obtain

$$B = 2\pi^2 r^3 \sigma + \frac{12\pi^2}{\kappa^2} \left[\frac{1}{V_-} \left(\left(1 - \kappa r^2 V_-/3\right)^{3/2} - 1 \right) - \frac{1}{V_+} \left(\left(1 - \kappa r^2 V_+/3\right)^{3/2} - 1 \right) \right]. \tag{4.98}$$

The coefficient B is stationary at $r = R$ which satisfies

$$\frac{1}{R^2} = \frac{\epsilon^2}{9\sigma^2} + \frac{\kappa(V_+ + V_-)}{6} + \frac{\kappa^2 \sigma^2}{16}, \tag{4.99}$$

where $\epsilon = V_+ - V_-$. So

$$B_{tw} = 2\pi^2 R^3 \sigma + \frac{4\pi^2}{\kappa} \left[R_-^2 \left(\left(1 - H_-^2 R^2\right)^{3/2} - 1 \right) - R_+^2 \left(\left(1 - H_+^2 R^2\right)^{3/2} - 1 \right) \right] \tag{4.100}$$

where $H_\pm^{-1} = R_\pm = (\kappa V_\pm/3)^{-1/2}$ and the subscript "tw" means the thin-wall approximation. Note that the last term is proportional to κ^2 and so is very small most of the time. According to Eq.(4.99), we can easily check that the bubble radius at the moment of materialization is not larger than the event horizon R_+ of the de Sitter space in false vacuum. This is reasonable; otherwise the bubble cannot be generated causally.

For the special case with $R \ll R_+$, the bubble size is much smaller than the curvature radius of the background and gravity does not play a big role. In this limit B becomes

$$B = 2\pi^2 r^3 \sigma - \frac{\pi^2}{2} r^4 \epsilon. \tag{4.101}$$

Here, B is stationary at

$$r = R_0 = \frac{3\sigma}{\epsilon}, \tag{4.102}$$

so

$$B_{tw} \sim \frac{27\pi^2}{2} \frac{\sigma^4}{\epsilon^3}. \tag{4.103}$$

In the other limit of $R \simeq R_+$ which corresponds to $V_+ \simeq V_- = V \gg V_s = 2\epsilon^2/3\kappa\sigma^2 + 3\kappa\sigma^2/8$. This happens at the high energy scale in the landscape, and the bubble radius is given by $R \simeq \sqrt{3/\kappa V}$. Now B is dominated by the first term in Eq.(4.98), namely

$$B_{tw} \simeq 6\sqrt{3}\pi^2 \tau (\kappa V)^{-3/2} = \frac{2\pi^2 \sigma}{H^3} \tag{4.104}$$

In the units where $M_p = 1$, or equivalently $\kappa = 1$, the tension of the bubble satisfies $\sigma \ll 1$. In Planck region ($V \sim 1$), $B \ll 1$ and $\Gamma \sim 1$. At low energy scale, the background curvature radius is quite large and the bubble size is relatively small, and then the tunneling rate is insensitive to the vacuum energy of the false vacuum.

The familiar CDL thin-wall approximation occurs in case (I), however, a solution of the case (I) is not necessarily the "thin-wall" solution, i.e., the tunneling factor B_{tw} determined by the thin-wall approximation may not be very accurate. To illustrate this point we compare the values of B_{tw} with our computation for case (I).

We fix $G = 1$, $\lambda = 1 \times 10^{-7}$, $\phi_T = 0$, $\phi_+ = -0.005$ and vary the variables ϕ_- and

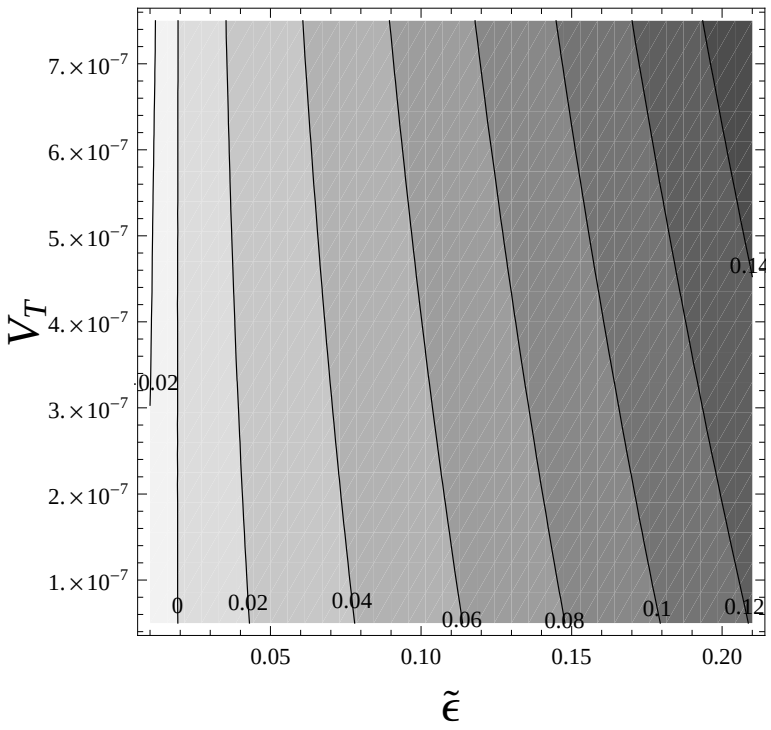

Figure 4.7: The contour plot of $(B_{tw} - B)/B$ as the function of $\tilde{\epsilon}$ and V_T. The horizontal axis is $\tilde{\epsilon}$ and the vertical axis is V_T. The contour line labels the value $(B_{tw} - B)/B$ and the darker regions have larger differences.

V_T. We define

$$\tilde{\epsilon} = \frac{\epsilon}{\Delta V_+} = \frac{V_+ - V_-}{V_T - V_+} = \frac{\phi_- - |\phi_+|}{|\phi_+|} \tag{4.105}$$

which is always positive and we may expect that when $\tilde{\epsilon}$ is close to 0, the thin-wall approximation is accurate. We reserve B for our result for the tunneling exponential factor from Eq.(4.45), Eq.(4.46) and Eq.(4.47) while B_{tw} denotes the counterpart of the thin-wall approximation formula (4.100) given in Ref.[45]. We plot the relative deviation of the two methods, $(B_{tw} - B)/B$, as a function of r and V_T in the contours of Figure 4.7.

In the contour figure we draw the range $0.01 < \tilde{\epsilon} < 0.2$ and $5 \times 10^{-8} < V_T < 7.5 \times 10^{-7}$. The reason for the V_T range choice is that if V_T is too small then our

expansion is not good and if V_T is too large, case (I) will turn into case (II). From the figure we can see

- The contour lines are roughly vertical and the relative difference $(B_{tw}-B)/B$ increases from the left to right. It means that when $\tilde{\epsilon}$ is small the thin-wall approximation coincides with our computation and so verifies that the thin-wall appoximation is good when ϵ is small.
- However, the contour lines are not completely vertical but tilt from the top left to the bottom right. It means when $\tilde{\epsilon}$ is fixed and V_T is increasing, the difference is getting larger and larger. An immediate explanation is: in this situation the solution is moving toward case (II) and finally when tunneling becomes case (II) the difference is very large, since the solution does not reach ϕ_- in contrast to the thin-wall approximation. Or by the Euclidean equation of motion, if V_T is large, H, which serves as a damping term, is also large and slows the evolution of the Euclidean solution. So the wall is not "thin" as before.

Although unlike case (IV), it is hard to get the analytic form of B for case (I) because of the transcendental Eq.(4.92). However, it is helpful to look at the numerical computation. For example, for a potential with small $\epsilon = V_+ - V_-$, like $\lambda = 1 \times 10^{-7}$, $V_T = 0.2 \times 10^{-6}$, $\Delta\phi_+ = 0.005$ and $\Delta\phi_- = 0.0055$, the zero-order of the S_E, by Eq.(4.46), is $S_{E,0} = -1.875 \times 10^6$. Eq.(4.47) gives the leading order correction $S_{E,1} = S_{E,1,\delta r} + S_{E,1,\phi}$, where $S_{E,1,\delta r} = 4787$ is the first term in (4.47) from δr contribution and $S_{E,1,\phi} = -7691$ is the second term induced by ϕ. Therefore, we explicitly see that the leading-order corrections $S_{E,1,\delta r}$ and $S_{E,1,\phi}$ are much smaller than the zero order $S_{E,0}$ and the perturbation series for S_E is valid. To

get the factor B, we needs to compute $S(\phi_+)$ which is -1.879×10^6, so

$$\begin{aligned} B &= S_E - S(\phi_+) \sim S_{E,0} + S_{E,1,\delta r} + S_{E,1,\phi} - S(\phi_+) \\ &= 1794 \end{aligned}$$

which is quite close to the thin-wall approximation result $B_{tw} = 1848$ by Eq.(4.98).

We see that it is crucial to include the back-reaction effect due to δr here. In fact, if we drop the contribution from δr in Eq.(4.47), then $B(\delta r\text{-excluded}) \sim S_{E,0} + S_{E,1,\phi} - S(\phi_+) \sim -2992$, which is negative and has no physical meaning. The importance of the δr term in Eq.(4.47) cannot be over-emphasized.

4.6 Discussion

Let us comment on the physical meaning of the cases other than case (I). For case (II), after the realization of quantum tunneling, the field will evolve by the classical equation. Coleman [15] points out that, instead of going back to solve the Minkowski (Lorentz) equation, we can get the classical solution directly from the Euclidean solution by analytical continuation. For [50], we can verify that, after the quantum tunneling, the field will continue to roll down until reaching the true vacuum. This also happens in de Sitter space. After the creation of the nucleation bubble with radius R at time $t = 0$, the evolution of the surface of the bubble is described by the Lorentzian action, where $\xi^2 = R^2 \to \mathbf{r}^2 - t^2$. The center of the bubble starts at $\xi = 0$ and as t increases, $\xi^2 = -t^2$ becomes negative at the center. By analytic continuation, starting with $\phi(r = 0, t = 0) < \phi_-$, $\phi(0, t)$ falls towards ϕ_-. It may overshoot and oscillates about the true vacuum at ϕ_-. With Hubble (or any additional) damping, it will eventually settle at the

true vacuum as the nucleation bubble continues to grow. In case (III) and case (IV), ϕ at the bubble outside is also expected to follow classical motion and roll down towards the false vacuum at ϕ_+ (while in a GH thermal bath). However, since the bubble is growing rapidly at the same time, the true vacuum may be reached before ϕ has time to roll to the false vacuum.

Let us show the different features of the tunneling by an explicit example. The type of tunneling is determined by the parameters of the potential, V_T, λ_+, λ_-, $\delta\phi_+$ and $\delta\phi_-$. First, we want to see the dependence of the exponent B on H, for large H. We set $G = 1$ and fix $\phi_T = 0$, $\Delta\phi_- = 0.007$, $\Delta\phi_+ = 0.005$, $\lambda_\pm = 1 \times 10^{-7}$ so the shape of the potential is fixed. We can move the potential up and down by varying V_T (hence H) to see the dependence of B on H.

- The condition for case (IV), $\alpha\gamma < 1$ reads $V_T > 9.494 \times 10^{-7}$. For example, we can plot the solution of $\phi(r)$ for $V_T = 2\times10^{-6}$ in the last picture of Figure 4.4 and it is clear that neither ϕ_+ nor ϕ_- is reached. The exponential factor B can be obtained by Eq.(4.64), $B \sim 41.73$. The HM tunneling exponential factor for this potential is $B_{HM} \sim 46.88$ hence the case (V) tunneling rate is close to the HM tunneling but faster than it. The relative difference of B is about 11%.

- When $\alpha\gamma \geq 1$, we need to consider the condition

$$\frac{\lambda}{H^2} I\left(\frac{H^2\Delta\phi_+}{\lambda}\right) < \Delta\phi_-. \tag{4.106}$$

  which reads $9.494\times10^{-7} \geq V_T > 6.465\times10^{-7}$. If it is satisfied, the tunneling is of case (II). For example, we plot the solution for $V_T = 9.0\times10^{-7}$ in Figure 4.4 and find that ϕ reaches ϕ_+ but not ϕ_-.

- If this condition is also violated, i.e., $V_T \leq 6.465\times10^{-7}$, the tunneling is case

(I). [2] For example, the solution of $V_T = 3.0 \times 10^{-7}$ is plotted in Figure 4.4 and ϕ reaches both ϕ_+ and ϕ_-. Eq.(4.47) gives $B \sim 928.7$ while the thin-wall approximation Eq.(4.100) gives $B_{tw} \sim 1019$. The relative difference is about 9.8% due to the finite difference of V_+ and V_-. (So the bubble wall is not "thin" enough for this potential.)

As H is decreased from a large value, the tunneling type goes from case (IV) to case (II) and finally to case (I). The corresponding exponent B for different cases are plotted in Figure 4.2 as a function of H. It is straightforward to see the dependence on the shape of potential, say, by varying $\lambda = \lambda_\pm$ and fixing $\Delta\phi_- = 0.007$, $\Delta\phi_+ = 0.005$, $V_T = 8 \times 10^{-7}$, we can also see the transition among the three cases. Notice the combination $xI(1/x)$ is monotonically increasing function of x, so the conditions can be solved easily in λ,

- For $\lambda < 8.425 \times 10^{-8}$ we have case (IV).
- For $8.4257 \times 10^{-8} \leq \lambda < 1.237 \times 10^{-7}$ we have case (II).
- for $\lambda \geq 1.237 \times 10^{-7}$ we have case (I).

Therefore case (IV), which is close to HM tunneling, happens for a "flatter" barrier (small λ) while case (I), of which thin-wall tunneling is a special case, happens for a "sharper" barrier (large λ).

We may write the factor B (4.2) as composed of two terms,

$$B = [S_E(\phi_{f+}) - S_E(\phi_+)] + [S_E(\phi_{bounce}) - S_E(\phi_{f+})] \tag{4.107}$$

where $\phi_T \geq \phi_{f+} \geq \phi_+$. For cases (I) and (II), we have $\phi_{f+} = \phi_+$, so the first term vanishes. For cases (III) and (IV), $\phi_{f+} > \phi_+$, so both terms contribute. In the limit

[2] Notice that our approximation works for $V_T \gg \Delta V_-$, which reads $V_T \gg 7 \times 10^{-10}$.

$\phi_{f+} \to \phi_T$, $\phi(\xi) \to \phi_T$, so the second term vanishes and the resulting formula reduces to the HM limit. The picture is consistent with the interpretation in [53, 54, 55]. However, as we have pointed out, corrections and back-reaction can introduce large corrections to the HM formula.

Brown and Weinberg [47] showed that the CDL tunneling rate can be derived by treating the field theory on a static patch of de Sitter space as a thermal system. In this thermal system, tunneling does not need to occur from the bottom of the false potential well. Instead, tunneling proceeds by a combination of thermal excitation part way up the barrier followed by quantum tunneling through the barrier. The tunneling rate is a thermal average of the energy-dependent quantum tunneling rates [60],

$$\Gamma \sim \int dE e^{-(E-E(\phi_+))/T} e^{-J(E)} \tag{4.108}$$

where E is the energy of the field configuration. Here the quantum tunneling rate is given by WKB approximation $J(E) = 2\int_{\phi_{f+}}^{\phi_{t-}} d\phi \sqrt{2(V(\phi)-E)}$ where the integral is along a Euclidean path from one classical turning point ϕ_{f+} to the other classical turning point ϕ_{t-}. This integral is dominated by the energy E_* that maximizes the integrand. Using the saddle-point approximation it follows that

$$\begin{aligned} \frac{1}{T} &= 2\int_{\phi_{f+}}^{\phi_{t-}} d\phi \frac{1}{\sqrt{2(V(\phi)-E)}} \\ &= 2\int_{\phi_{f+}}^{\phi_{t-}} d\phi \frac{1}{\sqrt{(\frac{d\phi}{d\tau})^2}} \qquad (4.109) \\ &= 2\Delta\tau \qquad (4.110) \end{aligned}$$

since the integral is along a solution to the Euclidean equations of motion. Fixing $T = T_H$ determines E_* (and so ϕ_{f+} and ϕ_{t-}). This yields $J(E_*) = S_E(\phi_{bounce}) - S_E(\phi_{f+})$. This result also implies that the tunneling takes a Euclidean

time $\Delta\tau = 1/2T_H$ and

$$S_E(\phi) = \int_{-\frac{1}{2T_H}}^{\frac{1}{2T_H}} E(\phi) d\tau \simeq E/T_H \tag{4.111}$$

That is, $E_*/T_H = S_E(\phi_{f+})$ and $E(\phi_+)/T_H = S_E(\phi_+)$. Using this result in the saddle-point approximation to (4.108), one finds

$$\Gamma \sim e^{-(S_E(\phi_{f+})-S_E(\phi_+))} e^{-(S_E(\phi_{bounce})-S_E(\phi_{f+}))} \tag{4.112}$$

which reproduces the standard CDL tunneling rate. So our result (4.107) agrees with this result of Ref.[47]: the first term in (4.107) corresponds to a thermal (i.e., Gibbons-Hawking temperature) fluctuation from the false vacuum (at ϕ_+) part way up the barrier to ϕ_{f+} and the second term in (4.107) corresponds to a quantum tunneling. Note that the derivation of Ref.[47] assumes a fixed de Sitter background., while the back-reaction (which can be large) is included in our derivation. In this sense, our result is a big improvement. In Sec. 5.1, we calculated the $S_E(\phi_{bounce})$ and determined ϕ_{f+} for a given triangular potential. This allows us to compare quantitatively the contribution from the GH thermal effect to the contribution from the quantum effect in such a tunneling.

4.7 Thermal Tunneling

At finite temperature, the transition from V_+ to V_- can also occur via thermal fluctuations [61]. So there is another contribution due entirely to the GH temperature fluctuation. The dominant thermal tunneling process is the formation of $O(3)$ symmetric bubbles of V_- that minimize the change in entropy ΔS. Let us evaluate the rate of this process and compare it to the above tunneling process. The thermal tunneling rate is given by

$$e^{\Delta S} = e^{\Delta F/T} \tag{4.113}$$

where ΔF is the change in the free energy. We can think of the free energy as a three-dimensional action

$$\Delta F = S_3 = \int d^3x \left(\frac{1}{2}(\partial\phi)^2 + V(\phi) \right) \tag{4.114}$$

for a scalar field with a standard kinetic term. In this case the equations of motion are

$$\phi'' + \frac{2r'}{r}\phi' = \frac{dV}{d\phi} \tag{4.115}$$

$$r'^2 = 1 + \frac{r^2}{3M_p^2}(\frac{1}{2}\phi'^2 - V). \tag{4.116}$$

We restrict our attention to the symmetric triangle potential as before. In the large V_T limit considered above, the general solution to (4.116) is

$$\phi = \frac{\lambda}{H^2}(A + \frac{H\xi}{2}\cot(H\xi) + B\cot(H\xi)) \tag{4.117}$$

Like the Euclidean case discussed above, there are also four types of thermal tunneling solutions:

- Case I. $\phi(\xi)$ reaches both ϕ_+ and ϕ_-.
- Case II. $\phi(\xi)$ reaches ϕ_+ but not ϕ_-.
- Case III. $\phi(\xi)$ reaches ϕ_- but not ϕ_+.
- Case IV. $\phi(\xi)$ reaches neither ϕ_+ nor ϕ_-.

We will begin our discussion with case IV as it is the simplest.

4.7.1 Case IV

In this case, we need to solve (4.115) with the boundary conditions (4.53). The solution to these equations is

$$\phi_1(\xi) = \phi_T + \frac{\lambda}{H^2}\frac{H\xi}{2}\cot(H\xi) \tag{4.118}$$

$$\phi_2(\xi) = \phi_T - \frac{\lambda}{H^2}\left(\frac{H\xi}{2}\cot(H\xi) - \frac{\pi}{2}\cot(H\xi)\right) \tag{4.119}$$

$$\xi_T = \frac{\pi}{2H} \tag{4.120}$$

This solution is valid if

$$\frac{H^2\Delta\phi_+}{2\lambda} < 1. \tag{4.121}$$

Comparing (4.121) to (4.59) we see that the existence of a case (IV) Euclidean tunneling solution implies the existence of a case IV thermal tunneling solution and that some potentials will admit a case IV thermal tunneling solution and a case (II) Euclidean tunneling solution.

Evaluating (4.114) using (4.120) we find that, for a specific background temperature,

$$S_3/T_H = \frac{8\pi\Delta V_+}{3H^4} + O\left(\frac{\lambda^2 M_p^6}{V_T^3}\right). \tag{4.122}$$

To compare to the HM bounce (4.4) we find the ratio at leading order

$$\frac{B_{HM}}{S_3/T_H} \sim 1. \tag{4.123}$$

Based on the discussion in the last section, this result is expected and consistent with [59]. One should compare this thermal tunneling to the stochastic tunneling process of [53, 54, 55].

4.7.2 Case II

Case III tunneling only occurs when $\lambda_+ \neq \lambda_-$ as in the Euclidean case. Since it does not show any special new feature, we shall skip this case.

In case II, we need to solve (4.115) with the boundary conditions (4.83). Imposing the condition $\phi_1'(0) = 0$ we find

$$\phi_1(\xi) = \frac{\lambda}{H^2}\left(A_1 + \frac{H\xi}{2}\cot(H\xi)\right) \tag{4.124}$$

$$\phi_2(\xi) = \frac{\lambda}{H^2}\left(A_2 - \frac{H\xi}{2}\cot(H\xi) + B\cot(H\xi)\right) \tag{4.125}$$

$$\tag{4.126}$$

As in the Euclidean case we can eliminate A_1 and A_2 by rewriting the boundary conditions (4.83) as

$$-\frac{H\xi_T}{2}\cot(H\xi_T) + \frac{H\xi_+}{2}\cot^2(H\xi_+) + B(\cot(H\xi_T) - \cot(H\xi_+)) = \frac{H^2\Delta\phi_+}{\lambda} \tag{4.127}$$

$$\cot(H\xi_T) - H\xi_T\csc^2(H\xi_T) - B\csc^2(H\xi_T) = 0 \tag{4.128}$$

$$\frac{1}{2}\cot(H\xi_+) - \frac{H\xi_+}{2}\csc^2(H\xi_+) - B\csc^2(H\xi_+) = 0 \tag{4.129}$$

which we can solve numerically for B, ξ_T, and ξ_+ as functions of $\frac{H^2\Delta\phi_+}{\lambda}$. We can then use these solutions in the original equations (4.83) to determine A_1 and A_2.

For our solution to be consistent, we need $\phi_1(0) - \phi_T < \Delta\phi_-$ or equivalently

$$I_{S_3}\left(\frac{H^2\Delta\phi_+}{\lambda}\right) = \frac{1}{2} - \frac{H\xi_T}{2}\cot(H\xi_T) < \frac{H^2\Delta\phi_-}{\lambda}. \tag{4.130}$$

Numerically we find that $I_{S_3}(\frac{H^2\Delta\phi_+}{\lambda}) > \frac{H^2\Delta\phi_+}{\lambda}$ so case II thermal tunneling is always from V_+ to some V_F where $V_+ > V_F > V_-$ as we saw above in case (II) Euclidean tunneling.

4.7.3 Case I

When (4.121) and (4.130) are both violated we have case I thermal tunneling. Here we need to solve (4.115) with the boundary conditions (4.92) numerically if the thin-wall approximation is not valid. In general the solutions have the same qualitative features as in case I Euclidean tunneling, but the Euclidean bounce B is smaller than S_3/T_H.

Thin-wall CDL tunneling is a special case of I. The thin-wall approximation greatly simplifies calculations so for the remainder of this section we consider a general potential that satisfies the thin-wall conditions. The difference between the CDL and thermal tunneling rates has to do with R^4 space in CDL versus $R^3 \times S^1$ space in the thermal case, where S^1 corresponds to $\beta = 1/T = 2\pi/H$. In the thin-wall approximation we can divide the integration in 4.114 into three parts. For a bubble of radius r we have $S_{3,out} = 0$ and $S_{3,wall} = 4\pi r^2\sigma$. Using Eq.(4.96), the integral inside the bubble becomes

$$S_{3,in}(\phi) = -\frac{24\pi}{\kappa}\int_0^r d\tilde{r}(1-\kappa V(\phi)\tilde{r}^2/3)^{1/2}. \tag{4.131}$$

The free energy is given by

$$S_3 = 4\pi r^2\sigma + \frac{12\pi}{\kappa}\left[r\left(1-r^2/R_+^2\right)^{1/2} + R_+\arcsin\left(\frac{r}{R_+}\right) - r\left(1-r^2/R_-^2\right)^{1/2} - R_-\arcsin\left(\frac{r}{R_-}\right)\right]. \tag{4.132}$$

Maximizing S_3, we find R given by

$$\frac{1}{R^2} = \frac{1}{(R_0^{(3)})^2} + \frac{(H_+^2+H_-^2)}{2} + \frac{\kappa^2\sigma^2}{36} \tag{4.133}$$

where $R_0^{(3)} = 2\sigma/\epsilon$. In the $R \ll R_+$ case; this yields

$$S_3 = 4\pi R^2\sigma - 4\pi R^3\epsilon/3 \tag{4.134}$$

For critical size radius $R = R_0^{(3)}$, we have

$$S_3/T = 32\pi^2\sigma^3/3\epsilon^2 H \tag{4.135}$$

To see which path dominates, we compare this to $B = S_E$,

$$\frac{B}{(S_3/T)} = \frac{27}{64}\frac{R_0^{(4)}}{R_+} \tag{4.136}$$

Since $R \ll R_+$, we see that the Euclidean S^4 bounce B is smaller so it dominates.

For large, $R \lesssim R_+$,

$$S_3/T = 8\pi^2\sigma/H^3 \tag{4.137}$$

so we see that B (4.104) is smaller than S^3/T by a factor of four,

$$\frac{B}{(S_3/T)} = \frac{1}{4} \tag{4.138}$$

It is easy to understand the origin of this factor of four. In CDL, we have S^3 with size $2\pi^2$ versus $S^2 \times S^1$ with size $4\pi \times 2\pi = 8\pi^2$ in the thermal case. This just shows that the $O(4)$ symmetry lowers the Euclidean action B and so yields the correct answer.

Note that this is true only for $B \gg 1$. Recall that

$$\Gamma = A_0 e^{-B} + A_T e^{-S_3/T} + ... \sim A_1 e^{-B} + A_T e^{-4B} \tag{4.139}$$

If this condition is not satisfied, say when $B \gtrsim 1$, then this factor of four difference may be overcome by the difference in the prefactors A_0 and A_T. Callan and Coleman [16] show that, for bounce B,

$$\Gamma = \left(\frac{B}{2\pi}\right)^2 \left(\frac{\det(-\partial^2 + V''(\phi_+)}{\det'(-\partial^2 + V''(\phi)}\right)^{1/2} e^{-B} \tag{4.140}$$

where the prime on the determinant implies that the four zero modes are removed, yielding the first factor. This prefactor is difficult to evaluate in general,

so here we shall use dimensional arguments to find an order of magnitude estimate.

For $B \lesssim 1$, the above formula for CDL tunneling actually breaks down. Linde [61] argued that

$$\Gamma \sim T^4 \left(\frac{S_3}{2\pi T}\right)^{3/2} e^{-S_3/T} \tag{4.141}$$

The difference is that here, the temperature T is the Gibbons-Hawking temperature T_H, which strictly speaking is a gravitational, not thermal, effect.

This means that the potential V should now include the finite temperature effect: $V(\phi_i) \rightarrow V(\phi_i, T_H)$. The effective potential in de Sitter space has been calculated for some simple potentials in [48], [49]. As expected based on the GH temperature interpretation, the effective potential for scalar electrodynamics in de Sitter space calculated in [48] shows the same behavior as one varies the inverse radius of de Sitter space as the effective potential in Minkowski space as one varies the temperature. For a phenomenological potential (as in a slow-roll inflationary scenario), one may assume this finite temperature effect (and other quantum effects) is already built into the potential. However, in string theory applications to cosmology, where the effective potential can be calculated given a specific model, such finite GH temperature effects should be included. Here let us consider some specific examples.

4.8 Tunneling in the Cosmic Landscape

We consider a type IIB compactification with the moduli stablized by a combination of fluxes and a nonperturbative superpotential as in [4]. These compactifications typically have a large number of axions ϕ_i corresponding to integrals of

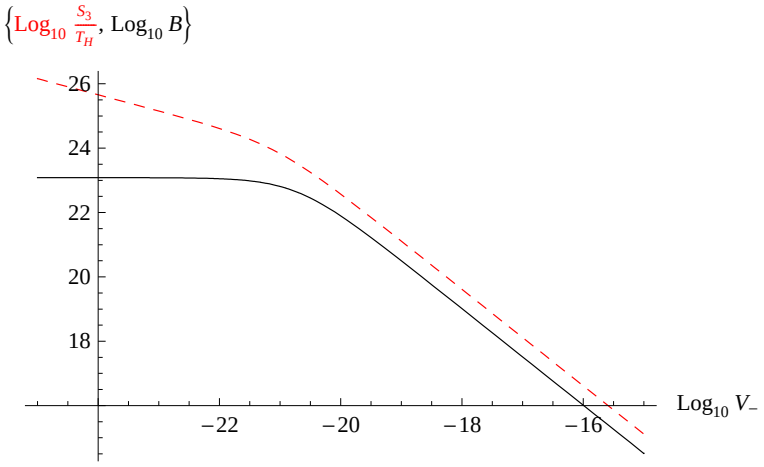

Figure 4.8: Comparison of the Euclidean action and the free energy divided by the GH temperature. $\log_{10} B$ (the black solid curve) and $\log_{10}(S_3/T_H)$ (the red dashed curve) plotted against $\log_{10} V_-$ with $\sigma = 10^{-10}$ and $\epsilon = 10^{-22}$ (in reduced Planck units) constant. In the thin-wall approximation, CDL tunneling has an exponentially faster rate than thermal tunneling. We see that B varies by 25 orders of magnitude. Tunneling is exponentially enhanced when the wavefunction is higher up (i.e., larger V_T) in the landscape.

the four-form potential over each of the independent four-cycles. Independent nonperturbative effects in the flux-induced superpotential give rise to a periodic potential

$$V(\phi_i) = M^4 e^{-S^i_{inst}}\left(1 - \cos\left(\frac{\phi_i}{f_i}\right)\right) + V(\rho) \tag{4.142}$$

where f_i is the decay constant, M is a natural mass scale (say, the string scale), and the ith instanton has action S^i_{inst}. $V(\rho)$ contains the potential coming from the moduli and includes D-term contributions. The shift symmetries associated with these axions are broken by nonperturbative effects. Including the effect of a single Euclidean D3-brane for each independent four-cycle the axion potential becomes [62]

$$V(\phi_i) = V_0(\phi_i) + \sum_i \hat{\alpha}_i \cos\left(\frac{\phi_i}{f_i}\right) + \sum_{ij} \beta_{ij} \cos\left(\frac{\phi_i}{f_i} - \frac{\phi_j}{f_j}\right) \tag{4.143}$$

where $V_0(\phi_i)$ is a smooth function of ϕ_i due to D-terms. Here, typical $\hat{\alpha}_i$ are exponentially small compared to the string scale. It is easy to estimate σ_i along the ϕ_i direction. Let $\alpha_i = \hat{\alpha}_i + \sum_{j\neq i}\beta_{ij}$, so the height of the potential barrier in the ϕ_i direction is $2\alpha_i$. Then, using Eq.(4.95), we have

$$\sigma_i = \int_{\phi_-}^{\phi_+} d\phi \sqrt{2(2\alpha_i)\cos(\frac{\phi_i}{f_i})} = \frac{\pi}{2}\sqrt{\frac{\alpha_i}{2}}f_i \tag{4.144}$$

and a crude estimate of the prefactor gives

$$\Gamma \simeq \left(\frac{B}{2\pi}\right)^2 |V''(\phi_t)|^2 e^{-B} \tag{4.145}$$

where

$$B = 2\pi^2\sigma/H^3 \tag{4.146}$$

and $|V''(\phi_t)| = \alpha/f^2$, yielding

$$\Gamma = \frac{\pi^4}{8H^9}\sum_{i=1}^{N}\frac{\alpha_i^3}{f_i^2}e^{-B_i} \tag{4.147}$$

Tunneling can be fast if the axion decay constant f is sufficiently small. Cosmological upper bounds on the amount of axionic dark matter constrain f to be below 10^{12} GeV, and astrophysical measurements of the cooling of red giants constrain f to be at least 10^9 GeV [63]. For example if we take $f_i = 10^{10}$ GeV within this observationally preferred region and choose $\alpha_i = (2 * 10^{-7}M_p)^4$, then $\Gamma \sim 1$ for $H = 10^{-7}M_p$ and $N \sim 10$. For smaller f the tunneling rate Γ can be order one for even smaller H. For model-independent axions in heterotic string theory f is generically between $1.1 * 10^{16}$ GeV and the reduced Planck mass [63]. If we choose $f_i \geq 1.1 * 10^{16}$ GeV for $N \leq 100$ there is no choice of $\alpha_i = \alpha$ and H in the regime where effective field theory is valid ($\alpha \ll M_p^4$ and $H < M_p$) so that $\Gamma \sim 1$.

For relatively large H or T, we have, instead

$$\Gamma \simeq \left(\frac{S_{i3}}{2\pi T}\right)^2 |V''(\phi_{it})|^2 e^{-S_{i3}/T} \tag{4.148}$$

where ϕ_{it} is the value of ϕ_i at the top of the barrier.

So it is reasonable to expect that the wavefunction of the universe tends to spread along some of the axionic directions. This what we expect for the QCD vacuum; that is, the wavefunction is a Bloch wave with angle θ_{QCD}. As we go up in the cosmic landscape (say, turning on D-terms), tunneling will be faster and so the wavefunction will be Bloch wave-like in more of the axionic directions. If we start with the wavefeunction localized as a classically stable vacuum site, it will take time for the wavefunction to spread. This time will be shorter when we are higher up in the landscape and when there are more axionic directions present.

However, here $V(\phi_i)$ should be replaced by $V(\phi_i, T)$. Instead of calculating this, we can make another estimate. In quantum mechanics, tunneling through a barrier becomes less suppressed when the energy of the particle increases. This happens when the particle is in a thermal bath with rising temperature. In quantum field theory, thermal effects typically lift the potential in a way such that the tunneling becomes faster, until the barrier disappears (i.e., the tunneling probability approaches unity).

For $\lambda\phi^4$ theory, with

$$V(\phi, T = 0) = -\frac{m^2}{2}\phi^2 + \frac{\lambda}{4!}\phi^4$$

we have, for high temperature T,

$$V(\phi, T_H) = \frac{1}{2}\left(\frac{\lambda T_H^2}{24} - m^2\right)\phi^2 + \frac{\lambda}{4!}\phi^4 + ... \tag{4.149}$$

so the effective mass term is no longer tachyonic for $T > T_c$, where the critical temperature is given by $T_c^2 \simeq 24m^2/\lambda$.

For any direction in the moduli space, if

$$T_H^2 > \frac{24m_i^2}{\lambda_i}, \qquad i = 1, 2, ..., d \tag{4.150}$$

Expanding the above potential about a maximum (top of a barrier), we have

$$V(\phi) = -\frac{\alpha}{2f^2}\phi^2 + \frac{\alpha}{4!f^4}\phi^4 + ...$$

we see that, if in any direction,

$$24f_i^2 < T_H^2 \tag{4.151}$$

then there is no barrier in that direction so the wavefunction is coherent along that direction. Even if this condition is not satisfied, we see that the finite T_H effect will enable to wavefunction to be coherent along some direction quickly, approaching a wavefunction similar to a Bloch wave.

In fact, compactification and moduli stabilization usually introduces a term like $H^2\phi^2$, which will tend to remove a lot of barriers. This term arises from Gauss' Law. Actually, this is the term that causes the η problem for slow-roll inflation.

In a single dimension at low scales these effects are probably negligible without a large degree of fine-tuning. For example consider a de Sitter vacuum in flux compactification in string theory with all moduli fixed. In the KKLT model [4], a highly warped type IIB compactification with nontrivial fluxes is stabilized using non-perturbative effects from Euclidean D-branes and gaugino condensation. The resulting anti-de Sitter minimum for the imaginary part of the volume

modulus σ is uplifted to a de Sitter minimum by adding a small number of $\overline{D3}$ branes. The presence of the $\overline{D3}$ branes induces a term D/σ^3 where D depends on the warp factor and the number of $\overline{D3}$ branes. The potential is:

$$V = \frac{aAe^{-a\sigma}}{2\sigma^2}\left(\frac{1}{3}\sigma aAe^{-a\sigma} + W_0 + Ae^{-a\sigma}\right) + \frac{D}{\sigma^3} \tag{4.152}$$

In this model if one tunes the parameters to have the de Sitter minimum be the cosmological constant observed today the tunneling rate is exponentially long.

The Gibbons-Hawking temperature effects are unimportant in the KKLT model because in the regime where the calculation is under control ($\sigma \gg 1$), the de Sitter vacuum is necessarily exponentially suppressed compared to the Planck scale. Increasing D both increases the false vacuum and decreases the barrier. The de Sitter vacuum disappears classically if the D-term uplifting is too large. Since the true vacuum is always Minkowski in this model HM tunneling dominates if the de Sitter vacuum is large. The HM bounce is $B_{HM} = 24\pi^2 M_p^4 \Delta V_+ / V_T^2$. Since $M_p^4/V_T \gg 1$ in this model, and $\Delta V_+/V_T \ll 1$ only when the barrier is about to disappear classically, the GH temperature corrections are small in this case. Numerical calculations approximating the maximum with a quartic potential and computing the finite temperature corrections using the GH temperature also show that the region of parameter space in which the de Sitter minimum is present classically but unstable quantum mechanically is extremely small.

4.9 Summary and Remarks

In this chapter, we discuss the relation between CDL thin-wall tunneling and HM tunneling. The picture is in agreement with the qualitative understanding

one has already, but the details allow us to obtain a quantitative understanding of the validity of each approximation and the sizes of the corrections. This result does allow us to say something about the stringy cosmic landscape. Here are a few comments that may be relevant, in no particular order:

• When we are high up in the cosmic landscape, gravitational effects exponentially enhance the tunneling rate. Qualitatively, one may interpret this as a GH temperature effect, but the actually enhancement is exponentially larger than a naive estimate based on the usual temperature effect, due to the enhanced $O(4)$ symmetry of the Euclidean action (versus the $SO(3)\times U(1)$ symmetry in the finite temperature case).

• Above the GUT scale, quantum gravity effects become important and we have nothing to say in this case. Around or slightly below the GUT scale, the tunneling can easily be enhanced by so much that there is simply no exponential suppression at all and the semi-classical formula simply breaks down. This is in the single field case, with only one tunneling direction. In the multi-field ($d > 1$) case, as we expect to be the situation in the cosmic landscape, there are typically many tunneling directions for any false vacuum, so one expects fast tunneling to take place.

• As is well known (see Appendix A in Ref. [45]), for a generic spherical potential in $d > 3$ spatial dimensions, the extra dimensions acts as an angular momentum like repulsive potential (with angular momentum $l = (d-3)/2$). So it is harder to form a bound state in higher dimensions, as is the case in the cosmic landscape. Instead of having a bound wavefunction that has to tunnel out, we may have a resonance like situation where the decay time can be very short. Even if the wavefunction is trapped, it is more likely to be weakly trapped, so

the wavefunction has a long tail outside the classically allowed region, rendering less suppressed tunneling.

• It is again well known that the finite temperature effect on the effective potential tends to decrease the barrier, allowing faster tunneling. In fact, compactification and moduli stabilization usually introduces a term like $H^2\phi^2$, which will tend to remove a lot of barriers. This term, a finite volume effect, arises from the equivalent of the Gauss's Law. (Actually, this is the term that causes the η problem for slow-roll inflation [64]) Here, a similar term arises due to the finite temperature effect on the potential. One may re-interpret this effect as a finite volume effect, due to the presence of the Gibbons-Hawking horizon $1/H$.

• Even if the barriers are still present (that is, not completely lifted), we see that the finite T_H effect will enable the wavefunction to be coherent along some direction more quickly. This is particularly likely along the axionic directions since the effective potential is periodic or close to being periodic and the heights of the barriers can be very low. In this situation, the wavefunction approaches a Bloch wave. Presumably, the QCD θ vacuum we live in today is described by such a Bloch wave.

• Since there are many vacua in the stringy landscape, resonance tunneling effects should play an important role in the landscape [17]. This also enhances the tunneling among the vacua in the landscape. Such enhancement can be substantial. In particular, its role in the development of the Bloch wave is well known.

• With all these observations, one suspects that the wavefunction of the universe in the cosmic landscape may be quite mobile; that is, it does not stay at

any particular vacuum site long enough to allow eternal inflation. However, without a detailed knowledge of the structure of the landscape (vacuum sites and their nearby neighbors as well as the barriers between them), it is difficult to make definitive statements. As we just pointed out, the wavefunction most likely is spread out along the periodic directions (i.e., the axionic directions) as Bloch waves; so what happens to the aperiodic directions? If we treat such directions randomly, i.e., as a random potential, one may borrow the insight obtained in condensed matter physics to argue that the wavefunction should be fully mobile along these directions as well [18]. This implies that eternal inflation in the landscape is very unlikely.

This argument is based on the large dimensionality of the landscape and does not use the gravitational effects discussed in this chapter; so it should apply all the way to very low vacuum energy density sites.

CHAPTER 5

HAWKING-MOSS TUNNELING WITH A DIRAC-BORN-INFELD ACTION

Quantum tunneling in gravity is a well studied subject. The Coleman-de Luccia instanton [6] plays an important role in cosmology, e.g., in gauge theory phase transitions, in inflation and recently, in the cosmic landscape. In IIB string theory, where the extra dimensions are compactified, the motion of D3 branes play a crucial role in brane inflation. As is well-known, the kinetic term of a D3 brane is given by the Dirac-Born-Infeld action. Recently, Brown, Sarangi, Shlaer and Weltman showed that Coleman-de Luccia tunneling with a DBI action can be significantly enhanced when compared to that with a canonical kinetic term [65]. Hawking-Moss tunneling arises in the same contexts as Coleman-de Luccia tunneling when the potential barrier is broad instead of narrow. In many cases of interest the potential is not known. A natural question to ask is what is the impact of a DBI action on the Hawking-Moss tunneling rate. Potential applications include both inflation and vacuum selection [66], [18], [67]. During the observable stage of inflation observations disfavor large field space velocities for the inflaton in models with a DBI action [66]. For this reason we focus on the case where the field space velocity is small throughout the tunneling event.

Hawking and Moss used a Euclidean approach in [7] to calculate the tunneling rate in de Sitter space from a metastable state A to over a wide barrier with a maximum at B to the true minimum of the potential C. Two constant instanton solutions $\phi(\tau, \mathbf{x}) = \phi_A$, $\phi(\tau, \mathbf{x}) = \phi_B$ satisfy the classical equations of motion. Claiming that the tunneling rate is the exponential of the difference in the Euclidean action of these two instanton solutions $P(A \to C) \sim \exp(-(S(\phi_A) - S(\phi_B)))$

Hawking and Moss found the tunneling rate to be

$$P_{A\to C} \sim \exp\Big(-\frac{3M_P^4}{8}\Big(\frac{1}{V_A} - \frac{1}{V_B}\Big)\Big). \tag{5.1}$$

Several problems have been pointed out with this approach in the appendices of [4],[18]. The instanton solution $\phi(\tau) = \phi_B$ does not interpolate between the metastable state and the true vacuum. However since the Euclidean scale factor $b(\tau) = H^{-1}\sin(2\pi H\tau)$ vanishes at $\tau = 0$ and $\tau = H^{-1}$ large modifications can be made to the instanton solution $\phi(\tau, \mathbf{x}) = \phi_B$ near the endpoints without changing the action significantly although the modified solution will no longer solve the classical equations of motion. This problem is particularly severe when there are several metastable vacua between the initial metastable state and the true vacuum. Naively we could pick any of the instanton solutions sitting at a local maximum between the initial metastable state and the true vacuum to calculate the tunneling rate but generically the result depends on this choice of a local maximum. For these reasons we will not use the Euclidean approach of [7].

We find that the tunneling rate is modified to be

$$P_{A\to C} \sim \exp\Big(\frac{3M_p^4}{8}\Big(\frac{1}{\gamma V(\phi)} - \frac{(\gamma+1)(\gamma-1)}{2(V(\phi))^2}T(\phi)\Big)\Big|_{\phi_A}^{\phi_B}\Big) \tag{5.2}$$

when the inflaton ϕ is described by the DBI action. Here H is the Hubble parameter given by $H^2(\phi) = \frac{8\pi}{3M_p^2}\rho$, T is the warped brane tension, and

$$\gamma = \frac{1}{\sqrt{1 - \frac{\dot\phi^2}{T(\phi)}}} = \frac{1}{c_s} \geq 1 \tag{5.3}$$

where c_s is the sound speed. For small brane tensions $T(\phi)/V(\phi) \ll 1$ the tunneling rate in Eq.(5.2) is enhanced over the rate in Eq.(5.1). In the limit that $\gamma = 1$ Eq. (5.2) reduces to Eq.(5.1). Our results are valid in the limit that the curvature of the potential is small compared to the Hubble scale, that the energy density

is dominated by the potential for the entire region in field space through which the tunneling occurs, and that the inflaton has a small field space velocity so that $\gamma \gtrsim 1$.

Instead of the Euclidean approach we will use the more clearly physically motivated stochastic approach of [53], [54], [55], [68]. The basic physical idea is that the quantum fluctuations of the short wavelength components of the inflaton field act as a random force on the long wavelength parts. If the inflaton is trapped in a metastable minimum, these fluctuations can drive the field up to a nearby maximum. From the maximum the inflaton has a probability of order unity to roll classically to a different minimum.

We consider a D3 brane probe moving in a type IIB background described by the DBI action

$$S = -\int d^4x a^3(t)(T\sqrt{1-\frac{\partial\phi^2}{T}} - T + V) \tag{5.4}$$

where T is the warped D3 brane tension, ϕ is the canonically normalized inflaton, and V is the potential. In this theory ϕ has a speed limit because of the non-minimal form of the kinetic term in Eq.(5.4).

We follow closely the treatment of [53]. The essential physical idea is that if we divide the field $\phi(\mathbf{x})$ into a long-wavelength part Φ and a short-wavelength part, the short-wavelength part acts as a random force on the long-wavelength part.

The average value of the field ϕ over the coordinate volume b^3 is given by

$$\phi_b = \frac{1}{(2\pi)^{3/2}}\frac{1}{b^3}\int d^3x \mathrm{e}^{-|\mathbf{x}|^2/2b^2}\phi(\mathbf{x}). \tag{5.5}$$

Assuming the metric is flat, we can use the momentum space expansion

$$\phi(\mathbf{x}) = \int \frac{d^3k}{(2\pi)^{3/2}} \{a_{\mathbf{k}} \phi_{\mathbf{k}} e^{i\mathbf{k}\cdot\mathbf{x}} + a^\dagger_{\mathbf{k}} \phi^*_{\mathbf{k}} e^{-i\mathbf{k}\cdot\mathbf{x}}\} \tag{5.6}$$

to obtain

$$\phi_b = \int \frac{d^3k}{(2\pi)^{3/2}} e^{-k^2 b^2/2} \{a_{\mathbf{k}} \phi_{\mathbf{k}} + a^\dagger_{\mathbf{k}} \phi^*_{\mathbf{k}}\}. \tag{5.7}$$

Here $a_{\mathbf{k}}$ and $a^\dagger_{\mathbf{k}}$ are the ordinary creation and annihilation operators satisfying $[a_{\mathbf{k}}, a^\dagger_{\mathbf{q}}] = \delta(\mathbf{k} - \mathbf{q})$. For calculational simplicity we replace Eq. (5.7) with

$$\phi_b = \int \frac{d^3k}{(2\pi)^{3/2}} \Theta(-k + b^{-1}) \{a_{\mathbf{k}} \phi_{\mathbf{k}} + a^\dagger_{\mathbf{k}} \phi^*_{\mathbf{k}}\}. \tag{5.8}$$

We are interested in the macroscopic evolution of the field ϕ on a de Sitter space background with metric $ds^2 = a^2(t)(dx^2 + dy^2 + dz^2)$. The coordinate length associated with the physical length scale $\gtrsim H^{-1}$ of interest is $b = \frac{1}{\epsilon a} H^{-1}$ where $\epsilon \ll 1$. A more precise restriction on ϵ will be obtained below. If we let Φ denote the value of ϕ averaged over this volume, then

$$\Phi = \int \frac{d^3k}{(2\pi)^{3/2}} \Theta(-k + \epsilon a H) \{a_{\mathbf{k}} \phi_{\mathbf{k}} + a^\dagger_{\mathbf{k}} \phi^*_{\mathbf{k}}\} \tag{5.9}$$

and the rate of change of Φ is

$$\begin{aligned} \dot{\Phi} &= \int \frac{d^3k}{(2\pi)^{3/2}} \Theta(-k + \epsilon a H)(a_{\mathbf{k}} \dot{\phi}_{\mathbf{k}} + a^\dagger_{\mathbf{k}} \dot{\phi}^*_{\mathbf{k}}) \\ &+ \epsilon a H^2 \int \frac{d^3k}{(2\pi)^{3/2}} \delta(-k + \epsilon a H)(a_{\mathbf{k}} \phi_{\mathbf{k}} + a^\dagger_{\mathbf{k}} \phi^*_{\mathbf{k}}) \\ &\equiv \int \frac{d^3k}{(2\pi)^{3/2}} \Theta(-k + \epsilon a H) \{a_{\mathbf{k}} \dot{\phi}_{\mathbf{k}} + a^\dagger_{\mathbf{k}} \dot{\phi}^*_{\mathbf{k}}\} + g(t). \end{aligned} \tag{5.10}$$

We will see that $g(t)$ plays the role of a random force due to the short-wavelength parts of ϕ.

To find the equation of motion of ϕ we use the results of [70] to calculate the energy density. Using $p = T - T\sqrt{1 - \frac{\dot{\phi}^2}{T}} - V$ and $\rho = 2X\partial_X p - p$ where $X = \frac{1}{2}(\nabla\phi)^2$

we obtain

$$\rho = 2\gamma X + T/\gamma - T + V. \tag{5.11}$$

From Eq.(5.11) and the Friedman equations we find that the equation of motion of ϕ on the background is

$$\ddot{\phi} + \frac{3H}{\gamma^2}\dot{\phi} + \left(2 - \frac{3}{\gamma^2}\right)\frac{\nabla^2}{a^2}\phi + \frac{1}{\gamma^3}V' - \frac{(\gamma+1)(\gamma-1)}{2\gamma^2}T' = 0 \tag{5.12}$$

where $'$ denotes a partial derivative with respect to ϕ.

If $\phi = \phi_0$ is a metastable state then we can write $V(\phi) = V_0 + \frac{m^2}{2}(\phi - \phi_0)^2 - \frac{\lambda}{4}(\phi - \phi_0)^4$ in a neighborhood of $\phi = \phi_0$. Assuming $T(\phi)$ is analytic in a neighborhood of $\phi = \phi_0$ we write $T(\phi) = T_3(\alpha_0 + \frac{\alpha_2}{2}(\phi - \phi_0)^2 + \cdots)$. Using these Taylor expansions we see that the mode ϕ_k approximately satisfies the equation

$$\begin{aligned}\ddot{\phi}_k + \frac{3H}{\gamma^2}\dot{\phi}_k + \left(\frac{3}{\gamma^2} - 2\right)\frac{k^2}{a^2}\phi_k + \frac{1}{\gamma^3}(m^2\phi_k - \lambda\langle\phi^2\rangle\phi_k) \\ -\frac{(\gamma+1)(\gamma-1)}{2\gamma^2}T_3(\alpha_2\phi_k + \cdots) = 0.\end{aligned} \tag{5.13}$$

If the short-wavelength modes of ϕ are to act as a stochastic force on the spatially averaged Φ, then these modes should obey the equation of a free field. For modes with $k \gg \epsilon aH$ only the first three terms are important if three conditions are satisfied:

1) $m^2/\gamma^3 \ll (3/\gamma^2 - 2)k^2/a^2$

2) $\lambda\langle\phi^2\rangle/\gamma^3 \ll (3/\gamma^2 - 2)k^2/a^2$

3) $\frac{(\gamma+1)(\gamma-1)}{2\gamma^2}T_3(\alpha_2 + \cdots) \ll (3/\gamma^2 - 2)k^2/a^2$.

The first two conditions restrict the shape of the potential for which our approximation is valid. These conditions are weaker than the conditions for the

validity of the Hawking-Moss tunneling rate (5.1) obtained by [53]. Our conditions reduce to the conditions of [53] when $\gamma = 1$. Condition 3 is always valid for small field space velocities (sufficiently close to $\gamma = 1$) and we know that $\gamma \gtrsim 1$ in a metastable state. Condition 2 is always valid in the neighborhood of a metastable state because the effective square of the mass $M^2 = m^2 - \lambda\langle\phi^2\rangle$ is always positive. This positivity combined with condition 1 implies

$$\lambda\langle\phi^2\rangle < m^2 \ll (3\gamma - 2\gamma^3)k^2/a^2 \tag{5.14}$$

By [70] the expectation value of ϕ^2 is given by

$$\langle\phi^2\rangle = \frac{3H^4}{8\gamma^2\pi^2m^2} \tag{5.15}$$

which gives us a bound on λ

$$\lambda < \frac{8\pi^2}{3}\frac{m^4\gamma^2}{H^4} \ll \frac{8\pi^2}{3}(3\gamma^3 - 2\gamma^5)\epsilon^4. \tag{5.16}$$

When our three conditions are satisfied the modes with $k \gtrsim \epsilon aH$ satisfy the equation

$$\ddot{\phi}_k + \frac{3H}{\gamma^2}\dot{\phi}_k + \left(\frac{3}{\gamma^2} - 2\right)\frac{k^2}{a^2}\phi_k = 0 \tag{5.17}$$

where $a = e^{Ht}$. Using the results of [70]

$$\phi_k \approx -\imath\frac{H}{\gamma(2k^3)^{1/2}} \tag{5.18}$$

at the sound horizon. Substituting the expansion of ϕ in momentum space into our equation of motion we find

$$\begin{aligned}\int \frac{d^3k}{(2\pi)^{3/2}} \\ \{a_{\mathbf{k}}(\ddot{\phi}_{\mathbf{k}} + \frac{3H}{\gamma^2}\dot{\phi}_{\mathbf{k}} + \left(\frac{3}{\gamma^2} - 2\right)\phi_{\mathbf{k}})e^{i\mathbf{k}\cdot\mathbf{x}} + \text{H.C.}\} \\ +\frac{1}{\gamma^3}V' - \frac{(\gamma+1)(\gamma-1)}{2\gamma^2}T' = 0\end{aligned} \tag{5.19}$$

The integral in Eq.(5.19) is equal to

$$\int \frac{d^3k}{(2\pi)^{3/2}}\Theta(\epsilon aH - k)\{a_{\mathbf{k}}(\ddot{\phi}_{\mathbf{k}} + \frac{3H}{\gamma^2}\dot{\phi}_{\mathbf{k}} + \left(\frac{3}{\gamma^2} - 2\right)\phi_{\mathbf{k}})e^{i\mathbf{k}\cdot\mathbf{x}} + \text{H.C.}\} \tag{5.20}$$

because

$$\int \frac{d^3k}{(2\pi)^{3/2}}\Theta(k - \epsilon aH)\{a_{\mathbf{k}}(\ddot{\phi}_{\mathbf{k}} + \frac{3H}{\gamma^2}\dot{\phi}_{\mathbf{k}} + \left(\frac{3}{\gamma^2} - 2\right)\phi_{\mathbf{k}})e^{i\mathbf{k}\cdot\mathbf{x}} + \text{H.C.}\} \tag{5.21}$$

vanishes identically by Eq.(5.17). In Eq. (5.19) the first derivative term is the most important if $\gamma \gtrsim 1$ which must be the case if the inflaton starts out in a metastable state. We assume $\gamma \gtrsim 1$ for the entire region in field space through which tunneling occurs. Thus

$$\int \frac{d^3k}{(2\pi)^{3/2}}\Theta(\epsilon aH - k)\{a_{\mathbf{k}}\dot{\phi}_{\mathbf{k}}e^{i\mathbf{k}\cdot\mathbf{x}} + \text{H.C.}\} = -\frac{1}{3H}\left(\frac{1}{\gamma}V' - \frac{(\gamma+1)(\gamma-1)}{2}T'\right) \tag{5.22}$$

Averaging this equation over the volume b^3 we find that

$$\dot{\Phi} = -\frac{1}{3H}\left(\frac{1}{\gamma}\frac{\partial V}{\partial \Phi} - \frac{(\gamma+1)(\gamma-1)}{2}\frac{\partial T}{\partial \Phi}\right) + g(t) \tag{5.23}$$

where

$$g(t) = \epsilon aH^2 \int \frac{d^3k}{(2\pi)^{3/2}}\delta(-k + \epsilon aH)\{a_{\mathbf{k}}\phi_{\mathbf{k}} + a^\dagger_{\mathbf{k}}\phi^*_{\mathbf{k}}\}. \tag{5.24}$$

Equation (5.23) is a Langevin equation with a random force $g(t)$. The correlation functions $\langle g(t)\rangle$, $\langle g(t_1)g(t_2)\rangle$, etc. characterize the statistical properties of $g(t)$. We compute these functions by averaging over the vacuum state $|\rangle$ that satisfies $a_{\mathbf{k}}|\rangle = 0$. Clearly all of the odd correlation functions vanish. The two-point correlation function is given by

$$\langle g(t_1)g(t_2)\rangle = \epsilon^2 H^4 a_1 a_2 \int \frac{d^3k d^3q}{(2\pi)^3}\delta(k - \epsilon a_1 H)\delta(q - \epsilon a_2 H)$$

$$
\begin{aligned}
&\langle a_{\mathbf{k}} a_{\mathbf{q}}^{\dagger}\rangle \phi_{\mathbf{k}} \phi_{\mathbf{q}}^{*} \\
= \;& \frac{\epsilon^2 H^6 a_1 a_2}{(2\pi)^2 \gamma^2} \int \frac{dk}{k} \delta(k - \epsilon a_1 H)\delta(k - \epsilon a_2 H) \\
= \;& \frac{\epsilon^2 H^6 a_1 a_2}{(2\pi)^2 \gamma^2} \frac{1}{\epsilon a_1 H} \delta(\epsilon a_1 H - \epsilon a_2 H) \\
= \;& \frac{H^3}{4\pi^2 \gamma^2} \delta(t_1 - t_2)
\end{aligned} \tag{5.25}
$$

It can be shown by induction that $\langle g(t_1) \cdots g(t_n)\rangle = \sum \prod \langle g(t_i) g(t_j)\rangle$ for all even n where the sum is taken over all possible products of two-point functions. Therefore $g(t)$ is a Gaussian variable and Eq.(5.23) leads to the standard Fokker-Planck equation

$$
\frac{\partial \rho}{\partial t} = \frac{\partial}{\partial \Phi}\Big(\frac{1}{3H}\Big(\frac{1}{\gamma}\frac{\partial V}{\partial \Phi} - \frac{(\gamma+1)(\gamma-1)}{2}\frac{\partial T}{\partial \Phi}\Big)\rho\Big) + D\frac{\partial^2 \rho}{\partial \Phi^2} \tag{5.26}
$$

with $D = H^3/8\pi^2\gamma^2$.

There is a finite probability for a particle initially in a metastable state at $\phi = \phi_A$ to stochastically climb up the potential to a nearby maximum at $\phi = \phi_B$. Once at the maximum the particle has a probability of order unity to classically roll down to an adjacent minimum $\phi = \phi_C$. By integrating the Fokker-Planck equation

$$
\frac{\partial \rho}{\partial t} = \frac{\partial}{\partial \Phi}\Big(\frac{1}{3H}\frac{\partial V}{\partial \Phi}\rho\Big) + D\frac{\partial^2 \rho}{\partial \Phi^2} \tag{5.27}
$$

in [69] it was found that the mean time during which a particle initially at $\phi = \phi_A$ passes over the barrier at $\phi = \phi_B$ of height ΔV is given by

$$
\Delta t \sim \exp\Big(\int_{\phi_A}^{\phi_B} d\phi \frac{\partial}{\partial \phi}\frac{V(\phi)}{3H(\phi)D(\phi)}\Big) \tag{5.28}
$$

up to some subexponential prefactors. Using the same technique and (5.26) we see that

$$
\Delta t \sim \exp\Big(\frac{8\pi^2}{3}\Big(\int_{\phi_A}^{\phi_B} d\phi \frac{\partial}{\partial \phi}\Big(\frac{V}{\gamma H^4} - \frac{(\gamma+1)(\gamma-1)}{2H^4} T\Big)\Big)\Big) \tag{5.29}
$$

if the argument of the exponential is large. Equivalently the probability per unit volume is given by

$$\begin{aligned} P_{A\to C} &\sim \exp(-B_{HMDBI}) \\ &\sim \exp\Big(\frac{3M_P^4}{8}\Big(\frac{1}{\gamma V} - \frac{(\gamma+1)(\gamma-1)}{2V^2}T\Big)\Big|_{\phi_A}^{\phi_B}\Big) \end{aligned} \tag{5.30}$$

so the effect of the DBI action is to modify the tunneling rate from the result of [7]

$$\begin{aligned} P_{A\to C} &\sim \exp(-B_{HM}) \\ &\sim \exp\Big(-\frac{3M_P^4}{8}\Big(\frac{1}{V(\phi_A)} - \frac{1}{V(\phi_B)}\Big)\Big). \end{aligned} \tag{5.31}$$

For example in a warped type IIB compactification with fluxes [4] and D7-branes wrapped on 4-cycles, the potential for a probe D3-brance can have discrete minima in the angular directions of the compact space [72]. If at a fixed radial position at the bottom of the throat the D3-brane is in a false vacuum, it can tunnel in an angular direction. If we have $T = (1.0 * 10^{-5}M_P)^4$, $V(\phi_A) = (3.00 * 10^{-4}M_P)^4$, $V(\phi_B) = (3.01 * 10^{-4}M_P)^4$, $\gamma_A = 1.02$, and $\gamma_B = 1.01$, then $B_{HM}/B_{HMDBI} \sim 3.91$ so tunneling is exponentially faster than one would expect using (5.31). This result could have important applications for inflation when the inflaton is described by the DBI action, or for vacuum selection in the landscape. We leave these implications to future work.

After completing this work the author became aware of [73] in which a result is derived that agrees with Eq.(5.2) in the limit that $T/V \ll 1$. See also [74] for a related discussion.

BIBLIOGRAPHY

[1] A. G. Riess *et al.* [Supernova Search Team Collaboration], "Observational evidence from supernovae for an accelerating universe and a cosmological constant," Astron. J. **116**, 1009 (1998) [arXiv:astro-ph/9805201].

[2] E. G. Adelberger, B. R. Heckel and A. E. Nelson, "Tests of the gravitational inverse square law," Ann. Rev. Nucl. Part. Sci. **53**, 77 (2003) [arXiv:hep-ph/0307284].

[3] G. D. Coughlan, W. Fischler, E. W. Kolb, S. Raby and G. G. Ross, "Cosmological problems for the polonyi potential," Phys. Lett. B **131**, 59 (1983).

[4] S. Kachru, R. Kallosh, A. D. Linde and S. P. Trivedi, "de Sitter vacua in string theory," Phys. Rev. D **68**, 046005 (2005) [arXiv:hep-th/0301240].

[5] V. Balasubramanian, P. Berglund, J. P. Conlon and F. Quevedo, "Systematics of moduli stabilisation in Calabi-Yau flux compactifications," JHEP **0503**, 007 (2005) [arXiv:hep-th/0502058].

[6] S. R. Coleman and F. De Luccia, "Gravitational Effects On And Of Vacuum Decay," Phys. Rev. D **21**, 3305 (1980).

[7] S. W. Hawking and I. G. Moss, "Supercooled Phase Transitions In The Very Early Universe," Phys. Lett. B **110**, 35 (1982).

[8] A. H. Guth, "Eternal inflation and its implications," J. Phys. A **40**, 6811 (2007) [arXiv:hep-th/0702178].

[9] B. Freivogel, "Making predictions in the multiverse," arXiv:1105.0244 [hep-th].

[10] S. Weinberg, "Anthropic Bound on the Cosmological Constant," Phys. Rev. Lett. **59**, 2607 (1987).

[11] S. M. Feeney, M. C. Johnson, D. J. Mortlock, H. V. Peiris, "First Observational Tests of Eternal Inflation," [arXiv:1012.1995 [astro-ph.CO]].

[12] See e.g., E. Merzbacher, Chapter 7 in *Quantum Mechanics*, 2*nd* edition, John Wiley, 1970.

[13] L. L. Chang, L. Esaki, and R. Tsu, "Resonant tunneling in semiconductor double barriers," Appl. Phys. Lett. **24**, 593 (1974).

[14] E.g., M. Sweeny. "Resonant interband tunnel diodes". Applied Phys. Lett. 54: 546 (1989); D. J. Day, "Double quantum well resonant tunneling diodes". Applied Phys. Lett. 57: 1260 (1990); K. K. Ng, "Complete Guide to Semiconductor Devices (2 ed.)", Wiley-Interscience (2002).

[15] S. R. Coleman, "The Fate Of The False Vacuum. 1. Semiclassical Theory," Phys. Rev. D **15**, 2929 (1977) [Erratum-ibid. D **16**, 1248 (1977)].

[16] C. G. . Callan and S. R. Coleman, "The Fate Of The False Vacuum. 2. First Quantum Corrections," Phys. Rev. D **16**, 1762 (1977).

[17] S. H. H. Tye, "A new view of the cosmic landscape," arXiv:hep-th/0611148.

[18] S.-H. H. Tye, "A Renormalization Group Approach to the Cosmological Constant Problem," arXiv:0708.4374 [hep-th].

[19] E. J. Copeland, A. Padilla and P. M. Saffin, "No resonant tunneling in standard scalar quantum field theory," JHEP **0801**, 066 (2008) [arXiv:0709.0261 [hep-th]].

[20] P. M. Saffin, A. Padilla and E. J. Copeland, "Decay of an inhomogeneous state via resonant tunnelling," JHEP **0809**, 055 (2008) [arXiv:0804.3801 [hep-th]].

[21] S. Sarangi, G. Shiu and B. Shlaer, "Rapid Tunneling and Percolation in the Landscape," Int. J. Mod. Phys. A **24**, 741 (2009) [arXiv:0708.4375 [hep-th]].

[22] J. L. Gervais and B. Sakita, "WKB wave function for systems with many degrees of freedom: A unified view of solitons and pseudoparticles," Phys. Rev. D **16**, 3507 (1977).

[23] K. M. Bitar and S.-J. Chang, "Vacuum Tunneling And Fluctuations Around A Most Probable Escape Path," Phys. Rev. D **18**, 435 (1978); "Vacuum Tunneling Of Gauge Theory In Minkowski Space," Phys. Rev. D **17**, 486 (1978).

[24] T. Banks, C. M. Bender and T. T. Wu, "Coupled anharmonic oscillators. 1. Equal mass case," Phys. Rev. D **8**, 3346 (1973);

[25] S.-J. Chang, Chapter 9 in *Introduction to Quantum Field Theory*, World Scientific, 1990.

[26] D. D. Osheroff, R. C. Richardson and D. M. Lee, "Evidence for a New Phase of Solid He^3," Phys. Rev. Lett. **28**, 885, 1972;
for reviews, see e.g., A. J. Leggett, "A Theoretical Description of the New Phases of Liquid ^3He", Rev. Mod. Phys. **47**, 331, 1975;
Superfluid ^3He, edited by L. P. Pitaevskii and W. P. Halperin (North Holland, Amsterdam, 1989).

[27] D. D. Osheroff and M. C. Cross, "Interfacial Surface Energy between the Superfluid Phases of He^3," Phys. Rev. Lett. **38**, 905 (1977);
M. C. Cross, "Calculation of Surface Energies in A and B Phases of ^{3}He," in *Quantum Fields and solids*, 1977, S. B. Trickey, E. D. Adams and J. W. Dufty, eds (Plenum, New York, 1977).

[28] R. Kaul and H. Kleinert, "Surface Energy and Textural Boundary Conditions Between *A* and *B* Phases of ^{3}He," Journal of Low Temperature Physics, Vol. 38, 539 (1980).

[29] See e.g., P. Schiffer, D. D. Osheroff, "Nucleation of the AB transition in superfluid He-3: Surface effects and baked Alaska," Rev. Mod. Phys. **67**, 491-501 (1995).

[30] A. J. Leggett and S. K. Yip, "Nucleation and growth in the supercooled A-phase," in *Helium Three* ed. by L. P. Pitaevskii and W. P. Halperin.

[31] D. Bailin and A. Love, "Instantons in superfluid ^{3}He," Journal Physics A : Math. Gen. **13** L271 (1980).

[32] A. J. Leggett, "Nucleation of ^{3}He-B from the *A* Phase: A Cosmic-Ray Effect?," Phys. Rev. Lett **53**, 1096 (1984); **54**, 246 (1985).

[33] G. W. Swift, "John Wheatley Memorial Conf.", Los Alamos, NM, October 1986, unpublished; as quoted in Ref[30].

[34] D. S. Buchanan, G. W. Swift and J. C. Wheatley, "Velocity of Propagation of the ^{3}He A-B Interface in Hypercooled ^{3}He-A," Phys. Rev. Lett. **57**, 341 (1986);
G. W. Swift and D. S. Buchanan, "Nucleation and Growth of ^{3}He-B in ^{3}He-A," in "*Proceedings of the 18th International Conference on Low Temperature Physics*", published in Jpn. J. Appl. Phys. **26-3** 1828 (1987).

[35] P. J. Hakonen, M. Krusius, M. M. Salomaa and J. T. Simola, "Comment on "Nucleation of ^{3}He-*B* from the *A* Phase: A Cosmic Ray Effect ?"," Phys. Rev. Lett. **54**, 245 (1985).

[36] J. S. Langer, "Statistical theory of the decay of metastable states," Ann. Phys., **54**, 258 (1969).

[37] See e.g., M. R. Douglas and S. Kachru, "Flux Compactification," Rev. Mod. Phys. **79**, 733 (2007) [arXiv:hep-th/0610102].

[38] See e.g., G. E. Volovik, *The Universe in a Helium Droplet*, Oxford University Press, 2003.

[39] Y. M. Bunkov, "^{3}He Experiments: Insights into Cosmology and Atomic Physics," J. Low Temp. Phys. **158** 118 (2010).

[40] Ü. Parts, V. M. H. Ruutu, J. H. Koivuniemi, Y. N. Bunkov, V. V. Dmitriev, M. Fogelström, M. Huenber, Y. Kondo, N. B. Kopnin, J. S. Korhonen, M. Krusius, O. V. Lounasmaa, P. I. Soininen, G. E. Volovik, "Single-vortex nucleation in rotating superfluid ^{3}He-B", EPL **31**, 449-454 (1995).

[41] V. M. H. Ruutu, V. B. Eltsov, A. J. Gill, T. W. B. Kibble, M. Krusius, Yu. G. Makhlin, B. Placais, G. E. Volovik, Wen Xu, "Vortex formation in neutron-irradiated superfluid 3He as an analogue of cosmological defect formation", *Nature*, **382** 334-336 (1996).

[42] R. Blaauwgeers, V. B. Eltsov, G. Eska, A. P. Finne, R. P. Haley, M. Krusius, J. J. Ruohio, L. Skrbek, and G. E. Volovik, "Shear flow and Kelvin-Helmholtz instability in superfluids", Phys. Rev. Lett. **89**, 155301 (2002).

[43] A. D. Linde, "Eternally Existing Selfreproducing Inflationary Universe," Phys. Scripta **T15**, 169 (1987).

[44] A. S. Goncharov, A. D. Linde and V. F. Mukhanov, "The Global Structure of the Inflationary Universe," Int. J. Mod. Phys. A **2**, 561 (1987).

[45] Q.-G. Huang and S.-H. H. Tye, "The cosmological constant problem and inflation in the string landscape," ArXiv:0803.0663 [hep-th].

[46] L. G. Jensen and P. J. Steinhardt, "Bubble nucleation and the Coleman-Weinberg model." Nucl. Phys. B **237**, 176 (1984).

[47] A. R. Brown and E. J. Weinberg, "Thermal derivation of the Coleman-De Luccia tunneling prescription," Phys. Rev. D **76**, 064003 (2007) [arXiv:0706.1573 [hep-th]].

[48] B. Allen, "Phase Transitions in de Sitter Space," Nucl. Phys. B **226**, 228 (1983).

[49] G. L. Kane, M. J. Perry, A. N. Zytkow, "Spontaneous Symmetry Breaking and Tunneling in de Sitter Space," [arXiv:hep-th/0407217v2].

[50] M.J. Duncan and L. G. Jensen, "Exact tunneling solutions in scalar field theory" Nuclear physics B **291**, 109 (1992).

[51] E. Mottola and A. Lapedes "Existence of finite-action solutions to the Coleman-De Luccia equations" Phys. Rev. D **29**, 773 (1984).

[52] V. Gen and M. Sasaki, "False vacuum decay with gravity in non-thin-wall limit," Phys. Rev. D **61**, 103508 (2000) [arXiv:gr-qc/9912096].

[53] A. S. Goncharov and A. D. Linde, "Tunneling in an expanding universe: Euclidean and Hamiltonian approaches," Sov. J. Part. Nucl. **17** 369 (1987).

[54] A. A. Starobinsky, "Stochastic DeSitter (Inflationary) Stage in the Early Universe," in Field Theory, Quantum Gravity and Strings, edited by H.J. De Vega and N. Sanchez (Springer New York 1986).

[55] A. S. Goncharov, A. D. Linde and V. F. Mukhanov, "The Global Structure of the Inflationary Universe," Int. J. Mod. Phys. A **2**, 561 (1987).

[56] K. Lee and E. J. Weinberg, "Decay of the true vacuum in curved space-time," Phys. Rev. D **36**, 1088 (1987).

[57] B. H. Lee and W. Lee, "The vacuum bubble and black hole pair creation," ArXiv:0809.4907v2 [hep-th].

[58] S. Parke, "Gravity and the decay of the false vacuum," Phys. Lett. B **121**, 313 (1983).

[59] E. J. Weinberg, "Hawking-Moss bounces and vacuum decay rates," Phys. Rev. Lett. **98**, 251303 (2007). [arXiv:hep-th/0612146].

[60] I. Affleck, "Quantum-Statistical Metastability," Phys. Rev. Lett. **46**, 388 (1981).

[61] A. D. Linde, "Decay of the False Vacuum at Finite Temperature," Nucl. Phys. B **216**, 421 (1983); [Erratum: **B** 223, 544 (1983)].

[62] R. Easther and L. McAllister, "Random Matrices and the Spectrum of N-flation," [arXiv:hep-th/0512102].

[63] P. Svrcek and E.Witten, "Axions in String Theory," JHEP **0606**, 051 (2006), arxiv:0605206 [hep-th].

[64] S. Kachru, R. Kallosh, A. Linde, J. Maldacena, L. McAllister and S. P. Trivedi, "Towards inflation in string theory," JCAP **0310** (2003) 013, hep-th/0308055;
S. Shandera, B. Shlaer, H. Stoica and S.-H. H. Tye, "Inter-brane interactions in compact spaces and brane inflation," JCAP **0402**, 013 (2004), hep-th/0311207.

[65] A. R. Brown, S. Sarangi, B. Shlaer, and A. Weltman, "A Wrinkle in Coleman - De Luccia," Phys. Rev. Lett. 99, 161601 (2007); arXiv:hep-th/0706.0485.

[66] R. Bean, S. E. Shandera, S.-H. H. Tye, J. Xu, "Comparing Brane Inflation to WMAP", JCAP 2007; [arXiv:hep-th/0702107].

[67] D. Podolsky and K. Enqvist, "Eternal inflation and localization on the landscape," [arXiv:0704.0144v3].

[68] A. D. Linde, Particle Physics and Inflationary Cosmology, (Harwood, Switzerland 1990), [arXiv:hep-th/0503203].

[69] A. A. Starobinskii, "Fundamental'nye vzaimodeistviya," Moscow State Pedagogical Institute, Moscow, 55 (1984).

[70] V. Mukhanov, "Physical Foundations of Cosmology," Cambridge University Press, Cambridge, 2005.

[71] E. Silverstein and D. Tong, "Scalar Speed Limits and Cosmology: Acceleration from D-cceleration," Phys. Rev. D 70, 103505 (2004); [arXiv:hep-th/0310221].

[72] D. Baumann, A. Dymarsky, I. R. Klebanov, and L. McAllister, "Towards an Explicit Model of D-brane Inflation," [arXiv:hep-th/0706.0360].

[73] A. J. Tolley and M. Wyman, "Stochastic Inflation Revisited: Non-Slow Roll Statistics and DBI Inflation," [arXiv:hep-th/0801.1854].

[74] A. Brown, "Brane tunneling and virtual brane-antibrane pairs"; [arXiv:0709.3532v1].